UCL Université catholique de Louvain

Faculté des Bioingénieurs

Impact of food components and digestive enzymes on silver nanoparticles cytotoxicity in a coculture model of the intestinal barrier

Présenté par Donika Kastrati

Promoteurs : Prof. Yves-Jacques Schneider (UCL/ISV/BCNT)
Prof. Jean-François Rees (UCL/ISV/BNTE)

Lecteurs : Prof. Melissa Page (UCL/ISV/BNTE)
Prof. Cathy Debier (UCL/ISV)

Mémoire de fin d'études présenté en vue de l'obtention du diplôme de Bioingénieur : **Sciences agronomiques**

AGRO LOUVAIN

Année académique 2017-2018

Acknowledgments

As a preamble to this thesis, I would like to thank all the people who have been implicated in its elaboration.

First, I would like to thank Professor Yves-Jacques Schneider for welcoming me in his lab and giving me advices and comments throughout the whole year. I thank also Professor Jean-François Rees for accepting to be my copromotor.

I would also like to thank the professors Melissa Page and Cathy Debier for accepting to be part of my jury and for taking the time to read and review the present work.

My special gratitude goes to Laurie Laloux, my supervisor. Thank you for all the advices, explanations, reviews and countless feedbacks of my works but also for your patience, availability and support. Many thanks to Camille Van Craynest, who was a great help at many moments during the experiments in the lab and Madeleine Polet for the daily good mood, advices and precious help in computer science.

Thanks also to Audrey Leurquin with whom I shared this captivating topic, i'll never forget the good moments we had in the lab.

To all the members of the BNTE lab that I met during this second quadrimester, thanks for the welcome and practical advices.

Finally, I would like to thank my friends and family for helping and supporting me throughout the writing of this thesis and my life in general.

Table of content

Acknowledgments .....

Table of content .....

Abstract .....

List of abbreviations .....

List of figures .....

List of tables .....

INTRODUCTION 1

1. Principles of digestion 2

1.1 Human digestive system 2

1.1.1 General overview 2

1.1.2 Histology 3

1.1.3 Stages of *in vivo* digestion 4

1.2 *In vitro* digestion 10

1.3 The intestinal barrier 11

1.3.1 Description at the cellular level 11

1.3.2 *In vitro* models of the intestinal barrier 12

2. Food Matrix 13

2.1 General considerations on nutrition and energy metabolism 13

2.2 Ingested foodstuffs 13

2.2.1. Carbohydrates 13

2.2.2 Fats 13

2.2.3 Proteins 14

2.3 *In vitro* model of the food matrix 14

3. Nanomaterials 14

3.1 Definitions 14

3.2 Nanoparticles in the society 16

3.3 General characteristics of NPs 17

3.4 Interaction between biological fluids and nanoparticles 18

4. Silver nanoparticles 19
4.1 Importance of AgNPs in the society 20
4.2 Properties of AgNPs 21
4.2.1 Antibacterial activity 21
4.3 Applications of AgNPs 23
4.3.1 AgNPs in the food sector 23
4.4 Toxicity studies about AgNPs 24
4.5 Characterization of AgNPs 26
4.5.1 UV-visible spectroscopy 26
4.6 Safety regulations 27
5. Objectives 29

MATERIAL & METHODS 30

1. Material 31
1.1 Cell lines 31
1.2 Silver nanoparticles 31
1.3 Food matrix 31
2. Cell culture 32
2.1 Caco-2 & HT29-MTX cells 32
2.2 Cell density assessment 32
2.3 Culture in 48 well plates 33
3. *In vitro* digestion 33
3.1 Principle 33
3.2 Method 33
4. Impact of the food matrix and digestive enzymes on intestinal cells 34
4.1 Sample preparation and *in vitro* digestion 35
4.2 Sample dilution and cytotoxicity assays 35
5. Impact of AgNPs included in a digested food matrix on intestinal cells 35
5.1 Sample preparation and *in vitro* digestion 35
5.2 Sample dilution and cytotoxicity assays 36
6. Cytotoxicity assays 36
6.1 CellTiter-Glo assay 36

6.1.1 Principle 36
6.1.2 Method 37
6.2 CellTiter-Blue assay 37
6.2.1 Principle 37
6.2.2 Method 38
6.3 Crystal Violet cell detachment assay 38
6.3.1 Principle 38
6.3.2 Method 38
7. AgNPs characterization 39
7.1 UV-visible spectroscopy 39
7.1.1 Principle 39
7.1.2 Method 39
8. Protein corona assay 39
8.1 Isolation of AgNPs-proteins complexes 40
8.1.1 Principle 40
8.1.2 Method 40
8.2 Protein quantification : microBCA assay 41
8.2.1 Principle 41
8.2.2 Method 42
9. Statistical Analysis 43

RESULTS AND DISCUSSION 44

1. Preliminary remarks 45
1.1 AgNPs concentrations 45
1.2 Food matrix concentrations 45
2. Impact of the food matrix and digestive enzymes on intestinal cells 46
2.1 Impact of dilution on the cytotoxicity of the digested HBSS control 46
2.2 Impact of dilution on the cytotoxicity of the undigested food matrix 47
2.3 Impact of dilution on the cytotoxicity of the digested food matrix 48
2.4 Discussion 49
3. Impact of the digestive enzymes and food components on AgNPs toxicity on intestinal cells . 51
3.1 Interference 52

3.2 Cytotoxicity assays 53
3.3 Results analysis 55
3.4 Discussion 56
3.4.1 Effect of the food matrix 56
3.4.2 Effect of digestive enzymes 58
3.4.3 Joint effect of digestive enzymes and food matrix 61
4. Characterization of AgNPs included in a food matrix during in vitro digestion 62
4.1 Macroscopic observations 63
4.2 UV-visible spectroscopy 65
4.3 Results Analysis 66
4.4 Discussion 67
5. Quantification of the protein corona 71
5.1 Protein quantification results 72
5.2 Discussion 74

CONCLUSION & PERSPECTIVES 76

BIBLIOGRAPHY 80

Abstract

Known as “the material of the 21st century”, nanomaterials have revolutionized many industrial sectors during the last decades. Concerning the food industry, engineered nanomaterials (ENMs) have been added intentionally in commercial food products to enhance their quality, safety or shelf-life but also to provide specific flavors or colors. Silver nanoparticles (AgNPs) are currently the nanomaterial found in the highest number of consumer products thanks to their antibacterial properties: dietary supplements, plastic food containers, fridges, …

The inevitable use of these products leads to the unintentional exposure of consumer’s digestive system to AgNPs. Indeed, the risk of AgNPs ingestion due to their migration from the products is recognized and reported in many studies, such as their deleterious effects *in vitro* and *in vivo*. Such considerations raise the need of toxicological studies about AgNPs, especially that account for the physico-chemical transformations of AgNPs occurring when they are incorporated into food and digested as they transit the gastro-intestinal tract (GIT). Although the GIT and food have been demonstrated to alter AgNPs cell’s interactions, only few studies take in account these effects.

In this master thesis however, we investigated the impact of food components and digestion on the toxicity of AgNPs. Thanks to a modelized food matrix and an *in vitro* digestion process, these two effects could be reproduced and their impact on the cytotoxic effect of AgNPs assessed in a coculture model of the human intestinal epithelium consisting of Caco-2 and HT29-MTX cells.

The food matrix seemed to reduce AgNPs inherent toxicity while digestive enzymes worsened it. Together, digestive enzymes and food component induced such changes that the toxicity of AgNPs was also increased. Further characterization and protein quantification experiments gave us lines of explanations. Indeed, the presence of a protein corona is strongly indicated and can explain the protective effect of food components. Digested enzymes were suggested to alter AgNPs characteristics or have a potential higher activity consequently to their interaction with AgNPs. Our results indicate that toxicity of AgNPs can be strongly influenced by the presence of food components and digestive enzymes and reproducing both parameters is important to draw realistic and truthful interpretations.

Further experiments should focus on the characterization of the composition of the protein corona upon incubation of AgNPs with the food matrix but also throughout the whole digestion process to have an insight of the new biological identity acquired by AgNPs.

List of abbreviations

AcOH: Acetic Acid

Ag^+: Silver ions

AgNPs: Silver nanoparticles

ATP: Adenosine Triphosphate

BCA: *Bicinchoninic acid*

BSA: *Bovine Serum Albumin*

CTB: *CellTiter-Blue*

CTG: *CellTiter-Glo*

CV: Crystal Violet

DLS: Dynamic Light Scattering

DMEM: *Dulbecco's modified Eagle's minimal essential medium*

ENMs: Engineerd nanomaterials

FBS: *Foetal Bovine Serum*

GIT: Gastro-intestinal tract

HBSS: *Hank's Balanced Salt Solution*

JRC: Joint Research Center

NEAA: Nonessential Amino Acids

NMs: Nanomaterials

NPs: Nanoparticles

PBS: *Phosphate Buffer Solution*

PEST: Penicillin and Streptomycin

PFA: paraformaldehyde

ROS: Reactive oxygen species

RT: Room temperature

TEM: Transmission electron microscopy

List of figures

Figure 1. Major functions of the digestive system

Figure 2. Layers of the gastrointestinal tract

Figure 3. Structural adaptations of the small intestine

Figure 4. Main stages of *in vivo* digestion

Figure 5. Structure of intestinal epithelium at the cellular level (Meng *et al.*, 2015)

Figure 6. Schematic diagrams of nanoparticle, nanofiber and nanoplate (Calderón-Jiménez *et al.*, 2017)

Figure 7. Nano-engineered products reported in the Nanodatabase through years

Figure 8. Representation of the protein corona formation on a nanoparticle (Fleischer & Payne, 2014)

Figure 9. Pie chart of the type of nanomaterial used in products listed so far 2018 in the Nanodatabase

Figure 10. AgNPs interactions within the cell compartment (Völker *et al.*, 2013)

Figure 11. Human exposure routes to nanosilver (Wen *et al.*, 2016)

Figure 12. Extinction spectra of AgNPs with increasing diameter and extinction spectra of 50 nm AgNPs undergoing aggregation (Sigma Aldrich, 2011)

Figure 13. Dimensions of a Bürker counting chamber and one square of the grid

Figure 14. Schematic diagram of the *in vitro* digestion protocol

Figure 15. The Biochemistry of the CellTiter-Glo® assay (Promega, 2018)

Figure 16. The Biochemistry of CellTiter-Blue® assay (Promega, 2018)

Figure 17. The principle of BCA assay

Figure 18. CellTiter-Glo, CellTiter-Blue and crystal violet assays results after incubation of digested HBSS on the Caco-2/HT29-MTX cell model

Figure 19. Results of CTG, CTB and CV after the incubation of the undigested food matrix on the Caco-2/HT29-MTX cell model

Figure 20. Results of CTG, CTB and CV after the incubation of the digested food matrix on the Caco-2/HT29-MTX cell model

Figure 21. Results of CTG, CTB and CV after exposition on the Caco-2/HT29-MTX of undigested and digested AgNPs without food matrix and with food matrix

Figure 22. Samples of undigested AgNPs in HBSS and included in a food matrix

Figure 23. Samples collected after the salivary stage: AgNPs in HBSS and in the presence of food matrix

Figure 24. Samples collected after the gastric stage: AgNPs in HBSS and included in the food matrix

Figure 25. Samples collected after the intestinal stage: AgNPs in HBSS (left) and in the food matrix

Figure 26. UV-visible absorbance spectra of AgNPs at different concentrations after each stage of *in vitro* digestion either diluted in HBSS or in the food matrix model

Figure 27. UV–vis spectra recorded as a function of interaction of BSA with Ag nanoparticles and UV-vis spectra of BSA coated AgNPs recorded as a function of pH (Ravindran *et al.*, 2010)

Figure 28. Results of the protein quantification with microBCA assay.

Figure 29. Interference between AgNPs at different concentrations included in HBSS or in a food matrix, digested or not, and CellTiter-Blue ® assay or crystal violet assay

Figure 30. Direct and indirect interference between CellTiter-Glo® reagent and digested or undigested AgNPs solution at different concentrations included in HBSS or in a food matrix

List of tables

Table 1. Macronutrients and energy reference intakes

Table 2. Amount of digestive fluids produced daily

Table 3. Estimates parameters from Loglogistic model for each cytotoxicity assay: CellTiter-Glo (CTG), CellTiter-Blue (CTB) crystal violet (CV)

Table 4. Values of SPR peaks (maximum wavelength λ_{max} and maximum intensity I_{max}) of the absorbance spectrum obtained after each digestive step of the *in vitro* digestion in the presence or absence of the food matrix for different AgNPs concentrations.

Table 5. Protein concentration values at the different AgNPs concentration tested with microBCA assay.

INTRODUCTION

1. Principles of digestion

1.1 Human digestive system

1.1.1 General overview

The gastrointestinal (GI) system, also called alimentary canal, is the most complex set of organs in the body, outside of the brain. It is responsible for the ingestion and digestion of dietary substances, the absorption of nutrients, and waste products elimination (Bornstein, 2009). The main function is to process food and transfer nutrients, water, and electrolytes into the body's internal environment. Ingested food is essential as an energy source from which the cells can generate ATP (adenosine triphosphate) to carry their energy-dependent activities such as active transport, contraction, secretion, and synthesis. Food is also a source of building blocks for the renewal and addition of muscles, bones and cellular tissues (Sherwood, 2012). Proteins, fats, carbohydrates are broken down into small units that can be absorbed, principally in the small intestine. The products of digestion and the vitamins, minerals, and water cross the intestine mucosa and enter the lymph or the blood while excess and unabsorbed nutrients are eliminated through feces (Ganong, 2003). Across the lifetime, our diet shapes also the intestinal bacterial population, the gut microbiota, which plays a crucial role in maintaining host's immunity, metabolism and protection against pathogens (Thursby and Juge, 2017).

The digestive system fulfills four major functions without taking in account ingestion and elimination (Figure 1) (Sherwood, 2012):

- The **motility** refers to the muscular contractions of the digestive tract that enable the alimentary bolus to progress through the tract. There are propulsive movements that push the content forward and mixing movements that favor digestion by blending and increasing surface contact of the food with the enzymes. The rate of transit depends on the tract's part: rapid along the esophagus and slow in the small intestine, the main absorptive site. Acts of chewing, swallowing and defecation are considered as voluntary movements since they are under the control of skeletal muscles. However, motility achieved by smooth muscle throughout the rest of the tract is controlled by involuntary mechanisms (Sherwood, 2012; Wilson, 2007)

- The **secretion** of digestive juices in the lumen by exocrine glands along the progress of the food. Each digestive secretion consists of water, electrolytes, and specific organic constituents responsible for the digestive process, such as enzymes, bile salts, or mucus. Secreting enzymes requires energy for active transport of raw materials into the cells and synthesis by the endoplasmic reticulum (Sherwood, 2012).

- The term **digestion** refers to the biochemical breakdown by the digestive secretions of the structurally complex foodstuffs of the diet into smaller, absorbable units. Practically, we define also a mechanical digestion, meaning the physical breakdown of foodstuffs occurring from the mouth (by chewing) to the small intestine (peristalsis) (Sherwood, 2012).

- The **absorption** of small absorbable units such as nutrients, water, vitamins, and electrolytes. The enterocytes, special small intestine cells, exhibit both active and passive membrane transporters in order to carry out nutrients absorption. The large intestine is for its part responsible for water and electrolytes absorption (Sherwood, 2012).

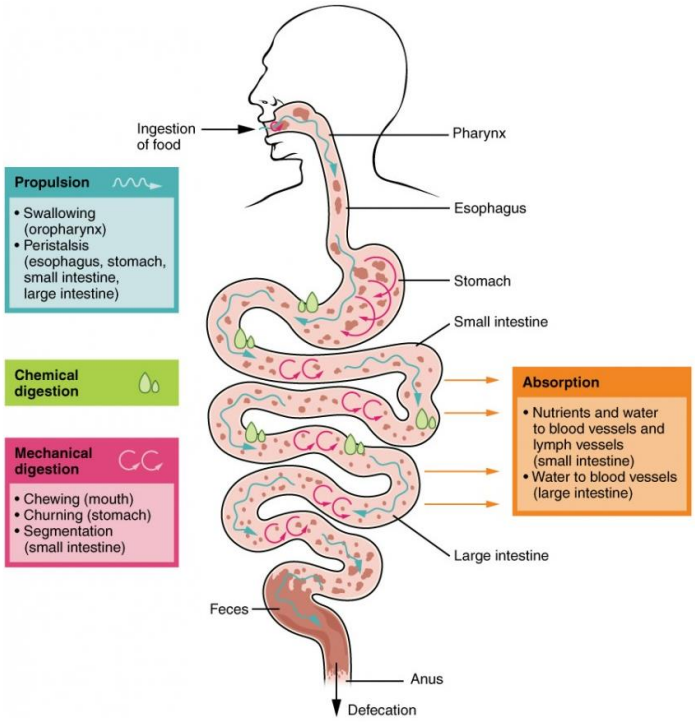

Figure 1. Major functions of the digestive system.

Source : http://digikalla.info/process-of-digestion/process-of-digestion-the-function-of-the-digestive-system-in-the-human-body-science-download/

1.1.2 Histology

The digestive tract has the same histological structure throughout most of its length, with some local structural variations depending on the segment 's function. A cross section of the digestive tube presents four major concentric tissue layers (Figure 2). From the innermost layer outward, we find the mucosa, the submucosa, the muscularis externa, and the serosa, each of them having a specific purpose for digestion (Sherwood, 2012; Histology@Yale,2018):

- The **mucosa**, lining the luminal surface of the digestive tract, is in direct contact with food components. It consists of a thin epithelial/mucous layer supported by a layer of connective tissue called the *lamina propria*, itself supported by a layer of smooth muscle cells, the *muscularis mucosa* that provides support and ability to move and fold. (Sherwood, 2012; Guénard,2009)

- The **submucosa**, a thick layer of connective tissue provides the digestive tract with its expandability and elasticity. It contains the larger blood and lymph vessels; both innerve inward to the mucosal layer and outward to the surrounding thick muscle layer. In addition, a nerve network known as Meissner's plexus lies within the submucosa and controls mucosal glands and the *muscularis mucosa* (Sherwood, 2012; Histology@Yale, 2018).

- The ***muscularis externa*** surrounds the submucosa. This third layer is the major smooth muscle coat of the digestive tube. In most part of the GI tract, the *muscularis externa* consists of two layers: an inner circular layer and an outer longitudinal layer. Those two layers move perpendicularly one to another, producing propulsive and mixing movements that form the base of peristalsis. The fibers of the inner smooth muscle layer run circumferentially around the tube, while those of the outer layer are oriented lengthwise (Guénard, 2009; Histology@Yale, 2018).

- The **serosa,** the outermost layer, covers the digestive tract and fixes it to the organism. Also called *adventitia*, the serosa is a connective tissue that secretes a watery fluid that lubricates and prevents friction between the digestive organs and the surrounding viscera (Sherwood 2012).

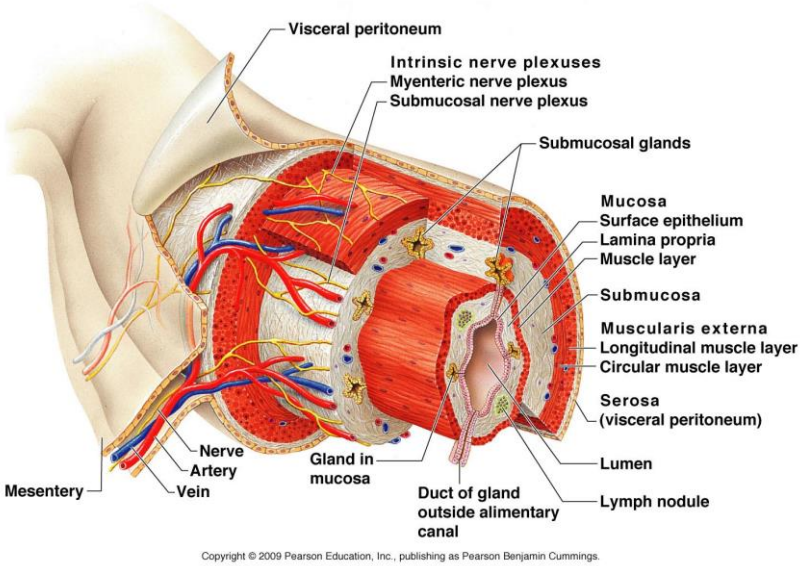

Figure 2. Layers of the gastrointestinal tract.

Source : https://inneorgans.com/layers-of-the-gastrointestinal-tract/

1.1.3 Stages of *in vivo* digestion

The digestive system is a set of organs working together to transform food into basic digestible nutrients and energy, essentials for life. The gastrointestinal system consists of the gastrointestinal tract (GIT) and the accessory gastrointestinal glands (Yoder *et al.*, 2010).

The digestive tract is essentially a tube of 4.5 m in length in its normal state. Running through the middle of the body, the GIT is divided into several segments: the mouth, pharynx, esophagus, stomach, small intestine and large intestine. Although these organs are continuous with one another, they are considered as separate parts because of their regional modifications, which allow them to specialize in distinct digestive activities (Yoder *et al.*, 2010; Guénard, 2009).

Lying outside the digestive tract, the accessory digestive organs include the salivary glands, exocrine pancreas, and the biliary system, which is composed of the liver and gallbladder. They discharge secretions participating to biochemical digestion into the digestive lumen. Since the lumen is continuous with the external environment, the luminal content is technically outside the body. This is essential to the digestion because some luminal conditions are intolerable in human cells e.g. the pH 2.0 in the stomach is incompatible with the pH life range of 6.8 to 8.0 (Sherwood, 2012).

A. Oral cavity

The mouth or oral cavity is the portal through which enters the food. The opening is formed by the muscular lips, which help attain, guide and contain the food into the mouth. The palate forming the roof of the oral cavity, separates the mouth from the nasal paths. The tongue composed of voluntary skeletal

muscles helps guiding food within the mouth during chewing and swallowing. Furthermore, the major taste buds are located on the tongue (Sherwood, 2012).

The first step in the digestive process is mastication involving the slicing, grinding and mixing of the food by the teeth. Chewing breaks down large food particles into smaller pieces, which facilitates swallowing and increases food surface area in contact with saliva. Once food is in the mouth, a reflex secretion of saliva is triggered (Ganong, 2003).

Saliva is the first digestive secretion in contact with the foodstuffs. Secreted by three pairs of salivary glands, about 1 L are produced in a day (Hollebeeck *et al.*, 2013). The pH of saliva rises from 7.0 to 8.0 during active secretion (Ganong, 2003). While 99.5% of saliva is water, the rest 0.5 % is made of electrolytes and proteins. The most important salivary proteins are mucus, lysozyme, but also α-amylase and lingual lipase that are the two salivary digestive enzymes (Guénard, 2009).

The saliva achieves different functions such as:

- The beginning of the digestion of carbohydrates through the action of salivary α-amylase, that breaks down at neutral pH, α1-4 glucosidic bonds of starch (Sherwood, 2012).
- The beginning of the digestion of triglycerides by lingual lipase; it hydrolyzes medium and long-chain triglycerides into free fatty acids and diglycerides without the action of bile salts. (Guénard, 2009).
- The humidification of the food and the mucosa thanks to water and mucus (mucins).
- Promoting mouth hygiene; the flow helps indeed flushing away food residues and old cells. Moreover, saliva is rich in bicarbonate buffers, which maintain the oral pH at 7.0 and neutralize food and bacteria acids, thereby preventing dental caries. Saliva is also known to have antibacterial actions thanks to lysozyme, a glycopeptide that kills Gram+ bacteria (Nash *et al.*, 2006; Ganong, 2003).

Even if the hydrolysis of polysaccharides into disaccharides by α-amylase begins in the mouth, most of its digestion by α-amylase occurs in the stomach once the food mass and saliva have been swallowed. Acid gastric conditions inactivates α-amylase, but in the center of the food mass, where acid has not yet reached, α-amylase continues to act for several more hours (Sherwood, 2012).

B. Pharynx and esophagus

The pharynx is the cavity at the rear of the throat. It is common passageway for both the digestive system (it links the mouth and the esophagus, for food) and the respiratory system (it provides access between the nasal passage and the trachea, for air) (Sherwood, 2012).

The esophagus is a straight muscular tube that extends from the pharynx to the stomach; each extremity guarded by sphincters. The first one, the pharyngoesophageal sphincter keeps the entry of the esophagus closed to prevent air from entering during breathing. The other, the gastroesophageal sphincter stays contracted to keep barrier between the stomach and the esophagus, reducing the chance of acid gastric reflux into the esophagus. The esophagus secretes also a mucus, which facilitates the transit of the food and protects its walls against acidic reflux (Mittal, 2011).

The motility process taking place in the pharynx and esophagus is swallowing. Swallowing is the most complex reflex in the body; initiated voluntary when the tongue pushes the food into the pharynx, it

cannot be stopped once engaged. The pressure of the bolus stimulates pharyngeal pressure receptors, which send impulses to the swallowing center: a peristaltic wave is created that take the food from the pharynx to the stomach in 5 to 9 seconds. The esophagus has no digestive function, it is only a passageway for the bolus (Ganong, 2003).

C. Stomach

The stomach is the J-shaped segment of the GIT located between the esophagus and the duodenum. Three regions can be distinguished based on structural and functional distinctions (Sherwood, 2012; Histology@Yale, 2018):

- The fundus is the part that lies above the esophageal opening. Its glands are lined mostly by mucous secreting-cells.
- The middle or main part of the stomach is the body. Its glands contain chief and parietal cells and a smaller population of mucous secreting cells.
- The antrum is the third distal part of the stomach.

The smooth muscle layers in the fundus (proximal part of the stomach) and body are thin, but at the lower part of the stomach (antrum), musculature is thicker in order to provide strong mixing movements (Sherwood, 2012).

In the stomach, food is mixed with gastric secretions and reduced into a thick liquid mixture called chyme (Histology@Yale, 2018). Stomach's most important function is to store food and release it into the duodenum at an appropriate rate for digestion and absorption by the small intestine (Sherwood, 2012). Stomach has also a secretory function: about 2 to 2.5 L of gastric juice is secreted each day. Three types of gastric exocrine cells are found in the walls of the pits forming gastric glands. Collectively, they produce the three secretions found in the digestive gastric juice (Ganong, 2003):

- Mucous cells, secreting a thin, watery mucus along with HCO_3-.
- The deeper parts of the gastric pits are lined by chief cells that secrete gastric lipase and pepsinogen, the inactive precursor of pepsin.
- The parietal cells secrete HCl that kills most of ingested bacteria, activates pepsinogen into an active pepsin, and denatures proteins that expose more bonds for enzymatic breakdown. HCl secretion decreases the luminal content pH as low as 2.0 (Ganong, 2003).

Pepsinogen, once activated into pepsin by HCl, begins protein digestion. Pepsin cleaves some of the amino acids linkages: between phenylalanine or tyrosine and a second amino acid. Products of peptic digestion are polypeptides of diverse sizes. Pepsin must be stored and secreted in an inactive form so that it does not digest proteins of the cells in which it was synthesized (Sherwood, 2012).

Concerning lipids digestion, the stomach continues to breakdown fats by secreting a gastric lipase that cleaves preferentially the fatty acyl ester bond at position 3. Besides, lingual lipase is still efficient in the proximal part of the stomach and both with gastric lipase, they can digest about 30 % of dietary triglycerides. However, their importance is little compared to pancreatic lipase the main lipid digestive enzyme (Ganong, 2003; Feher, 2017).

In the body of the stomach, food remains semisolid since peristaltic contractions are too weak to mix food with gastric juice. Hence a very little digestion inside of the bolus. Gastric digestion therefore only happens in the antrum where food is mixed strongly with HCl and pepsin. No food or water is absorbed through the stomach mucosa (Ganong, 2003). Some acidic drugs (e.g. aspirin) and ethanol can however pass through it (Hogben *et al.*, 1957; Vivo Pathophysiology, 2018).

D. Pancreatic and biliary secretions

Pancreas is a mixed gland containing both exocrine and endocrine tissues. Acinis that are grapelike clusters of secretory cells, secrete pancreatic enzymes while the endocrine tissue, composed of the islets of Langerhans, produces insulin and glucagon (Sherwood, 2012).

The pancreatic juice consists of pancreatic enzymes secreted by the acinar cells and an aqueous alkaline solution rich in $NaHCO_3$ conferring a pH 8.0 that neutralizes chyme's acidity and creates optimal conditions for the pancreatic enzymes. The volume of pancreatic secretion ranges between 1 and 2 liters per day. Pancreatic enzymes are essential since they can almost completely digest food in the absence of all other digestive secretions. Proteolytic enzymes, α-amylase and pancreatic lipase are the main constituents of the pancreatic juice, but ribonucleases, co-lipases and phospholipases are also found (Guénard, 2009).

Polypeptides formed after gastric digestion are further degraded by the proteolytic enzymes, the main being trypsin, chymotrypsin and carboxypeptidases A and B, each secreted in a primary inactive form (trypsinogen, chemotrypsinogen and procarboxypeptidases). Trypsinogen remains inactive until it reaches the duodenal lumen, where an enterokinase converts it into active trypsin. Trypsin then catalyzes the conversion of chemotrypsinogen and procarboxypeptidase into their active form. Each of these proteolytic enzymes cleaves different peptide linkages, leading to end products made of small peptides and a small fraction of free amino acids (Ganong, 2003; Sherwood, 2012).

Pancreatic α-amylase continues to break down polysaccharides into di- or tri-saccharides such as maltose, isomaltose and maltotriose (Sherwood, 2012).

Pancreatic lipase is the most important enzyme digesting lipids throughout the entire digestive system; lingual and gastric lipases having only a minor action. This enzyme hydrolyzes the 1- and 3- bonds of triglycerides easily but the 2-bond at a very low rate. So, final products are mainly free fatty acids and 2-monoglycerides. Its action is largely facilitated on emulsified fats. Cholesterol esterase, phospholipases and bile salt-activated lipase are also secreted and digest cholesterol, phospholipids and esters of cholesterol as well as fat-soluble vitamins respectively (Ganong, 2003; Ribet *et al.*, 2018).

Besides the pancreatic juice, the other secretion emptied in the duodenum is bile. Bile contains several organic constituents such bile salts, cholesterol, lecithin, and bilirubin in an aqueous alkaline fluid. Even though bile does not contain any digestive enzymes, it has a substantial role for the digestion and absorption of fats enabled above all through the activity of bile salts. Bile salts have a detergent action: fats are transformed into small lipidic droplets called micelles, which increases their surface and thus facilitates their digestion and absorption. After lipid digestion, micelles contain fatty acids, monoglycerides, and cholesterol in their hydrophobic center (Ganong 2003; Sherwood, 2012).

E. Small intestine

To meet its absorptive function, the small intestine has developed many strategies to amplify its surface (Figure 3). The following structures increase the total intestinal surface by 600-fold (Ganong, 2003):

- The intestinal barrier projects big circular folds of the mucosal epithelium, lamina propria, *muscularis mucosa* and submucosa called *plicae circularis*.
- At a second level, only the epithelium and lamina propria form the *villis*, 0.5- 1 mm long finger-like folds into the lumen. These have a central lymphatic vessel, the lacteal, crucial for lipids absorption. Depressions between villis, known as Lieberkühn crypts are compared to tubular intestinal glands; they contain various cell types important for digestion.
- Finally, enterocytes exhibit *microvillis* on their apical face, commonly called the brush border. *Microvillis* are covered with the glycocalyx, an amorphous layer rich in neutral and amino sugars. (Ganong, 2003; Histology@Yale, 2018)

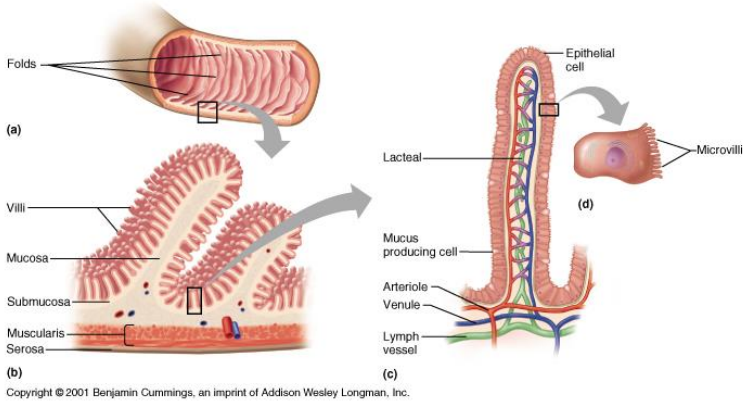

Figure 3. Structural adaptation of the small intestine (a) *plicae circularis* (b) *villis* (c) *microvillis.*

Source : https://socratic.org/questions/why-does-the-wall-of-the-small-intestine-need-a-large-surface-area

Beginning after the gastro-duodenal junction and ending at the ileo-cecal junction, the small intestine is divided into three sections (Guénard, 2009; Ganong, 2003):

- The duodenum (30 cm long) where most of the digestive processes occur through the combined action of pancreatic enzymes, duodenal enzymes and bile.
- The jejunum displaying the most prominent *plicae circularis* and highly implicated in non-selective absorption processes of amino acids, lipids and monosaccharides.
- The ileum that selectively absorbs vitamin B12 and biliary salts.

The small intestine is in contact with 9L of fluids per day (2L from dietary sources and 7 L of gastrointestinal secretions) whereas 1 to 2L reach the colon (Guénard, 2009).

End products of pancreatic α-amylase (maltose, maltotriose and isomaltose) such as sucrose and lactose are finally digested at the brush border of the intestine cell that secretes maltases and isomaltases as

well as lactases and sucrases. Final products of carbohydrates digestion are monosaccharides of glucose, fructose and galactose (Faure, 2012). Glucose is rapidly absorbed by intestine cells though SGLT1 co-transporters depending on Na^+ gradient and reach capillaries trough GLUT2 by facilitated diffusion at the basal side of the enterocytes. SGLT1 and GLUT2 are not glucose-specific, galactose takes the same passageway. Fructose has a specific facilitated diffusion transporter (GLUT5) at the apical side. Other pentoses are absorbed by simple diffusion (Guénard, 2009; Ganong, 2003).

Final digestion of peptides occurs in three sites: intestinal lumen, brush border and cytoplasm of the mucosal cells. Di- and tri-peptides reaching the intestinal lumen are either transported actively and specifically in the enterocytes (with a cotransporter H^+-peptide) where they will be broken down into amino acids (AA) by intracellular peptidases, or degraded into AA by peptidases (carboxypeptidases, endopeptidases, and dipeptidases) of the brush border. AA are transported at slower rate than di-and tripeptides. There are at least seven different transport systems of amino acids identified in enterocytes. Five of these require Na^+ cotransport, similar to Na^+ glucose transport; two others require Cl^- cotransport (Guénard, 2009; Ganong, 2003).

Final products of lipid digestion (fatty acids, monoglycerides, cholesterol and lysophospholipids) enter the enterocytes by passive diffusion and are transported to the endoplasmic reticulum. In the endoplasmic reticulum, lipidic molecules are transformed into triglycerides, cholesterol esters and phospholipids that will be gathered into lipoproteins: chylomicrons (95 % triglycerides, 2% proteins) or VLDL (very low-density lipoprotein) (60 % triglycerides, 15 % cholesterol, 10 % apoproteins). Both are excreted by exocytosis. While VLDL reach portal blood, chylomicrons join the lymphatic system because of their important size (Guénard, 2009).

Concerning the transport of toxic molecules, AgNPs especially, their uptake by enterocytes will be explained extensively in the section 4.4. of this introduction.

F. Large intestine

Last part of the GIT, the colon or large intestine extends from ileo-cecal junction to the anus. Its purpose is to absorb water and electrolytes from undigested foodstuffs and eliminate them through feces. The large intestine is segmented into two parts (Sherwood, 2012):

- Proximal colon composed by the caecum and right transverse colon. Its main function is water and electrolytes absorption.
- Distal colon formed by the left transverse colon, left colon, sigmoid colon and rectum; storage and elimination of food wastes are the main processes taking place.

Colon epithelium differs from intestinal one by its lack of *villi* and absorptive cells, and by a disproportionally large number of goblet cells especially in the rectum part since feces pass out of it (Guénard, 2009; Histology@Yale,2018).

The large intestine has major role in managing the volume and ionic composition of stools. At a basal state, the colon absorbs Na^+ and Cl^- and secretes K^+ and HCO_3^- through both active and passive transporters, which leads to water retention and therefore to the concentration of the stools. Water flow goes from 1L/day at the ileo-cecal junction to 0.1L/day at the anus. 90 % of the daily 7L water secreted by the gastrointestinal tube are reabsorbed (Guénard, 2009).

The colon is also known for hosting more than 99% of the total bacteria in the body. Estimated at 10^3 - 10^6 germs/ml, the colonic microflora displays more than 400 different species, most of it being anaerobic (Guénard,2009). Bacteria are very important for the metabolic activity of the colon. They are engaged in many critical processes: recycling of the endogenous proteins released by cellular desquamations, breakdown of 40 % of the urea produced by the liver into NH_3 and fermentation of nondigested carbohydrates, which produces intestinal gazes (CO_2, H_2, CH_4) and short-chain fatty acids (acetic acid (C2), propionic acid (C3), butyric acid (C4)) used as energy source for the colon epithelium (Guénard,2009; Rambaud *et al.*., 2004).

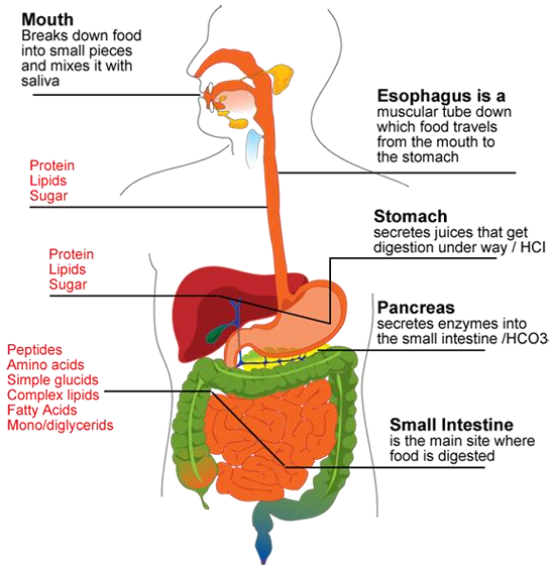

Figure 4. Main stages of *in vivo* digestion.

Source : http://www.cynergymed.com/en/clinical-studies

1.2 *In vitro* digestion

Taking into account the bioaccessibility (*i.e.* the fraction of an ingested substance that reaches the systemic circulation) of ingested foodstuff such as xenobiotics or unwanted nanoparticles, is crucial when their physiological effects at the intestinal barrier are assessed in *in vitro* studies (Hollebeeck *et al.*, 2013). To this end, many *in vitro* digestion models were developed in the literature converging in an international consensus about a standardized *in vitro* digestion method established in 2014 by Minekus *et al*.

Although the complexity of human digestion will never be perfectly represented by an *in vitro* model of the digestive tract, this approach has the advantages of being faster, cheaper, less labour intensive, and ethically more accepted than *in vivo* techniques (Minekus *et al.*, 2014).

A standardized, rapid and low-cost *in vitro* digestion has been developed in our laboratory in 2013 by Hollebeeck *et al.* They created a three-step protocol reproducing each stages of the pre-colonic digestion: salivary, gastric and duodenal step. pH, incubation time and enzyme concentration were adapted according to the digestive step in order to reproduce human digestion effectively. Digestive enzymes were α-amylase, pepsin and a mix of bile and pancreatic enzymes for the 3 stages respectively.

The *in vitro* digestion protocol used for this thesis is based on Hollebeeck's method and is completely described in the section 3.1 and 3.2. Food components were added to the *in vitro* digestion to complete simulation of a realistic human digestion.

1.3 The intestinal barrier

The intestinal epithelium is one of the largest mucosal surfaces of the body in contact with the external environment: the total surface area in the adult human being between 250-400 m^2 (Thursby and Juge, 2017). It acts as a gatekeeper by controlling the entry of nutrients or xenobiotics and preventing harmful luminal molecules from reaching the blood circulation (Le Ferrec *et al.*, 2011, Nollevaux *et al.*, 2006).

1.3.1 Description at the cellular level

The intestinal mucosa is composed of the epithelium, the *lamina propria* and the *muscularis mucosa* (Márquez *et al.*, 2016). From the duodenum to the rectum, the intestinal lining consists of a single cell layer renewing itself every 36-72 hours and comprised of six different type of cells (Figure 5) (Ganong, 2003):

- Enterocytes, the tall columnar cell the most present in the intestinal lining and performing most of the intestinal digestive and absorptive functions. Renewing every 5-6 days, they have specific features as a brush border made up of microvillis coated with glycocalyx on their apical border, tight junctions that link enterocytes between them and separates the lumen from intercellular spaces and many transporters and enzymes on their apical face that perform the last step of protein and sugars digestion (Guénard, 2009; Ganong, 2003).

- Goblet cells found in the Lieberkühn crypts and secreting the mucus, which lubricates the tract and embodies microorganisms. This mucus coat contains glycoproteins (mucins) capable of interacting with bacteria and toxins (Guénard, 2009).

- Paneth cells, located at the base of the crypts and serving an immune function by secreting antimicrobial peptides such as α-defensins and cathelicidins, growth factor, lysozymes, and phospholipase A2 (Garabedian *et al.*, 1997; Ouellette, 2006).

- Entero-endocrine cells, producing hormones (secretin and cholecystokinin) controlling motility and secretion. They have a luminal pole rich with microvilli and a basal pole containing secretory granula (Ganong, 2003).

- M, "microfold", cells located at the epithelium of Peyer's patches, lymphoid follicles found in human's lowest part of the small intestine (jejunum and ileum). M cells have a crucial role in the transport of antigen from the lumen to mucosal lymphoid tissues, where an immune response is initiated. They differ morphologically and enzymatically from enterocytes: poorly organized brush border, irregular microvilli and thin glycocalyx (Corr *et al.*, 2008).

- Stem cells, found at the depths of the crypts, they replenish the other cell types. According to their location, they will differentiate into various intestinal cell types. Migrating upwards the crypts, they will form enterocytes, goblets cells and endocrine cells while those who stayed at the base will become enterocytes or M cells (Corr *et al.*, 2008).

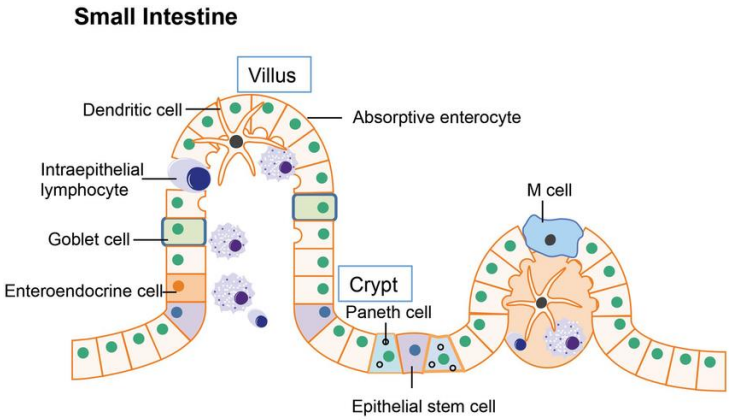

Figure 5. Structure of intestinal epithelium at the cellular level.

Source: Meng *et al.*, 2015.

1.3.2 *In vitro* models of the intestinal barrier

Since the intestinal barrier is the first site of absorption and the main fence preventing luminal molecules from reaching the blood system, many *in vitro* cell models have been developed to study the processes taking place across the intestinal epithelium (Pan *et al.*, 2015).

1.3.2.1 Co-culture of Caco-2 and HT29-MTX cells

To study the toxicity of silver nanoparticles on intestinal cells in laboratory conditions, a robust model of the intestinal barrier is necessary. For this master thesis, AgNPs cytotoxicity was assessed on a coculture of Caco-2 and HT29-MTX cells.

Caco-2 cell lines have been used frequently the last thirty years as an *in vitro* model for the intestinal epithelium (Sambuy *et al.*, 2005). Derived from human colon adenocarcinoma cells, they differentiate naturally and rapidly into a monolayer of cells highly similar to mature human enterocytes (Contado, 2015). They develop several key structures after differentiation: cylindrical polarized cells with brush border microvilli and glycocalyx on the apical side, tight junctions between cells and hydrolase enzymes activities (sucrase, isomaltase, lactase, aminopeptidase, peptidases …) (Sinnecker *et al.*, 2014; Sambuy *et al.*, 2005).

To improve Caco-2 cell model, co-culture of Caco-2 with other cell lines such as HT29-MTX cells that can differentiate into Goblet-like cells have been established (Pan *et al.*, 2015). The parental HT29 cells originally come from a human colorectal cancer. Their cellular differentiation is very similar to Caco-2's one; only the time is different: 30 days of culture are needed for HT29 cells against 21 days for Caco-2 cells (Martinez-Maqueda *et al.*, 2015). HT29-MTX are mucus secreting subclones, coming from the parental HT29 cell lines (Ferraretto *et al.*, 2018). They come from the isolation of HT29 cells adapted to methotrexate (MTX, 10^{-5} M), that secrete several mucins similar to Goblet's secretions as a result to the treatment (Nollevaux *et al.*, 2006).

Mimicking the two main cellular types found in the human intestinal epithelium, enterocytes and goblet cells, the coculture model of Caco-2/HT29-MTX cells with a 3:1 ratio, is very suitable for paracellular permeability studies (Nollevaux *et al.*, 2006).

2. Food Matrix

2.1 General considerations on nutrition and energy metabolism

Human body needs to oxidize foodstuffs such as carbohydrates, proteins and fats in order to produce CO_2, H_2O and recover the energy necessary for life processes. Around 60 T of food passes through the human GI tract in an average lifetime (Thursby and Juge, 2017). Food oxidation is a long and complex process, commonly called catabolism, which liberates energy used e.g. for physical activity, to maintain body functions, to digest and metabolize food and regulate body's temperature. Most energy liberated by catabolism is not directly used but is stored in energy-rich phosphate compounds like ATP. ATP contains high-energy phosphate bonds of 10-12 kcal/mol. Through its hydrolysis into adenosine diphosphate (ADP), ATP provides energy directly to processes as muscle contraction, active transport or synthesis of new chemical compounds (Ganong, 2003).

To achieve these energy-consuming tasks essential for life, the average adult must ingest between 2 000 and 2 500 kcal/day. Differences of caloric requirements depends on age, gender as well as the level of activity. An optimal diet includes, in addition to sufficient water, adequate calories, proteins, fats, minerals and vitamins. In the average middle-class European diet, approximately, 50 % of the calories come from carbohydrate, 11-15 % from proteins and 35 % from fats (Guénard, 2009). Supplying 9 kcal/g, fats are the most compact form of food. Carbohydrates and proteins however provide 4 kcal/g. In addition, a certain number of minerals and vitamins must be ingested daily for the maintenance of health like sodium and potassium, which are essential minerals (Ganong, 2003; USDA, 2015)

2.2 Ingested foodstuffs

2.2.1. Carbohydrates

The European average food intake provides 260 g of carbohydrates/day counting for 50 % of caloric daily needs (EU regulation N°1169/2011). 80 % of ingested carbohydrates are high glucose-polymers, essentially starch, the rest 20 % are disaccharides (saccharose, maltose, lactose) or monosaccharides like fructose or glucose (Guénard, 2009). Among dietary carbohydrates, fibers (pectins, lignins, hemicelluloses, celluloses, …) count also for a large part since they are the major feed for the intestinal microflora (Dhingra *et al.*, 2012).

Starch that is a polymer of amylose and amylopectin, and glycogen are the only polysaccharides digested to any degree in the GI tract. Glycogen is found in animals, whereas starch comes from plant. Glycogen is comprised of long glucose chains (α1-4 linkage) with some straight chains with only α 1-6 linkages. It is the storage form of glucose in human body: the major supplies are in the liver and skeletal muscles. Amylopectin, which constitutes 80-90% of dietary starch is similar but with less branches, whereas amylose is a straight chain with only α 1-4 linkages. (Sherwood, 2012; Guénard, 2009; Ganong, 2003).

The principal product of carbohydrate digestion is glucose. However, fructose and galactose occur also in significant amounts in the diet and are important for energy metabolism. About 10 % of the calories contained in the diet are supplied by fructose (~ 55g/day). The major source of fructose is sucrose, a disaccharide of fructose and glucose while most of galactose is found in lactose, disaccharide of galactose and glucose, obtained from milk and dairy products (Alzaharna, 2016).

2.2.2 Fats

About 70 g of lipids are provided daily in the average occidental feed. Lipids are essential since they provide essential fatty acids and liposoluble vitamins (A, D, E, K). 80 % of ingested lipids are triglycerides,

the rest are cholesterol and phospholipids (Guénard, 2009). Triglycerides are made up of three fatty acids bound to glycerol. Found in vegetable oils or animal fats, fatty acid chains vary in length and saturation but 16, 18 and 20 carbons chains are the most common. In human body, triglycerides become major components of VLDL and chylomicrons, which deliver fatty acids to the liver and fat cells, the adipocytes (PubChem, 2018). Generally, lipids in cells are of two types: structural lipids, inherent of the membrane, and neutral fats stored in adipose cells. While structural lipids are preserved, neutral fats can be mobilized during starvation. The fat depot is 15 % of male body weight and 21 % in women (Ganong, 2003).

2.2.3 Proteins

While carbohydrates and fats provide energy to cells, dietary proteins supply cells on nitrogen vital for growth and cellular turnover. 50 g of proteins must be ingested daily to meet caloric requirements (Guénard, 2009). Proteins are made up of chains comprised of 20 different amino acids linked by peptide bonds joining the amino group of one to the carboxyl group of the next one. Dietary protein digestion depends on their origin, the type of protein, the cooking mode and food shelf-life (Guénard, 2009).

2.3 *In vitro* model of the food matrix

To reproduce daily food intakes in this master thesis, three standard macronutrients were selected according to Hollebeeck's *in vitro* digestion method: starch, bovine serum albumin and triolein.

Bovine serum albumin (BSA) was chosen to represent the protein fraction. BSA is a globular protein yielded from bovine blood, which function is binding and transporting proteins in blood circulation. Thanks to its negative charge, BSA have an important binding capacity; it binds a wide range of molecules: water, salts, vitamins and hormones such as toxic substances. BSA counts approximately for 60 % of all proteins in animal serum. Besides, BSA is commonly used in cell culture protocols due to its stability to increase signal in assays and lack of interference within biochemical reactions. Another advantage is its low cost, since big amounts of it can be purified from bovine blood, a byproduct of the cattle industry (Biowest, 2013; Sigma-Aldrich, 2018; Rockland, 2018).

Carbohydrate part was represented by wheat starch. Starch in general, is the main energy source in human and animal food. Wheat starch in its unmodified form is considered as a by-product in the manufacture of wheat-gluten (International Starch Institute, 2018).

The third reagent, glyceryl trioleate or triolein stands for the lipid fraction. Triolein is a symmetrical triglyceride derived from glycerol and three units of oleic acid (C18:1, cis-9) (PubChem, 2018). Triolein represents 4-30 % of olive oil. Olive oil is indeed use in many *in vitro* food models such as in Lichtenstein *et al.*, 2015 or Kästner *et al.,*2017.

3. Nanomaterials

3.1 Definitions

The first time the word "nanotechnology" was used, dates back to 1974 when Prof. Norio Taniguchi used the word to describe semiconductor processes (Taniguchi, 1974). Since then, a lot of nanotechnology applications used engineered nanostructures for which the term "nanomaterial" (NM) was used indiscriminately. These materials, exhibiting different features compared to coarser materials

with the same chemical composition, have been introduced in a wide range of daily-life products even if a common acceptance on the term is still not established (Lövestam *et al.*, 2010).

Latterly, the European Union (EU) invested great efforts to define the term "nanomaterial". The European commission recommended the following definition in 2011 (Recommendation on the definition of a nanomaterial (2011/696/EU)):

"A nanomaterial is a natural, incidental or manufactured material containing particles, in an unbound state or as an aggregate or as an agglomerate and where, for 50 % or more of the particles in the number size distribution, one or more external dimensions is in the size range 1 nm - 100 nm."

The aggregate is defined as a particle composed of strongly bound particles while the agglomerate means the collection of weakly bound particles or aggregates (2011/696/EU). The purpose of the recommendation was to ensure conformity in the legislative area and a common acceptance of the meaning of the term "nanomaterial" by different sectors since no harmonized definition existed before (Calderón-Jiménez *et al.*, 2017).

In 2015, the International Organization for Standardization (ISO) proposed a very similar definition (ISO/TS 80004-1, 2015) and classified NMs into two main categories:

- Nanostructured materials are "*materials having internal structure or surface structure in the nanoscale*" (ISO/TS 80004-4, 2015).
- Nano-objects, described as "*discrete piece of material with one, two or three external dimensions in the nanoscale*" (ISO/TS 80004-2, 2015).

Nano-objects are classified into three categories depending on their size and shape characteristics: the nanoparticle (NP) that has all external dimensions at the nanoscale, the nanofiber exhibiting two external dimensions at the nanoscale while the third is larger and the nanoplate having only one external dimension at the nanoscale.

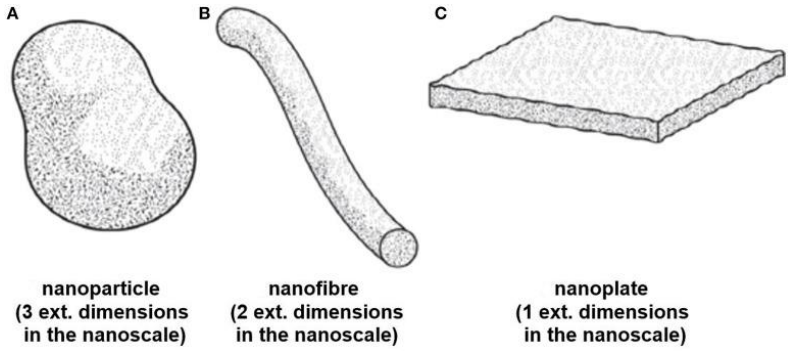

Figure 6. Schematic diagrams displaying shape designations for (A) nanoparticle (B) nanofiber (C) nanoplate.

Source : Calderón-Jimenez *et al.*, 2017

Besides ISO classification, NMs can be categorized as natural or anthropogenic:

- Natural NMs are provided by nature since ages. For example, volcanic ashes, sulfur and mineral particles in the air, sulfur and selenium nanoparticles produced by bacteria and yeasts are natural NMs (Griffin *et al.*, 2018).

- Anthropogenic NMs are either incidental or engineered (ENMs). Incidental NMs are the byproducts of human activities; their shape and size is poorly controlled and may be made of a mix of different elements. ENMs (inorganic non-metallic NMs, carbon-based NMs, metal NPs and organic polymeric particulate materials, …) are on the other side, specifically engineered and deliberately synthesized by human (Contado, 2015).

Despite various definitions proposed through years by federal agencies, more work needs to be done to standardize the vocabulary used in this field (Calderón-Jiménez, 2017). The term "nanoparticle" is indeed defined differently by ISO, ASTM (American Society for Testing and Materials) and IUPAC (International Union of Pure and Applied Chemistry) regarding the number of dimensions and shapes of NPs. This demonstrates that terms in the nanotechnology field are still evolving and highlights the importance of creating robust descriptors for these novel materials in order to develop relevant policies (Calderón-Jiménez, 2017).

3.2 Nanoparticles in the society

Since its introduction in the 70s, nanotechnology has impacted the world of science and engineering in a great extent, enabling the emergence of a plethora of new technologies and applications. Adding nanomaterials in every-day consumer products improved their features and quality by making them lighter, stronger, cleaner, less expensive, more efficient, more precise, or more aesthetic. Many fields are concerned about NMs incorporation in their products such as food, cosmetics, hygiene, medicine, electronic devices, household products, agronomy, aviation, textile, ceramics, polymers, construction or energy (Calderón-Jiménez *et al.*, 2017; Lövestam *et al.*, 2010).

To cite some products: sunscreens, coatings for easier cleaning glass, protective coatings for eyeglasses and cars glass, bumpers and catalytic converters on cars, stain-free clothing and mattresses, longer-lasting tennis balls and stronger tennis racquets, polymer films used in displays for laptops, phones and digital cameras, food packaging … (OSHA, 2018).

Most of products are sunscreen lotions or skin-care products (Lövestam *et al.*, 2010). The health care industry is indeed cited among many articles as being the one containing the greatest number of nano-engineered products (PEN, 2013; Vance *et al.*, 2015; The Nanodatabase, 2018). Since the incorporation of NPs in sunscreens (mostly TiO_2 and ZnO), the effectiveness and the stickiness improved because NPs can absorb and reflect UV-rays but are transparent at visible-rays range (Lövestam *et al.*, 2010; Alagarasi,2013).

The exponential growth in the development of NMs applications has and will have a major impact on the market and society. Estimated at 7.27 billion USD in 2017, the nanomarket is expected to grow by 17 % between 2017 – 2024 according to the 'Global Nanotechnology Market Outlook 2024' report and to reach 12.83 billion by 2021 (Research and Markets, 2018). This huge development reflects the continuous growth of consumer products incorporating NMs in their formulation. While 54 products were identified in 2005, more than 1800 NM-containing consumer products were produced in 2014 (Vance *et al.*, 2015). "The Nanodatabase" inventory created by the Danish Consumer Council and Ecological Council currently lists 3 037 products that are claimed to contain nanomaterials in 2018 (Figure 7) (The Nanodatabase, 2018).

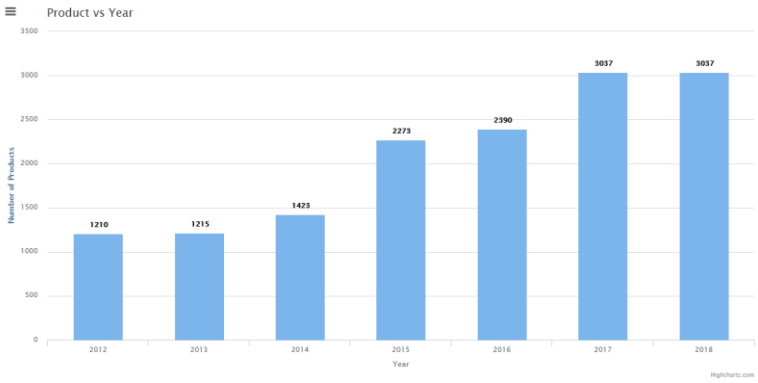

Figure 7. Nano-engineered products reported in the Nanodatabase through years.

Source : http://nanodb.dk/en/analysis/consumer-products/#chartHashsection

Some materials seen today as NMs have been industrialized a long time ago. Carbon black for example was used in industrial production over a century ago. Used in 1915 in production of car tyres, its annual production exceeds 10 million tons in 2010 (Lövestam *et al.* 2010). Other early NMs are silicon dioxide (SiO_2-NPs), titanium dioxide (TiO_2-NPs), and zinc oxide (ZnO-NPs). These are still, together with the recent AgNPs, the most used NMs in terms of commercial production amounts and represent the biggest volume introduced into consumer products. TiO_2-NPs, SiO_2-NPs and ZnO-NPs are produced in the greatest quantities worldwide (5500 t/year, 3000T/year, 550 T /year respectively) with AgNPs representing 2% of that TiO_2 (Piccinno *et al.*, 2012; Keller *et al.*, 2013).

While many NMs are introduced nowadays into the market, there is also a lack of knowledge about their toxicity on the environment and biology. Considering the high number of applications, the number of ENMS dispersed in the environment is potentially high. These considerations have led to many efforts around the world to study the impact of NMs on human and environmental health. But still, more research needs to be done (Lövestam *et al.*, 2010).

3.3 General characteristics of NPs

Nanomaterials exhibit unique chemical, physical and biological properties compared to materials with a coarser structure but with the same chemical composition (Contado, 2015). While some properties can be extrapolated from the macroscale, most of them change completely below a certain size (U.S. FDA, 2014).

For example, NPs have **a larger specific area** than their macro-equivalents. Specific surface area is inversely proportional to the diameter of spherical nanoparticles. For example, 10 g of spherical AgNPs have total surface area of almost 600 m^2 while a single solid silver sphere with the same mass exhibits a surface area of nearly 5 cm^2; giving an increase in total surface area of a factor of about 1,200,000. NPs are thus much more reactive than coarser structures since chemical and biochemical reactions take place at the surface. Decreasing the particle size increases the biological activity substantially. Concerning the toxicity, the size alone is not the unique responsible for its harmful effects; either it is the total number per unit volume that is important (Shin *et al.*, 2015).

Among their **physical properties**, we can highlight the strong capacity of some metal NPs to block UV (ZnO) hence their presence in sunscreens (Lövestam *et al.*, 2010). Metal NPs have also higher thermal conductivities than fluids or solid form: thermal conductivity of copper for example, at room

temperature, is 700 times greater than water and 3,000 times than engine oil. Thus, solutions containing suspended solid particles, called nanofluids, are expected to display improved thermal conductivities compared to conventional heat transfer fluids (Khan *et al.*, 2017). Another interesting property of NPs is their color that varies with size and shape, which is very useful in bioimaging applications (Khan *et al.*, 2017).

Their ability to form **stable suspensions** in aqueous media (water or organic solvents) is an important physical feature. Nanoparticles do not dissolve in water in the truest sense of the word, they remain insoluble at the nanometric scale. They form "suspensions" or "colloidal dispersion" in opposition to the "solution" obtained with soluble molecules (Labille & Brant, 2010). The stability of a suspension is due to an equilibrium between attractive and repulsive forces between suspended particles; aggregation and sedimentation due to the tendency of colloids to reduce surface energy results in an unstable colloidal dispersion (Khatab, 2016).

3.4 Interaction between biological fluids and nanoparticles

Among their abundant properties, nanoscale objects have the ability to interact with all biological components often differently than larger molecules (Lesniak *et al.*, 2012).

Once in contact with biological fluids, because of their high surface free energy, nanoparticles adsorb on their surface biomolecules such as proteins and lipids, leading to a complex biomolecular interface, commonly called the "corona" (Kokkinopoulou *et al.*, 2017). This corona is defined as a *"a durable, stabilizing coating of the bare surface of nanoparticle monomers that may present different subpopulations of particle assemblies, each presenting a durable protein coating*." (Monopoli *et al.*, 2011). Long described as uniformly distributed or well-rounded, the protein corona was recently analyzed by TEM (Transmission Electron Microscopy) by Kokkinopoulou *et al.*, (2017) and the morphology appeared to have a non-uniform structure and to be more as a *"network-like, loosely interconnected agglomeration of proteins surrounding a nanoparticle. "*

The adsorption of proteins (figure 8) is a kinetic (k) and thermodynamic (K) function of the proteins and NP's surface modification, composition and size (Fleischer and Payne, 2014). In a typical biological medium, biomolecules compete for the limited surface according to their affinity toward the NP's surface, leading the corona to be divided into the 'hard' and 'soft' corona (Giri *et al.*, 2016):

- The "hard" corona contains a few high affinity proteins that bind tightly to NPs, resulting in a relatively immobile layer. "Hard" is used in reference to the "long" exchange time of proteins that build it.
- The "soft" corona is formed by loosely bound proteins with high exchange rate. Low affinity proteins exhibit a dynamic absorption; they can freely exchange over time since they have a short exchange time (Kokkinopoulou *et al.*, 2017).

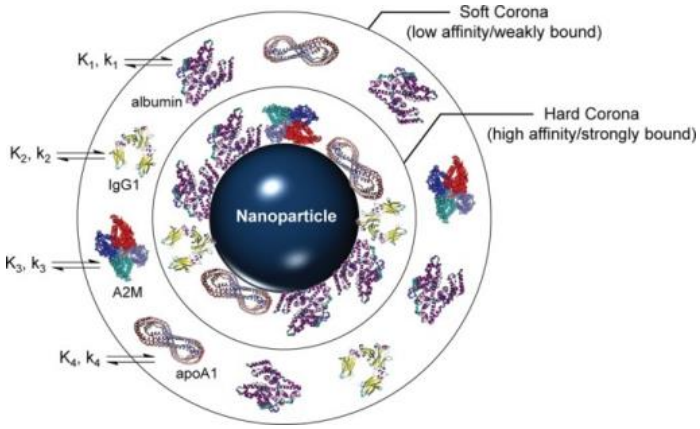

Figure 8. Schematic representation of the protein corona formation on a nanoparticle.

Source: Fleischer & Payne, 2014.

Composition of the corona depends on the composition of the surrounding media. In the gastrointestinal tract for example, the protein corona is made up of bile salts and digestive enzymes (Fröhlich & Fröhlich, 2016). Even if this complex coating is often called the "protein corona", other molecules than proteins constitute the corona, including a range of different lipids (Monopoli *et al.*, 2011).

The discovery of a protein complex formation around NPs has led to the distinction between the synthetic and biological identity of NPs. The biological identity of NPs acquired by molecules adsorbed on their surface becomes the interface that will be in contact with the cellular environment. The hard corona has indeed a life time sufficiently long (many hours), that the biological identity of the entire corona can be defined by the hard corona (Monopoli *et al.*, 2011). The corona disrupts NPs properties by simply reducing the surface free energy of the nanomaterial (Lesniak *et al.*, 2012). This special coating alters NP interactions in the long term, modifies physiological response such as cellular uptake, clearance, biodistribution and toxicity of the NPs (Giri *et al.*, 2016).

4. Silver nanoparticles

Found naturally is the earth crust (under mineral or alloy form), silver is a soft, ductile, and malleable element, slightly harder than gold. Silver is known to have the highest electrical and thermal conductivity of any metals (Chen & Schluesener, 2008; ATSDR, 2011). It had multiple uses throughout history: jewelry, currencies, photography, disinfectant for wounds and burns during World War I (Schneider, 2017). Silver salts have been used as treatments for epilepsy, gonorrhea, and gastroenteritis. Having a high absorptivity, soluble silver compounds can cause adverse health effects through dietary intake; a chronic ingestion of silver salts induces a poisoning known as argyria. Caused by silver precipitation in human tissues, argyria is associated with an irreversible pigmentation of the skin and the eye (Keat *et al.*, 2015)

However, since it has been established that silver is relatively non-toxic to human system (Chen & Schluesener, 2008), applications have been rising in recent years especially as antimicrobial agents for medical supplies. In the past years, with the outbreaks of infections and the emergence of antibiotic resistance, silver in the colloidal form (AgNPs) regained attention for prevention of bacterial, fungal and viral infections due to their effective antiseptic effect and the rareness of silver resistance. AgNPs are fine particles of elemental silver produced by the reduction of silver ions (Ag^+) in an aqueous solution,

resulting in Ag^0 (Bott *et al.*, 2014). AgNPs are to those days one of the most promising system offering advanced perspectives in sterilization and hygiene fields and more importantly in human health (Keat *et al.*, 2015; Le Ouay & Stellacci, 2015; Rai *et al.*, 2017, Zhang *et al.*, 2018).

4.1 Importance of AgNPs in the society

In the late 19th century, scientists started to produce nanosilver dispersions even if the term nanoparticle was not created. Since 1897, nanosilver was manufactured and commercialized under the name "Collargol" and has been used for medical purposes until the 1930s. After antibiotics had been invented, the use of nanosilver decreased but found a renewal when nanotechnology discipline arises (Schneider, 2017).

Currently, nanosilver is the most used nanomaterial in consumer products thanks to its versatile properties (Foldbjerg *et al.*, 2015). Nanosilver has a bigger marketing value than other NPs since its presence in consumer products is more advertised and their antimicrobial properties well-documented (Calderón-Jiménez *et al.*, 2017). The Consumer products Inventory (CPI) created by the project on emerging technologies (PEN) and the Woodrow Wilson International Center for Scholars (WWISC) reported that 24% of the listed products in 2014 (438/1814) were containing silver (Vance *et al.*, 2015). Another inventory, the Danish Nanodatabase, has listed 378 out of 3 037 products (12.4%) containing nanosilver in their formulation so far (The Nanodatabase, 2018).

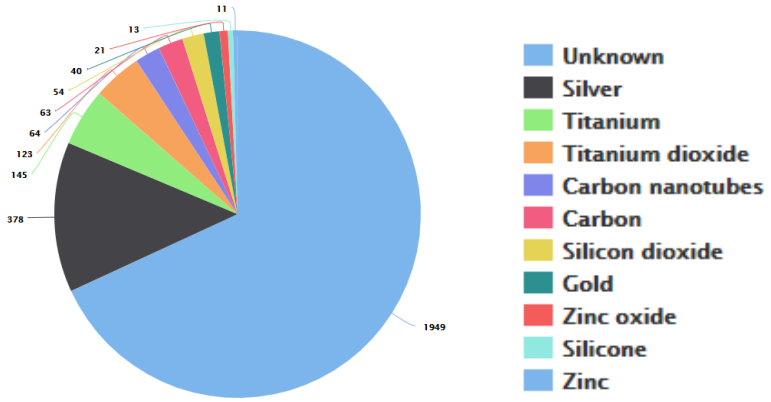

Figure 9. Pie chart representing the type of nanomaterial used in products listed so far 2018 in the Nanodatabase.

Source : http://nanodb.dk/en/analysis/consumer-products/#chartHashsection

Estimations on worldwide production have been largely issued but do not converge. Evaluated in 2010 at 22 T/year by European commission and 400 T/year by Keller *et al*. (2013), the global production of nanosilver is projected to reach 800 T by 2025 according to the optimistic estimates (Pulit-Prociak & Banach, 2016). Even if the data on nanosilver production do not overlap, its importance on the global market is substantial. The global nanosilver market was valued at more than 1 billion USD in 2016 and suppose to surpass 3.3 billion USD by 2024 consequently to an increasing demand for anti-microbial coating in the food and beverage industry, healthcare, and consumer products (Global Market Insights, 2017).

4.2 Properties of AgNPs

Among metallic nanoparticles, AgNPs have been the most intensively studied during the past decades because of their unique properties such as high electrical and thermal conductivity, catalytic activity, antibacterial, anti-viral and anti-fungal effects, chemical stability, nonlinear optical behavior and surface-enhanced Raman scattering (Tran *et al.*,2013; Ajitha *et al.*, 2014). These features depend strongly on the morphology of the particles including shape, size, and surrounding medium (Zhang *et al.*, 2018).

4.2.1 Antibacterial activity

The multitude properties of AgNPs have led them to a wide range of commercial and industrial applications in many sectors such as the medical field, the food sector, textiles, cosmetics, catalysis, bio-sensors, electricity and environmental uses (Keat *et al.*, 2015; Zhang *et al.*, 2018).

Among them, the antibacterial effect of silver nanoparticles is the main reason for their enormous development in recent years. An effective biocide effect has been observed against a wide range of fungi and bacteria (Gram+ and Gram-), including pathogenic strains (Marambio-Jones & Hoek, 2010; Tran *et al.*, 2013). In 2015, Le Ouay & Stellacci's study explained the effect of AgNPs in a large spectrum of bacteria by the non-specificity of AgNPs. Once in the cells, they act on a wide variety of targets, impairing simultaneously many pathways (Le Ouay & Stellacci, 2015) (Figure 10).

In addition to being dose-dependent (Shrivasta *et al.*,2007), shape-dependent (Pal *et al.*, 2007) and relying on the surface modifications (Kvitek *et al.*, 2008), the antibacterial activity of AgNPs is also size-dependent (Agnihotri *et al.*, 2014): the smaller the particle, the higher the antibacterial effect (Kholoud *et al.*, 2010). Indeed, when particle's size is reduced, surface area rises (a reduction in size of a uniform particle from 10 µm to 10 nm will increase surface area by 10^9) (Pal *et al.*, 2007). A large surface area increases contact with bacteria, allows the particles to attach to the cell membrane and easily penetrate the bacteria (Li *et al.*, 2010) and increases the release of ions (Foldbjerg *et al.*, 2014).

It is indeed accepted for a while among researchers that the antibacterial activity of AgNPs is not just conferred by the nanoparticles themselves but also by the silver ions released during the partial oxidation of the AgNPs in aqueous solution (Calderón-Jiménez *et al.*, 2017). Wasmuth *et al.,* 2016, measured 71 µg/L of Ag^+ after 7 days at pH 6 with an initial loading of 100 mg/L AgNPs. The amount of silver ions released is directly proportional to antimicrobial efficacy (Schneider, 2017). Elemental silver in the core and outer layers of silver oxide act as a reservoir releasing continuously silver ions at a steady state, for an effect lasting for years and remaining constant after UV or harsh cleaning procedures. (Schneider, 2017; Le Ouay & Stellacci, 2015). For Bone *et al*. (2012) the main toxic effect of Ag^+ is the inhibition of Na^+-/K^+-ATPases and mitochondrial dysfunction caused by the accumulation of reactive oxygen species. However, even if many studies agreed on the release of silver ions as the main toxic mechanism, a study showed that AgNPs were more effective against *E. Coli* compared to silver ions (Agnihotri *et al.*, 2013). Although the degree of importance of silver ion release in the bactericidal effect of AgNPs is still unclear and discussed among scientists, all agreed on different mechanisms of action behind the antibacterial activity of AgNPs (figure 10) (Durán *et al.*, 2016; Tran *et al.*, 2013).

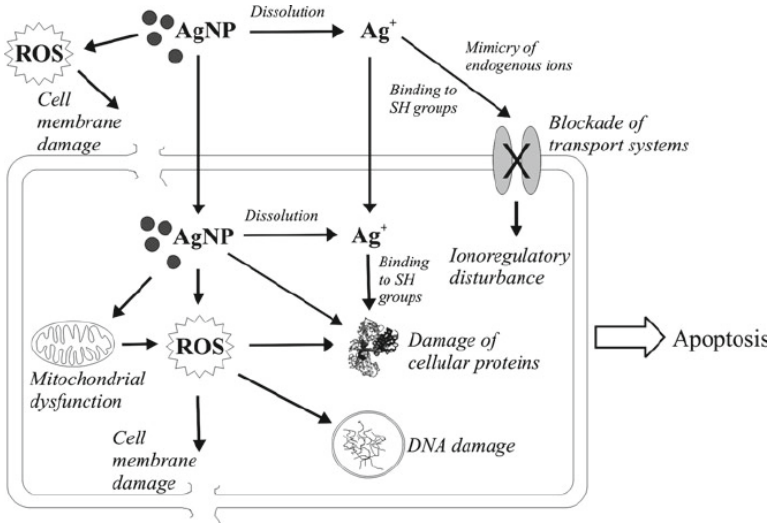

Figure 10. AgNPs interactions within the cell compartment.

Source: Völker *et al.*, 2013

First of all, AgNPs can attach to the cell membrane and disturb its functions such as permeability (Pal *et al.*, 2007; Williams *et al.*, 2016) and integrity (Le Ouay & Stellacci, 2012). For many studies, the anchoring and dissolution of the bacterial cell wall is the primary mechanism of action (Shrivastava *et al.*, 2007; McQuillan *et al.*,2012). When AgNPs are in contact with a bacterial membrane, they form aggregates, which lead to the perforation of the membrane (Le Ouay & Stellacci, 2015). Indeed, Mirzajani *et al.* (2011) showed that AgNPs destroyed the bacterial cell wall by releasing muramic acid that forms the peptidoglycan wall.

AgNPs were also suggested to act as a "Trojan horse" passing through membranes and releasing silver ions that will in turn cause many damages like interactions with sulfur and phosphorus compounds such as proteins and DNA (Park *et al.*, 2010). Silver ions have a very high affinity for organic amines, phosphates, and more importantly thiols group with which they form quasi-covalent bonds (Le Ouay & Stellacci, 2015). This affinity could explain the oxidative stress induced by AgNPs exposure by depleting antioxidants containing sulfide groups like glutathione (GSH), an effective silver ion chelator and redox balancer. GSH will adsorb Ag^+, which will in turn decrease their bioavailability in cell, inducing an imbalance between redox levels resulting in an oxidative stress (Foldbjerg *et al.*, 2014).

The induction of oxidative stress is also caused by the direct generation of reactive oxygen species (ROS) like superoxide anion, hydroxyls radicals, hydrogen peroxide in the mitochondria (Foldbjerg *et al.*,2015). When Ag^+ binds to respiratory chain enzymes, the passage of electrons to oxygen becomes inefficient leading to a large production of ROS. Consequently, interactions between Ag^+ and respiratory enzymes interrupt ATP formation and lead to cell death: ATP synthesis enables cell adhesion and proliferation (Asharani *et al.*, 2009; Reidy *et al.*, 2013).

This ROS formation has also been suggested as the common pathway of membrane, DNA and protein damages and apoptosis. Reactions happening are the formation of highly reactive and short-lived hydroxyl radicals causing DNA damage (Foldbjerg *et al.*, 2014). Concerning toxicity on genomics, Bouwmeester *et al.* showed that AgNPs could induce changes in gene expression of stress hormone, oxidative stress and apoptosis in Caco-2 cells (Bouwmeester *et al.*, 2011). Moreover, many studies

showed an up-regulation in metallothionein family, proteins expressed in response to metal exposure but also in response to oxidative stress (Foldbjerg *et al.*, 2012).

4.3 Applications of AgNPs

AgNPs were incorporated in high amount of everyday life products (textiles, bandages, detergents, cosmetics lotions, deodorants, toothpastes…) thanks to their effective antibacterial activity (Mao *et al.*, 2018; Zhang *et al.*, 2018). For example, silver coated textiles have durable bactericidal effect compared to other textiles, which lose their effect after washing cycles. Once the nanoparticles incorporated in the polymers, they stay fixed and release silver ions continuously. Textiles remain antimicrobial after 200 washings at 60 °C. Besides, since it avoids germ growth in the fabric, drying is not necessary (Schneider, 2017). AgNPs can also be fused with core materials of polymeric membranes to disinfect water or air contaminated with bacteria and viruses. In addition to prevent epidemic waterborne diseases due to poor drinking water filtration, AgNPs prevent biofilm formation in filtration device (Tran *et al.*, 2013).

In the medical field, nanosilver was certified as an effective agent for wound management in the 1920's by the US FDA (Food and Drug Administration). In the last years, we could find AgNPs in catheters, implants and prostheses, additive in wound dressings, surgical instruments and bone substitute materials. Originally used also as an effective disinfectant, it was relatively free of side effects (Suresh *et al.*, 2012; Foldbjerg *et al.*, 2014; Chopra, 2007).

Recently, the potential of AgNPs as antimalarial agent was discussed and great hopes are placed in it. Current malarial treatments fail because of the emergence of drug resistance and insecticide toxicity in human body. In this context, nanotechnology based-products and AgNPs especially, could be an effective solution for the control of malaria since they have demonstrated significant activity against malarial parasite (*Plasmodium falciparum*) and vector (Anopheles mosquito) (Rai *et al.*, 2017). In addition to the antibacterial effect, AgNPs are also killing agents of fungi and viruses such as HIV-1 or HBV (hepatitis) (Tran *et al.*, 2013).

4.3.1 AgNPs in the food sector

Even if most consumer products containing AgNPs are designed for topical application, the risk of cutaneous absorption is low since human epiderm is relatively impermeable (excepted in case of wounds) (Calderón-Jiménez *et al.*, 2017). However, AgNPs have many applications in the food sector, thus the risk of ingestion through oral exposure has to be taken seriously in account.

Referred as a food additive E174 in the food industry in EU, silver is allowed as a coloring agent in medicinal products and pastry decoration (Contado, 2015). Nanosilver, however, is not considered as a food ingredient like silver but might be ingested since the increasing number of food applications. The presence of NPs in our diet arises either from direct incorporation during food manufacturing or from migration from food contact materials (Bellmann *et al.*, 2015). AgNPs are indeed allowed in the processing, conservation and consumption of food as antiseptic coating in plastic food containers, in inner surfaces of fridges and dishes, in food packaging for sterilization purposes (*e.g*. soaker pads for fresh meat), but also as health supplements or as alginate gel coatings of carrots and asparagus for water loss prevention. Fresh fruits and vegetables are also a source of AgNPs in form of residuals of agricultural treatments (Contado, 2015; Bove *et al.*, 2017; Fröhlich & Fröhlich, 2016).

The potential migration of nanosilver from consumer products was investigated vastly. The release of Ag NPs from reusable food containers to food simulants in water was 5 ng/cm^2 over 10 days, polyethylene bags released 10 ng of silver /cm^2 after 12 days, this amount increasing with storage and temperature (Huang *et al.*, 2011), and 34 ng/cm^2 of Ag were released after 3 use cycles from food storage plastic containers (Von Goetz *et al.*, 2013). Silver migration from three commercial nanosilver plastic food containers ranged between 1.66–31.46 ng/cm2 (Echegoyen & Nerin, 2013). Nevertheless, other studies like Bott's *et al.* (2014), suggested that AgNPs would not be able to migrate from contact plastics (LDPE, low density polyethylene) (Bott *et al.*, 2014). While studies argued on nanosilver migrating or not from consumer-products, the World Health Organization estimated in 2003 the daily consumption of Ag through drinking water to amount 20-80 g/day. Wijnhoven *et al.*, 2009, however amounted the human dietary silver intake to 70-90 µg /day. However, these are estimations about silver daily intakes and not about nanosilver. To the best of our knowledge, total nanosilver daily intakes could not be found in literature. However, the Danish Ministry of Environment estimates that 1.25 mg/day were ingested through the release from food supplements.

4.4 Toxicity studies about AgNPs

Consequently to the massive introduction of AgNPs in everyday consumer products, the chance of public and environmental exposure has increased dramatically (Figure 11) (Foldbjerg *et al.*,2015). A lot of concerns was raised these times regarding unexpected toxicity of nanosilver. Several researches have been carried out to assess the fate, transport and deleterious effects of AgNPs on the environment such as in higher organisms (Calderón-Jiménez, 2017). AgNPs exhibit indeed diverse deleterious effects being related to the size, shape, surface area, agglomeration/aggregation state, dissolution rate, efficiency of ion release and surface coating of the particle (Foldbjerg *et al.* ,2015; Wen *et al.*, 2016).

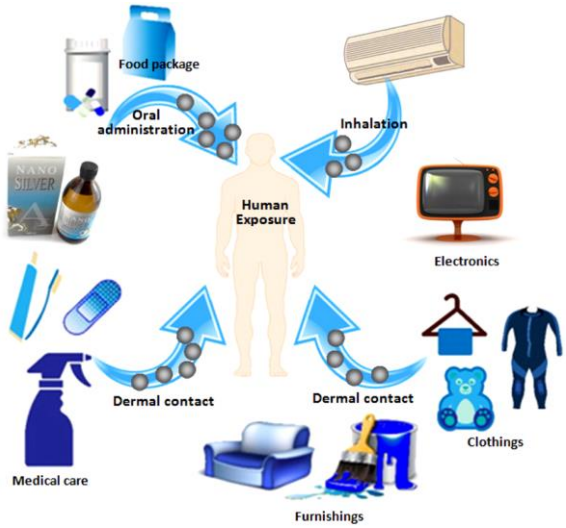

Figure 11. Human exposure routes to nanosilver. **Source**: Wen *et al.*, 2016

In vivo studies gave relevant information about the distribution, kinetics and accumulation of AgNPs within the organism. Intravenous administration of AgNPs in rodents showed that AgNPs target specific organs (liver, kidneys, lung and spleen) depending on the size of the particle (Lankveld *et al.*, 2010; Jarak *et al.*, 2017). The study of van der Zande *et al.* (2012) showed that AgNPs we are using for this thesis (NM-300K) were found in the highest level in the liver and the spleen upon 28-day oral administration to rats. They saw that concentration of Ag in the organs was highly correlated with the amount of Ag^+

in the suspension. Many studies (Ji *et al.*, 2007; Kim *et al.*, 2008, Park *et al.*, 2011) suggested the absorption of AgNPs through the GI tract followed by a systemic distribution by blood circulation towards hepatobiliary detoxification pathway; high levels of AgNPs were indeed found in feces. According to different studies in mice and rats, the distribution and biokinetic profile of AgNPs is also gender related (Xue *et al.*, 2012; Boudreau *et al.*, 2016).

Recently, other effects were highlighted in rodents upon oral exposure to AgNPs: aggravation of fatty liver diseases only in overweight mice (Jia *et al.*, 2017), disruption of bacterial population in the gut (van de Brule *et al.*, 2016) and increase of ATP production in the heart and inflammation in the lung (Jarak *et al.*, 2017). Other animal models were also used to assess AgNPs toxicity. AgNPs coated with starch and BSA impaired development of zebrafish embryos (delayed hatching, increased mortality, induce malformations and cardiac problems (Asharani *et al.*, 2008). In soil invertebrates *Enchytraeus crypticus*, AgNPs (NM-300K) induced oxidative stress with an increase of metallothionein production (Ribiero *et al.*, 2015) while they had no effect on reproduction and survival of arthropod *F. candida* below 700 mg Ag/kg dry soil (Waalewijn-Kool *et al.*, 2014).

As seen before, many studies assessed the effect of AgNPs in animal models, but very small number of studies report its real impact on human health (*in vivo* human studies) (Calderón-Jiménez *et al.*, 2017) despite the fact that humans are accessible to AgNPs exposure through many routes: oral ingestion, pulmonary inhalation, intravenous injection or dermal contact (Mao *et al.*, 2018). One of them was led by Munger *et al.* in 2014 where they prospected the effect of oral dosed commercial AgNPs (10-32 ppm Ag solutions) in a single blind, controlled design on 60 healthy subjects. They did not observe clinically important toxicity markers after 14 days ingestion of a commercial nanosilver product. They also recommended longer human exposure to better determine risks (Munger *et al.*, 2014).

However, many *in vitro* studies have been conducted on human cell lines and have provided results showing that AgNPs are transported inside the cell (Williams *et al.*, 2016). Once internalized, they induce DNA damage and repair mechanisms (Lim *et al.,* 2017), disrupt cell morphology and induce oxidative stress (Arora *et al.*, 2008; Asharani *et al.* 2009), and finally lead to cell cycle arrest and apoptosis (Arora *et al.*, 2008, Eom and Choi,2010; McCracken *et al.*, 2015).

In *in vitro* models of the human gut epithelium, AgNPs alter significantly the permeability of the cell monolayer (Williams *et al.*, 2016; Martirosyan *et al.*, 2014), decrease cell viability (Lichtenstein *et al.*, 2015; Abbott Chalew & Schwab, 2013) and increase cytokine production leading to inflammation and oxidative stress (Abbott Chalew & Schwab, 2013; McCracken *et al.*, 2015).

Concerning the uptake of AgNPs, studies show that ingested nanoparticles were absorbed via M-cells and enterocytes in the intestinal mucosa. The absorbed fraction of the administered dose ranges from 0.4% to 10% depending on the species (Florence, 2005). Different pathways were reported as uptake processes: clathrin-mediated and cavelin-mediated endocytosis but also phagocytosis and pinocytosis (Foldbjerg *et al.*, 2014). These mechanisms depend on the size of the particles (Liu *et al.*, 2010; Foldbjerg *et al.*, 2014) and their surface coating (Jiang *et al.,* 2015) but also the cell type (Greulich *et al.*, 2011; Wang *et al.*, 2012). Most studies summarize the uptake by formation of endosomes, fusing with lysosomes with endocytosis as the major mechanism underlying the cellular uptake (Gliga *et al.*, 2014; Jiang *et al.*, 2013).

4.5 Characterization of AgNPs

Characterize nanoparticles is crucial to control their synthesis and to understand their behavior since most NPs properties are size and shape-dependent (Pal *et al.*, 2007). Besides UV-visible spectroscopy, which has been used for this thesis, there are many other techniques of AgNPs characterization: X-ray diffractometry (XRD), dynamic light scattering (DLS), Fourier Transform Infrared (FTIR) spectroscopy, Scanning Electron Microscopy (SEM), Transmission Electron Microscopy (TEM), Atomic Force Microscopy (AFM), and Localized Surface Plasmon Resonance (LSPR) (Zhang *et al.*, 2016).

These techniques provide a multitude of information such as the size, shape, crystal form, fractal dimensions and surface area. TEM, SEM and AFM are generally used to determine the morphology and size of the particle while DLS is used for the particle size distribution and hydrodynamic diameter. AFM has the advantage over TEM and SEM of providing three-dimensions images, giving a deep insight of surface topography. XRD allows to examine crystallinity while FTIR spectroscopy can highlight interaction of AgNPs with functional groups. UV-visible spectroscopy is commonly used to confirm NP formation by showing the plasmon resonance (Kholoud *et al.*, 2010; Ajitha *et al.*, 2015).

4.5.1 UV-visible spectroscopy

UV-visible spectroscopy is a very common and reliable technique for the primary characterization of AgNPs. UV-visible spectroscopy has the advantages of being fast, simple, sensitive and selective for different types of NPs. Information about the size, presence of surroundings and aggregation state of digested AgNPs can be obtained with UV-visible spectroscopy (Zhang *et al.*, 2016).

Metallic NPs such as silver have free electrons that oscillate on the surface of the particles and can absorb light at specific wavelengths. These free electrons generate a surface plasmon resonance (SPR) absorption band (called SPR peak) occurring because of the mutual vibrations of conduction electrons of AgNPs in resonance with the light wave (Zhang *et al.*, 2016). The SPR band lies in the visible part of the spectrum, giving the colors of colloidal AgNPs solutions (Maayan & Liu, 2011). Smaller particles exhibit a plasmon band at smaller wavelength than larger particles or aggregates (Maayan & Liu, 2011).

Spherical AgNPs particularity, for example, is the SPR peak ‘s wavelength that can be set from 400 nm (violet light) to 530 nm (green light) by changing the size or shape of the NPs (Sigma Aldrich, 2011). As seen on the left extinction spectra of the figure, smaller AgNPs display peaks around 390-400 nm (10 – 40 nm diameter). As the diameter increases, SPR peaks shift towards higher wavelengths and widen simultaneously (phenomenon called red-shifting). From a diameter of 80 nm, a second peak at a lower wavelength appears because of a quadruple resonance that has a different electron oscillation pattern than the first peak (Sigma-Aldrich, 2011).

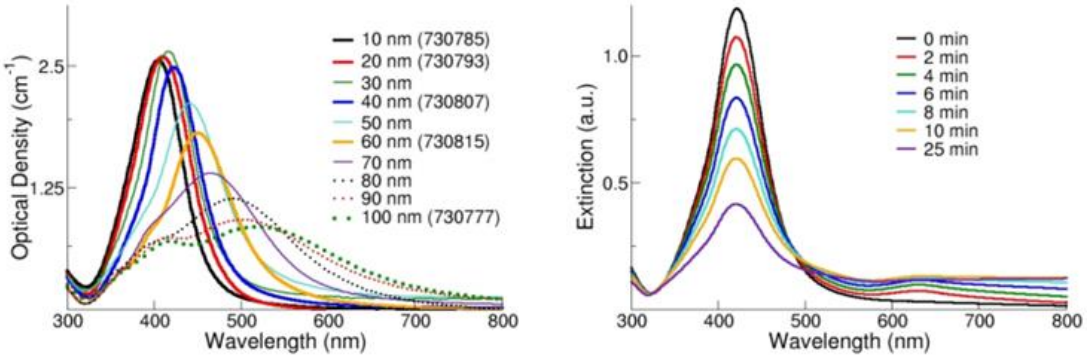

Figure 12. Extinction spectra of AgNPs with diameters ranging from 10 to 100 nm at concentration of 0.02 mg/ml (left). Extinction spectra of 50 nm AgNPs undergoing aggregation (right). Source: Sigma Aldrich, 2011.

Spectral curves can give interesting information about the changes in physical state of AgNPs over time, especially their aggregation state. Right figure above shows the optical response of AgNPs upon the addition of a saline solution of sodium carbonate. When particles aggregate, conductions electrons delocalize to nearby particle inducing a destabilization of the particles and triggering a shift of the SPR peak to lower energies. Over time, the original extinction peak is less intense due the depletion of stable nanoparticles and widens as the agglomeration increases. The solution is yellow when AgNPs are unaggregated and grey if the particles aggregate (Nanocomosix,2018).

Since SPR peaks depends on the size, shape, aggregation state and surface alterations of the NPs at the molecular level (Khan *et al.*, 2017), characterizing this peak enables to detect the formation of agglomerates or changes in the close environment of NPs such as the formation of a protein corona. Argentiere *et al.*, studied which of these three techniques: TEM, DLS and UV-visible spectroscopy is the best to characterize interactions between AgNPs and biological fluids found in both *in vivo* (mouse plasma) and *in vitro* (fetal bovine serum) conditions. They found that UV-vis more informative about AgNPs changes, especially for smaller particles, which showed more pronounced optical changes when interacting with surrounding proteins (Argentiere *et al.*, 2016).

4.6 Safety regulations

Legislation about the use of nanoparticles is very recent and generally little respected by producers. Indeed, the obligation to label products containing nanoparticles did not come into force until july 2013 for cosmetics (EU regulation n° 1223/2009), september 2013 for the use as a biocidal substance (BPR, EU regulation n°528/2012) and december 2014 for food products (EU regulation n° 1169/2011).

Concerning the last one, the regulation about the provision of food information to consumers, it recommends that all products containing ingredients in the form of engineered nanomaterials shall be clearly indicated in the list of ingredients with the 'nano' in brackets following the name of the nanomaterial used. To avoid any misunderstanding, the definition of engineered nanomaterials is also clarified (EU 1169/2011). Despite those regulations, few are the industries that apply them. The 2018 scandal over the unlabelling of TiO_2 or E171, used as a bleaching agent in sweeties, confirm that

nanotechnologies are still poorly regulated by the producers but also by the legislations (LCI, 2018). A nanomaterial added unintentionally does not have to be labeled, opening the door to abuses and frauds (LCI,2018).

No specific regulation about AgNPs has been released so far but a report providing extensive data on mammalian and ecotoxicity of the nanosilver product “agpure W10”, known as the reference material NM-300K used for this thesis was edited in 2007. Known as ‘the OECD WPMN Sponsorship Program for the Testing of manufactured Nanomaterials’, the report concludes that products containing NM-300K as antimicrobial additive are safe for humans and the environment (Klein *et al.*, 2011). Even if the impact on humans upon exposure to AgNPs through realistic doses is supposed safe, more toxicological studies need to be carried out in order to corroborate such affirmations.

5. Objectives

In the past 10 years, the use of AgNPs has increased exponentially in industry, food, medicine and textile largely thanks to their antimicrobial properties. In the food sector particularly, applications using AgNPs have exploded: sensors in food packaging, food additives, anticaking agents and clarifying agents for fruit juices. Many concerns have been raised about nanosilver included in consumer food products since they may migrate unintentionally into the food content. Orally ingested silver nanoparticles may then cross the intestinal barrier, reach the blood system, distribute to all parts of the human organism and finally cause harmful health effects. Knowing the toxic effects of AgNPs in human body is therefore important to protect consumer health and guaranty food safety.

To the best of our knowledge, only few studies reproduced the physicochemical transformations of orally ingested AgNPs. Indeed, AgNPs are incorporated into food products and should pass through the GIT before inducing potentially deleterious effects on intestinal cells. Taking in account these two effects is therefore essential to assess AgNPs cell toxicity in the most realistic way possible.

The first objective of this thesis was to assess the impact of food components and digestive enzymes on the cytotoxicity of silver nanoparticles in a coculture of Caco-2 and HT29-MTX cells. To this end, an *in vitro* digestion process such an *in vitro* food matrix model was used. A preliminary study assessing the effect of digestive enzymes and food components on cells has been undertaken. A characterization of AgNPs through UV-visible spectroscopy before and after each step of the *in vitro* digestion process was also performed.

Undigested and digested AgNPs included or not in the food matrix model were used to assess their toxicity on the Caco-2/HT29-MTX cells model. Previously tested in the lab, this model is largely accepted among researchers as a realistic simulation of human intestinal epithelium. The two main cell types found in gut epithelium, enterocytes and goblet cells are indeed represented. Toxicity of AgNPs has been evaluated trough different cytotoxicity assays: ATP content measured with CellTiter-Glo assay, cell viability with CellTiter-blue assay and cell detachment with crystal violet staining.

The second objective was to quantify the protein corona formed around AgNPs since its presence is assumed to change interactions between AgNPS and cells, a fact known for many years among researchers. A method using the microBCA assay was used to quantify the protein corona formed after AgNPs incubation in the food matrix model comprised of standard counterpart of the dietary macronutrients: bovine serum albumin, starch and triolein. At this point, it seems important to emphasize the fact that the effect of the digestion has not been taken into account in the characterization of the protein corona. Moreover, a characterization with UV- visible of the AgNPs during the *in vitro* digestion is also performed in order to give information about the changes in the optical and physical state.

MATERIAL & METHODS

1. Material

1.1 Cell lines

As model for the intestinal barrier, we used a coculture of Caco-2 and HT29-MTX cells.

- *Caco-2 cells*

Caco-2 cells were provided by Dr Maria Rescigno (first clone C2E, University of Milano-Bicocca, Milan, IT). Originally, the parental cell line was obtained from a human colon adenocarcinoma. Once in culture conditions, cells differentiate spontaneously into a monolayer of enterocyte-like cells. We used them from passage 10 to 30 for our model.

- *HT29-MTX cells*

HT29-MTX cells were added to this enterocyte-like monolayer to reproduce mucus secreting cells, the goblet cells. They come from a human colorectal carcinoma. They originate from isolation of HT29 cells treated with methotrexate (MTX, 10^{-5}M). This treatment induces the secretion of mucins by differentiated cells. HT29-MTX cells were used from passage 30 to 50 for our model.

1.2 Silver nanoparticles

Silver nanoparticles (NM-300K, JRC, Ispra, IT) were provided by the JRC, a scientific center of the European commission created, among other things, to" develop *innovative tools and make them available to policy makers"* (European Commission, 2018). The average diameter of these referenced AgNPs is 15 nm with a narrow size of distribution of 99 % of the particles exhibiting a diameter below 20 nm. NM-300K is a nanosilver colloidal dispersion, yellow-brown colored, with a silver content of 10.16 % (w/w). The aqueous solution contains stabilizing agents to avoid nanoparticles aggregation within the solution: 4 % (v/v) of polyoxyethylene (20) sorbitan mono-laurate (Tween 20) and 4% (v/v) of polyoxyethylene glycerol trioleate (JRC,2011). This stock solution has been stored at room temperature and protected from the light.

Concentrations of AgNPs used in our experiments (11.25, 33.75 and 101.25 µg AgNPs/ml) were obtained by dilution of the initial solution (called stock solution) in Hanks Balanced Salt Solution (HBSS, Lonza, Verviers, BE). HBSS is an aqueous solution containing different salts and glucose (1g/L) at pH 7-7.4.

1.3 Food matrix

Since the main goal of this thesis is to assess the impact of the food matrix in a toxicity study of silver nanoparticles, a modelized food matrix was used during experiments. The three main constituents found in food were represented by referenced equivalents in our food model.

To represent the protein fraction, we used the bovine serum albumin (BSA, lyophilized powder, A4503, > 96%, Sigma-Aldrich, Saint-Louis, MI) at 5.6 mg/ml, solubilized in HBSS.

We used starch (unmodified wheat starch, S5127, Sigma-Aldrich) to model the carbohydrate fraction. The final concentration (8.7 mg/ml) was obtained by mixing the starch powder with HBSS.

The third reagent, glyceryl trioleate (glyceryl trioleate, T7140, > 99%, Sigma-Aldrich), commonly triolein, stands for the lipid fraction. Triolein was used at a concentration of 7.8 mg/ml in the food matrix model.

2. Cell culture

2.1 Caco-2 & HT29-MTX cells

Both Caco-2 and HT29-MTX cells were grown separately in flasks of 75 cm^2 (Corning Incorporated, Corning, NY) in the Dulbecco's modified Eagle's minimum essential medium (DMEM, Lonza), a culture medium containing 4.5 g/L of glucose and a mix of salts, vitamins, and amino acids. DMEM has a red color due to the presence of phenol red, incorporated as a pH indicator of the medium. DMEM was supplemented with 10% (v/v) of heat inactivated fetal bovine serum (FBS, Thermo Scientific, Waltham, Massachusetts) providing essential proteins for cell growth, 1% (v/v) of L-glutamine 200 mM in a NaCl solution at 0.85 % (Lonza), 1% (v/v) of non-essential amino acids 100x (Lonza) and 1% (v/v) of a mix of penicillin-streptomycin (Lonza). This supplemented DMEM was the culture medium used in every experiment. Flasks were incubated in a vapor saturated atmosphere at 37°C and either 5 % or 10 % CO_2 for HT29-MTX and Caco-2 flasks respectively. After 7 days of culture, the flask reaches 90 to 100 % of confluence. A subculture can then be conducted to launch the next flask.

The subculture protocol is the same for Caco-2 and HT29-MTX cells. First, flasks were washed with 13 ml of phosphate buffered saline (PBS) that eliminates dead or unfixed cells and serum. Serum needs to be washed because it contains trypsin inhibitors. Otherwise, trypsin used right after wouldn't be effective to detach cells. Cell layer was then detached from the flask after 5-10 min incubation (37°C, 10 % CO_2) with 1.5 ml (v/v) of trypsin-EDTA 0.05% (Lonza). Detached cells were suspended in 20 ml of culture medium. Cell density of the suspension was then measured according to the method given in the next paragraph. Once cell density measured, cells were inoculated at 10 000 cells/cm^2 in a new culture flask with 25 ml of medium to reach confluence after 7 days of culture.

2.2 Cell density assessment

Cell counting is performed using the trypan blue dye (Lonza), a tetrasodium salt that enters in dead and alive cells but is actively expulsed from the living ones. Living cells appear uncolored while dead cells are colored in blue. 50 µl of trypan blue are added to 50 µl of cell suspension. 18 µl of colored cell suspension are then dropped in a Bürker cell that is observed under the microscope. The total amount of living cells found on 3 squares taken randomly on the grid was counted.

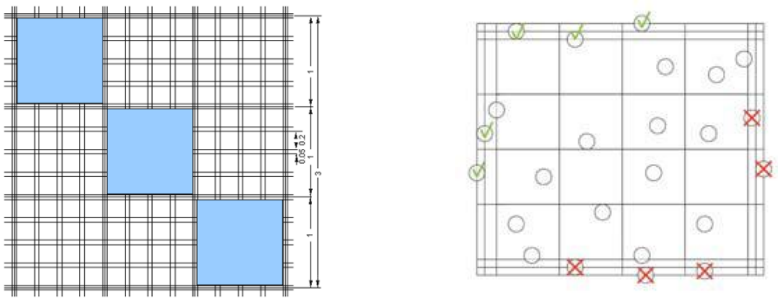

Figure 13. Dimensions of the entire grid (Bürker counting chamber) (left) and one square showing which cells to count: cells in the middle of the grid and cells that overlap edges on two sides (ticked) (right).

Sources:

https://openwetware.org/wiki/IGEM:University_of_Debrecen:_transfection#.2A__How_to_use_the_B.C3.BCrker_chamber: (left).

https://www.sigmaaldrich.com/technical-documents/protocols/biology/cell-quantification.html (right).

Cell density was assessed by the following formula:

$$\text{Cell density (cells/ml)} = \frac{\text{(number of living cells X dilution factor (2) X 10\^4}}{\text{number of counted squares (3)}}$$

Eventually, volumes for the next subcultures and the coculture were calculated once the cellular density was assessed. Cell lines for the coculture of Caco2/HT29-MTX cells were mixed at a proportion 3:1.

2.3 Culture in 48 well plates

Coculture of Caco-2/HT29-MTX cells was inoculated in polystyrene 48 well plates (Costar, Corning Incorporated) in order to carry out the cytotoxicity assays. The bottom surface of the wells measures 0.95 cm^2. Before seeding the plates, the 24 central wells were incubated 1 hour with 150 µl of collagen 1% (v/v) (Sigma-Aldrich) dissolved in PBS. The collagen coating provides a better anchoring base by preventing the detachment of the cell-layer.

After the incubation, wells were washed with PBS. 300 µl of coculture suspension at a density of 200 000 cells/ml were added in each central well. Seeded plates were incubated in the same conditions as culture flasks (37°C, 10 % CO_2, vapor saturation). Assays were performed on confluent cell monolayers obtained after 21 days of culture during which growth medium was renewed every two days.

3. *In vitro* digestion

3.1 Principle

In vitro digestion is carried out to reproduce human digestion beginning in the mouth and ending in the small intestine. Based on *Hollebeeck et al*, 2012 protocol, the *in vitro* digestion used for this thesis is separated into 3 stages: salivary, gastric and intestinal steps. *In vitro* conditions must be the closest to human digestion's one in order to have a realistic model. For each step, the main digestive enzyme was added in the bottle containing the digesting solution and pH was adjusted. Throughout the whole digestion, digestion bottles were kept at 37°C and the content was shaken with a 350 rpm speed to reproduce mechanical digestion.

3.2 Method

During the entire process, digesting solutions were poured in dark glass bottles (Duran, Wertheim, DE), incubated at 37°C in a water bath (SW22 Shaking water bath, Julabo GmbH, Seelbach, DE) and shaken at 350 rpm.

- Salivary stage

Previously, a stock solution of α-amylase (α-amylase from human saliva type IX-A, A0521, 210 units/mg solid content, 2400 U/mg protein, Sigma-Aldrich) at 166.7 U/ml was prepared in PBS, aliquoted and stored at -20°C.

The day of the experiment, the pH of the digesting solution was adjusted at 6.9 with HCl (1M). Next, 11.3 µl of α-amylase stock solution were added per ml of digesting solution. The bottle was thereafter incubated 10 min in the water bath.

- Gastric stage

A pepsin solution (pepsin from porcine gastric mucosa, P7000, 561 U/mg solid, Sigma-Aldrich) was freshly prepared with a final concentration of 0.04 g/ml HCl 0.1 M.

At the end of the salivary step, HCl 1M was added in the bottle to lower pH until 2.0. Then, 50 µl of pepsin solution was added per ml of digesting solution and if necessary, pH was readapted to 2.0 with HCl 1M.

As a final step, the bottle was flushed by N_2 to reproduce anaerobic conditions found in the stomach. The bottle was eventually incubated for 2 hours at 37°C.

- Intestinal stage

A bile-pancreatin solution containing 3.33 mg of bile (Bile extract porcine, B8631, Sigma-Aldrich) and 3.33 mg of pancreatin (pancreatin from porcine pancreas, P1750, Sigma-Aldrich) per ml of $NaHCO_3$ 0.1M was first prepared. The pancreatin stock solution contains enzymatic components including α-amylase, trypsin and other proteases, lipase, and ribonuclease excreted by the exocrine cells of the porcine pancreas (Sigma-Aldrich, 2018).

After the gastric step, pH was risen to 5.3 with $NaHCO_3$ 1M. Then, 150 µl of bile-pancreatin solution were added per ml of digesting solution. pH was adapted a second time with HCl 1M or $NaHCO_3$ 1M to reach 7.0. The bottle was finally flushed by N_2 and incubated at 37°C for 2 hours. The following figure shows a schematic representation of the *in vitro* digestion protocol.

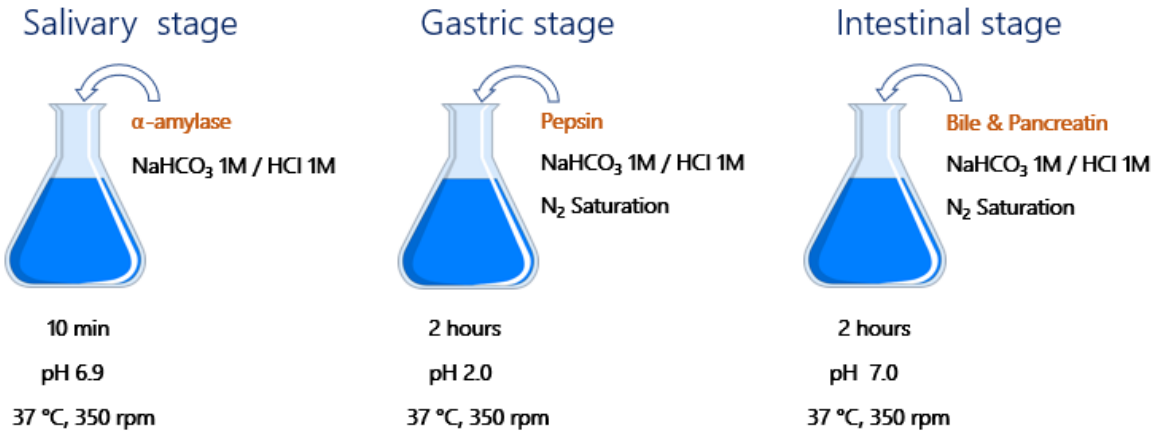

Figure 14. Schematic diagram of the *in vitro* digestion protocol.

4. Impact of the food matrix and digestive enzymes on intestinal cells

When the toxicity of digested AgNPs is assessed, we need to be sure that a potential toxic response is solely due to AgNPs and not to the intrinsic toxicity of the food matrix and the digesting solution. Enzymes used during the *in vitro* digestion may indeed present cell toxicity that we need to get rid of in order to assess AgNPs toxicity. Since the toxicity of digested food matrix without AgNPs on intestinal cells was never assessed before in our experimental model, different dilutions were realized in order to find nontoxic concentrations of the digestates.

To this end, *in vitro* digestions of HBSS and food matrix without AgNPs have been carried out. Toxicity of these two digesting solutions was tested for different dilutions (1-, 2-, 4-, 8-times diluted) by

performing cytotoxicity assays on 48 wells culture plates. These tests are explained in the point 8 of this Material & Methods part.

4.1 Sample preparation and *in vitro* digestion

Before digesting HBSS and the food matrix, two stock solutions were prepared:

- BSA solution at 16.8 mg/ml in HBSS.
- Starch solution at 26.1 mg/ml in HBSS.

Then, two digesting bottles were prepared. In the first one, 15,129 ml of HBSS are added. In the second one, 5 ml of HBSS, 5ml of starch solution, 5ml of BSA solution, and 129 µl of triolein are added to simulate the food matrix. Both bottles undergo the whole *in vitro* digestion process as explained in section Erreur ! Source du renvoi introuvable..

4.2 Sample dilution and cytotoxicity assays

After the *in vitro* digestion, digested HBSS and food matrix solutions were diluted 2X, 4X and 8X in HBSS and poured in 15 ml tubes. Non-diluted falcons of digested HBSS and digested food matrix were also prepared. In the same time, Falcon™ tubes containing dilutions (1,2,4,8X) of undigested food matrix were prepared. Two other controls were tested: undigested HBSS and Triton X-100. In total, 14 different treatments were assessed on intestinal cells.

For that, differentiated coculture of Caco-2/HT29-MTX cells previously seeded in 48 wells plates were used. After washing cells with PBS, each treatment was added in at least three wells. Plates were finally incubated 3 hours at 37 °C.

After incubation, plates were washed with PBS and cytotoxicity assays are performed according to the sections 6.1, 6.2 and 6.3.

5. Impact of AgNPs included in a digested food matrix on intestinal cells

Once toxicity of digested food matrix assessed, AgNPs can be included in the model to see their impact on intestinal cells. Since, digesting solutions will be diluted two times in order to suppress their potential toxic effect, the toxic impact of AgNPs only can be evaluated.

To do this, an *in vitro* digestion was performed on AgNPs solutions at different concentrations (11.25, 33.75 and 101.25 µg/ml) with and without food matrix. Cytotoxicity assays were then performed on culture plates to conclude on the toxic effect of AgNPs.

5.1 Sample preparation and *in vitro* digestion

Stock solutions of food matrix were prepared as explained below:

- BSA solution at 16.8 mg/ml in HBSS.
- Starch solution at 26.1 mg/ml in HBSS.

An AgNPs stock solution at 1822.5 µg/ml was also prepared in HBSS. Then, AgNPs solutions 3 times concentrated (67.5; 202.5 and 607.5 µg/ml) were prepared by a serial dilution of the AgNPs stock solution in HBSS.

Afterwards, two kinds of digesting bottles were prepared:

- 4 bottles containing AgNPs in HBSS at 0, 22.5, 67.5 and 202.5 µg/ml: 5 ml of the 3X concentrated AgNPs solutions or HBSS were added to 10.129 ml of HBSS.
- 4 bottles containing AgNPs included in the food matrix: each one contains 5 ml of HBSS or 3X concentrated AgNPs solution, 5ml of starch solution, 5ml of BSA solution, and 129 µl of triolein.

In total, 8 bottles went through the process of digestion as explained in section Erreur ! Source du renvoi introuvable.. After each digestive step, 1 ml of the different treatments is collected and analyzed by UV-visible spectroscopy.

1 hour before the end of digestion, undigested solutions (controls) were prepared:

- Undigested AgNPs without matrix (4 bottles) at 0, 22.5, 67.5 and 202.5 µg/ml by diluting in HBSS the 3X concentrated AgNPs solutions.
- Undigested AgNPs with food matrix (4 bottles) at 0, 22.5, 67.5 and 202.5 µg/ml by mixing 1.2 ml of 3X concentrated AgNPs solutions with 1.2 ml of both BSA and starch solutions and 31 µl of triolein.

These solutions were poured in 5 ml glass bottles and incubated 1h under stirring at 25 °C. After the incubation, addition and removal of solutions during digestion was simulated for the non-digested bottles in order to repeat the same conditions for every treatment.

5.2 Sample dilution and cytotoxicity assays

After the *in vitro* digestion, digested and undigested samples are diluted 2X in HBSS regarding the results obtained after assessing digested food matrix toxicity on intestinal cells. These are prepared in 15 ml Falcon™ tubes by mixing 2ml of HBSS with 2ml of sample solution. Then the toxicity of each sample is assessed on intestinal cells.

For that, differentiated cocultures of Caco-2/HT29-MTX cells previously seeded in 48 wells plates were used. After washing cells with PBS, each treatment was added in three wells. Plates were finally incubated 3 hours at 37 °C.

After incubation, plates were washed with PBS and cytotoxicity assays were performed according to the sections 6.1, 6.2 and 6.3.

6. Cytotoxicity assays

6.1 CellTiter-Glo assay

ATP content, one of the most sensitive cell viability indicator, is assessed by the kit CellTiter-Glo® Luminescent Cell Viability Assay (Promega Corp, Madison, Wisconsin). This kit contains a lyophilized CellTiter-Glo substrate and the CellTiter-Glo buffer, both stored at -20°C and defrosted before the assay.

6.1.1 Principle

The CellTiter-Glo® Luminescent Cell Viability Assay (CTG) is a homogeneous method to determine the number of viable cells in culture. After complete cell lysis, ATP content is measured thanks to luciferase that induces a simple exothermic reaction releasing light. In the presence of ATP, luciferase converts luciferin onto oxyluciferin that emits light detected with a luminometer (figure 15). The amount of ATP, translated by the quantity of light released, is directly proportional to the number of metabolically active cells.

CellTiter-Glo test uses a thermostable luciferase that can generate a stable “glow-type” luminescent signal while inhibiting at the same time endogenous enzymes released during cell lysis that may interfere with ATP measurement (ATPases, …). ATPase inhibitors are indeed added to the substrate to stabilize released ATP. This assay provides a simple way to measure cell viability with extremely high sensitivity: as few as 10 cells/well can be detected in 10 min after adding the reagent (Promega, 2018).

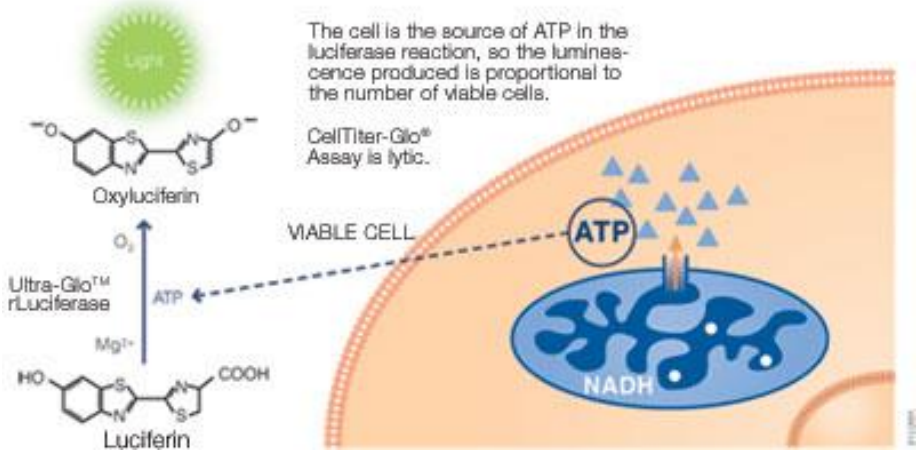

Figure 15. The biochemistry of the CellTiter-Glo® assay.

Source: Promega, 2018.

6.1.2 Method

After incubation with the samples, cells were first washed with PBS and 150µl of HBSS were added in each well. The plate needs to rest at room temperature for 15 min to prepare cells for the next step. CellTiter-Glo buffer was meanwhile transferred into the CellTiter-Glo substrate bottle and 150 µl of the reagent mix was added to the wells. Right after, 200 µl of the resulting solution were transferred in a white 96 well plate (Nunc).

Luminescence was then recorded for 15 minutes with a fluorimeter-luminometer (Fluoroskan Ascent® FL, Thermo Scientific) with an integration time of 0.5 sec and after 10 seconds of shake.

6.2 CellTiter-Blue assay

Measuring cell viability can be carried out through different ways. The CellTiter-Blue (CTB) assay uses the reducing property of viable cell as an indicator of the general cell viability. This assay was performed using the commercial substrate CellTiter-Blue® Cell Viability Assay (Promega). CTB assay is a blue solution kept at -20 °C and thawed before the assay.

6.2.1 Principle

The CellTiter-Blue® assay is based on the ability of living cells to convert a redox dye (resazurin) into a fluorescent product (resorufin). Non viable cells rapidly lose metabolic capacity and therefore are not able to generate a fluorescent signal. Resazurin is dark blue in color and has little intrinsic fluorescence until it is reduced to resorufin, which is pink and highly fluorescent (579 nm Ex/ 584 nm Em). Fluorescence is finally recorded with a fluorimeter (Fluoroskan Ascent® FL, Thermo Scientific). The fluorescent signal measured is directly proportional to the quantity of viable cells (Promega,2018).

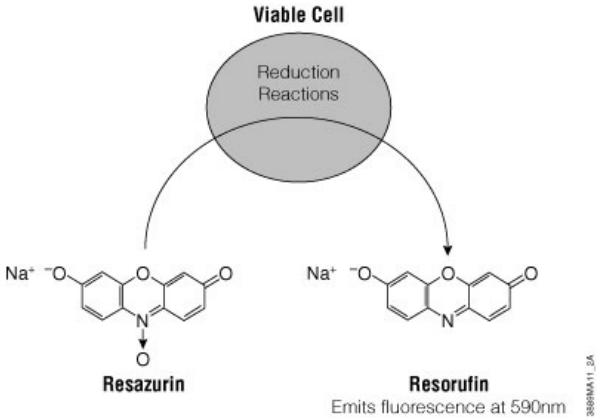

Figure 16. The Biochemistry of CellTiter-Blue® assay.

Source: Promega, 2018.

6.2.2 Method

Before performing the test, a 20% (v/v) CTB solution was prepared by adding 1.5 ml of CellTiter-Blue® to 7.5 ml of HBSS. The resulting mix, so-called "diluted solution", has been used for the assay.

After 3 hours of incubation with the different treatments, plates were first washed with PBS. After adding 357 µl of diluted CTB solution in each well, the plate was incubated 30 min at 37°C. Right after, 300 µl of each well solution were transferred in a black 96 well plate (Nunc). Fluorescence was immediately read with a fluorimeter (Fluoroskan Ascent® FL, Thermo Scientific).

6.3 Crystal Violet cell detachment assay

Commonly used as a histological stain and in Gram's bacteria classification method, crystal violet dye (CV, C3886, Sigma-Aldrich) has been used in this thesis to assess the detachment of the cell layer caused by silver nanoparticles.

6.3.1 Principle

If adherent cells die, they detach from cell culture plate. This simple characteristic can be used for the indirect quantification of cell death upon exposure to toxic agents, AgNPs in our case. A simple method, but not as precise as CTG or CTB assays, to quantify living cells is the staining of fixed cells with crystal violet, a triarylmethane dye that binds to DNA and proteins of adherent cells. Dead cells are lost from the population of cells, reducing the amount of crystal violet staining the culture (Feoktistova *et al.*, 2016).

Once CV is fixed to DNA and proteins, the remaining extracellular dye is removed from the wells. The intracellular CV is then solubilized with an acidic solution. After solubilization, fixed CV is measured with a spectrophotometer. The amount of crystal violet and intensity of the measured signal is proportional to the number of adherent cells.

6.3.2 Method

To perform this assay, 3 different solutions are prepared:

- The fixative solution: 2 % (w/w) PFA (paraformaldehyde, 158127, Sigma-Aldrich) in PBS;
- The coloring solution: 0.125 % (w/w) crystal violet, and 2% (w/w) PFA in 5% (v/v) ethanol (AnalaR NormaPUR, Ethanol absolute, VWR, Fontenay-sous-bois, FR) and 95 % (v/v) Milli-Q water;

- The extractive solution: 30 % (v/v) acetic acid (Acetic acid glacial, Fisher Scientific Chemicals, Leicester, UK) in Milli-Q water.

Once the 48 wells plates washed with PBS, 200 µl of the fixative solution was added per well, for 5 minutes at room temperature (RT). After a second PBS washing, 200 µl of coloring solution were added for 10 min at RT. Crystal violet enters cells and binds to DNA and proteins.

Colored plates were then rinsed 3 times with Milli-Q water that removes unfixed dye. The remaining dye, fixed to DNA and proteins, was then extracted by addition of 200 µl of the extractive solution. 50 µl of each well solution are then transferred in a 96 wells plate containing 200 µl of extractive solution (Nunc). A second transfer of 50 µl in a new 96 wells plate is needed if the coloration is too dark. Absorbance was finally read at 595 nm with a spectrophotometer.

7. AgNPs characterization

Toxicity of AgNPs depends on their physico-chemical properties such as size, shape, surface charge, surface coating, aggregation state and solubility (Zhang *et al.*, 2016).

Characterizing AgNPs becomes therefore very important to understand which properties are affected along their transition through the gastro-intestinal tract and the effect on their toxicity. During this thesis, UV-visible spectroscopy was used for AgNPs characterization.

7.1 UV-visible spectroscopy

7.1.1 Principle

The analyzed AgNPs solution is placed between a light source (UV-visible light beam) and a photon detector. The light beam scans the sample by 1 nm steps. A fraction of the light is absorbed by the sample while the rest is catch by the detector. Absorbance is obtained by measuring the difference between emitted light and transmitted light through the sample. An absorbance spectrum is obtained by reporting all absorbance measures to every wavelength measured (350 – 750 nm).

7.1.2 Method

AgNPs solutions (with and without food matrix) collected after each stage of digestion were poured in polystyrene cuvette (BRAND polystyrene (PS) cuvette, Semi-Macro, 1.5 ml, BrandTech Scientific, Essex, UK) and placed in the sample chamber of the spectrophotometer (Genesys 10S UV-vis, Thermo Scientific).

Absorbance was measured at every wavelength between 350 et 750 nm and saved in a .csv file. Absorbance spectrum was finally obtained after gathering all the data in an Excel sheet.

8. Protein corona assay

When AgNPs are in contact with a biological fluid e.g. a food matrix, they interact specifically with proteins, which modifies their properties. Their surface acquires a new biological identity that disrupt AgNPs stability and interaction with living materials (Rahman *et al.*, 2013). Regarding results of samples containing the food matrix, a hypothesis is assumed: the formation of a protein corona around AgNPs modifies their toxicity on intestinal cells. The goal of this section is therefore to prove the formation of a corona around AgNPs by quantifying the proteins adsorbed on them.

8.1 Isolation of AgNPs-proteins complexes

8.1.1 Principle

In order to quantify proteins of the corona, we need to separate unbound proteins from proteins bound to AgNPs. Generally, it's better to employ nonperturbing methods that do not disrupt the protein-particle complex or induce additional protein binding. The most widely used method separation of particle-associated proteins is centrifugation. After centrifugation, AgNPs sediment in the pellet with their corona while unbound proteins stay in suspension (Cedervall *et al.*, 2007). Supernatant is then discarded, and AgNPs-proteins complexes are resuspended in buffer. Three cycles of centrifugation and resuspension are performed to get rid of most unbound proteins.

8.1.2 Method

- Stock solution preparation

Before beginning the assay, 3 stock solutions were prepared:

- **BSA solution** at 16.8 mg/ml in HBSS.
- **Starch solution** at 26.1 mg/ml in HBSS.
- **AgNPs stock solution** at 911.25 µg/ml in HBSS.

AgNPs solutions 3X concentrated (33.75; 101.25; 303.75 µg/ml) were prepared by a serial dilution of AgNPs stock solution in HBSS.

- Samples preparation

Two kinds of bottles were prepared:

- 4 bottles containing AgNPs at different concentrations (0, 11.25, 33.75, 101.25 µg/ml) in HBSS: 3ml of HBSS and each AgNPs solution 3X concentrated were diluted in 6.078 ml of HBSS.
- 4 bottles containing AgNPs at different concentrations (0, 11.25, 33.75, 101.25 µg/ml) in food matrix: 3 ml of HBSS and each AgNPs 3X concentrated solution were diluted in the food matrix solution consisting of 3 ml of both BSA and starch solutions and 78 µl of triolein.

All samples were incubated one hour at 25°C under agitation (350 rpm).

- Isolation of AgNPs-proteins complexes by centrifugation

1 ml of each **control samples** (AgNPs included in HBSS) was first transferred in 3 microtubes (SuperSpin™ Microcentrifuge Tubes, Polypropylene, 1.5 ml, VWR®, Radnor, Pennsylvania) in order to have minimum three repetitions. These microtubes were especially chosen according to previous results showing that AgNPs were not able to adsorb on their walls.

All samples went then through a serie of 3 centrifugations, each one being conducted as follows:

I. Centrifugation at a speed of 14 000 xg during 40 min in a microcentrifuge (Microcentrifuge 5417 C, Eppendorf, Hamburg, DE).
II. Elimination of the supernatant in a chemical waste: about 30 µl corresponding to the pellet of AgNPs needs to remain in the Eppendorf.
III. Solubilization of the pellet in 1 ml of Milli-Q water at pH 7.

Samples containing the food matrix undergo a special process before centrifugation to get rid of the excess of starch. Starch can indeed disrupt the measure since it's heavy and troubles the solution.

1.2 ml of each solution was transferred in 3 microtubes in order to have triplicates. All microtube undergo a series of three centrifugations: first centrifugation at 200 xg for 1 minute and 2 other ones at 2000 xg for 1 minute. After each centrifugation, 1 ml supernatant is transferred in a new microtube. This aims at eliminating the starch of the pellet is to leave just a small fraction of it in solution when the following centrifugations will be carry out.

After the third centrifugation, 1 ml of samples was transferred in new microtubes. Then all samples went through a series of 3 centrifugations as follows:

I. Centrifugation at a speed of 6000 xg during 60 minutes in a microcentrifuge.
II. Elimination of the supernatant in a chemical waste: just as before, 30 µl of pellet remains in the microtube.
III. Solubilization of the pellet with 1 ml Milli-Q water.

Centrifugations of both kind of samples, control and matrix samples were carried out simultaneously in 2 different centrifuges to save time.

After both third centrifugations, the pellet was not solubilized but saved for the micro BCA assay.

8.2 Protein quantification : microBCA assay

To perform protein quantification, a commercial kit is used: the Thermo Scientific Micro BCA Protein Assay Kit (Thermo Fisher Scientific, Waltham, MA). This special kit, based on the same principle as the popular Pierce BCA Protein assay, is optimized to measure (A=562 nm) total protein concentration of a dilute protein concentration solution (Thermo Fischer Scientific, 2018).

8.2.1 Principle

This assay provides a colorimetric detection and quantitation of total protein. It is based on the reduction of Cu^{2+} to Cu^{+} by proteins in an alkaline environment. Cu^{+} is then chelated by two molecules of bincichoninic acid (BCA) and forms a water-soluble purple complex. This product shows a strong absorbance at 562 nm, which is directly proportional with protein concentration. Three parameters are known to be responsible for complex formation with BCA: macromolecular structure of proteins, the number of peptide bonds, and the presence of 4 amino acids (cysteine, cystine, tryptophan and tyrosine)

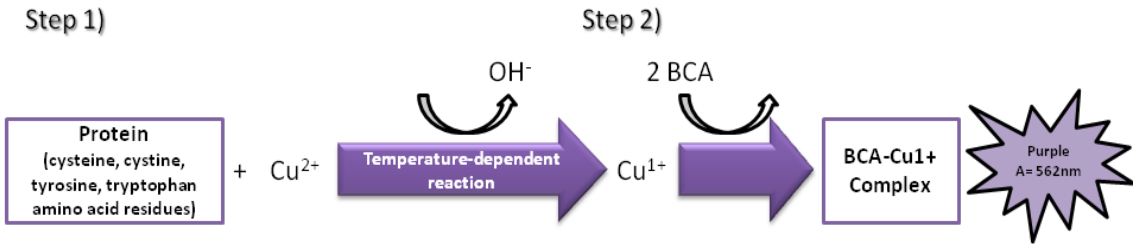

Figure 17. The principle of BCA assay.

Source : http://microamaze.blogspot.be/2015/10/bicinchoninic-acid-bca-assay-for.html

8.2.2 Method

- BSA standards preparation

In order to quantify the total amount of proteins in each sample, a BSA scale for each AgNPs concentration tested (0; 11.25; 33.75;101.25 µg/ml) needed to be prepared. These scales were then converted into standard curves, useful during results treatment.

To prepare these BSA scales, silver nanoparticles of each concentration have to go through a centrifugation process first. For that, an AgNPs stock solution was prepared at 607.5 mg/ml in Milli-Q water at pH 7. From this stock solution, solutions of AgNPs 2X concentrated at 22.5, 67.5 and 202.5 µg/ml were prepared by a serial dilution in Milli-Q water.

Each AgNPs solution 2X concentrated was then transferred into 6X1 ml microtubes. These 18 microtubes were centrifugated at 14 000 xg for 40 minutes, at the same time as the third centrifugation of control samples. The supernatant was eliminated in a chemical waste, so we used these pellets to create BSA scales.

During the third centrifugation of control samples, the BSA solutions 2X concentrated formerly prepared in Milli-Q water were thawed. These solutions contained respectively 0, 100, 200, 500, 1 000, 1 500, 2 000 and 3 000 µg/ml of BSA.

Eventually, 4 kinds of BSA standards scales were prepared by mixing 15 µl of each BSA solutions 2X concentrated with 15 µl of pellet of each AgNPs solutions 2x concentrated:

- A BSA scale (0-1500 µg/ml) without AgNPs
- A BSA scale (0-1500 µg/ml) with 11.25 µg/ml of AgNPs
- A BSA scale (0-1500 µg/ml) with 33.75 µg/ml of AgNPs
- A BSA scale (0-1500 µg/ml) with 101.25 µg/ml of AgNPs

- Micro BCA assay

First, the assay reagent is prepared by mixing the 3 reagents provided by the Micro BCA Protein Assay Kit: 12.5 ml of reagent A, an alkaline tartrate-carbonate buffer, 12 ml of reagent B, the bicinchoninic acid solution and 500 µl of reagent C, a copper sulfate solution. The resulting solution is called “working solution”.

30 µl of each pellet samples are transferred in new microtubes. So, besides the 4 BSA scales (32 microtubes), 12 microtubes contained control samples and 12 microtubes contained AgNPs in food matrix samples. 400 µl of working solution was added to all 56 microtubes. Each of them was vortexed before incubation at 60°C in the water bath for 60 minutes.

After incubation, all microtubes containing silver nanoparticles (including the BSA scales) were centrifugated 20 minutes at 14 000 xg. As a final step, 50 µl of each supernatant was transferred in a 96 wells plate (Nunc) and absorbance read at 562 nm.

9. Statistical Analysis

Each assay described previously has been repeated several times, following the same protocol. Throughout these repetitions, replicates were carried out; every condition (AgNPs concentration or dilution) was at least repeated three times.

Statistical analyses were performed using the JMP PRO 13.0 software (SAS Institute Inc, North Carolina). For all statistical tests, results were considered significant at the level α= 0.05. In case of multiple testing, a Bonferroni-Sidak correction was applied to the level α(α= 1-(1-0.05)(1/comparison number)) (Šidàk, 1967).

The same method was used for protein corona quantification and the cytotoxicity assays to measure the impact of the food matrix and digestive enzymes on intestinal cell.

First, normality of the data and homogeneity of the variance were assessed with the Shapiro-Wilk's test and Levene's test respectively. These two conditions determine if a one-way ANOVA could be used. As all data had unequal variances, one-way ANOVA could not be applied and a more robust ANOVA, called Welch ANOVA, was used. Finally, treatments were compared either individually to the control or with each other with Student's test.

For the cytotoxicity assays of AgNPs, a LogLogistic model was fitted to the data for each condition. The function of the LogLogistic model was:

$$f(AgNPs\ cc) = \frac{100}{1 + exp(b \times ln\left(\frac{AgNPs\ cc}{EC50}\right))}$$

where AgNPs cc is the concentration of AgNPs (µg/ml), b is the steepness of the dose-response curve and EC50 is the median effect concentration. The lower and upper limits of the response were set at 0 and 100 respectively.

The EC50s and their standard errors were obtained by estimating the parameters of these models. Finally, for each assay, Wheeler ratio tests were performed to highlight significant differences between EC50s from the four treatments (Wheeler *et al.*, 2006).

RESULTS & DISCUSSION

1. Preliminary remarks

1.1 AgNPs concentrations

AgNPs concentrations used for this thesis were 11.25, 33.75 and 101.25 µg/ml. They were chosen to obtain a definite cytotoxic effect in all assays. Clearly, these are overestimations of the nanosilver human daily ingestion, based for this thesis, on the worst-case scenario of 1.25 mg nano-Ag/day according to the Danish Ministry of Environment (2015). This estimation could underestimate the real amount of daily ingested AgNPs since it concerns only AgNPs found in food supplements while they are increasingly incorporated in many other food products (packaging coatings, kitchenware, …) (van den Brule *et al.*, 2016). Nevertheless, the goal of the present work is to assess the impact of digestive enzymes and food components on toxic amount of AgNPs. Hence the concentrations 10 to 100 times higher than the amount of AgNPs ingested daily through food supplements; insuring a harmful effect of AgNPs on intestinal cells.

1.2 Food matrix concentrations

For this master thesis, the three main food macronutrients were represented by their standard counterparts: bovine serum albumin (BSA), wheat starch and triolein, as used in Hollebeeck's protocol (2013). BSA was used at 5.6 mg/ml, starch at 8.7 mg/ml and triolein at 7.8 mg/ml. Concentrations were chosen to take in account volumes of ingested and secreted fluids such as relative proportions of the three major dietary macronutrients being carbohydrates, proteins and fats (Hollebeeck *et al.*, 2013). Concentrations were calculated in a way that is reflective of the concentrations found at the intestinal level. The calculation is simple: the amount of the macronutrient needed daily (taken from the macronutrients reference intakes Table 1) is divided with the total amount of gastro-intestinal fluids and water (Table 2) that are daily in contact with the ingested food:

- **BSA** : 50 g (proteins) / 9L = 5.55 g/L ~ 5.6 g/L.
- **Triolein** : 70 g (total fats) / 9L = 7.77 g/L ~ 7.8 g/L.
- **Starch**: 260 g (carbohydrates) / 9L = 28.88 g/L ~ 28.9 g/L. 30 g/L of starch being not soluble at all, we took 30 % of it for our food model: 0.3 x 28.9 g/L = 8.67 g/L ~ 8.7 g/L.

Macronutrients and energy reference intakes from "Regulation 1169/2011, Annex XIII, part B	
Energy or nutrient	**Reference intake**
Energy	8 400 kJ (2 000 kcal)
Total fats	70 g
Saturated fatty acids	20 g
Carbohydrates	260 g
Sugars	90 g
Proteins	50 g
Salt	6 g

Table 1. Macronutrients and energy reference intakes.

Source: adapted from EU regulation N°1169/2011 on the provision of food information to consumers.

Gastro-intestinal fluids	9L/day
Saliva	1 L
Gastric juice	2 L
Bile	1 L
Pancreatic juice	2 L
Intestinal juice	1 L
Water	2 L

Table 2. Amount of digestive fluids produced daily.

Source: Adapted from Hollebeeck *et al.*, 2013.

2. Impact of the food matrix and digestive enzymes on intestinal cells

Although the GIT and food have been demonstrated to alter AgNPs properties and cell's interactions, only few studies take in account these effects (Deloid *et al.*, 2017).

In this thesis however, we assess the impact of food components and digestion on the toxicity of AgNPs (NM-300K). To simulate transformations occurring in the GIT, AgNPs were incorporated into a modelized food matrix and subjected to an *in vitro* digestion. Then, we used an *in vitro* intestinal cell model, a co-culture model representing enterocytes (Caco-2 cells) and goblet cells (HT29-MTX) for *in vitro* assessment of cytotoxicity of the treated AgNPs.

To carry on such a study, the protocol used needs to assess AgNPs toxicity without being biased by the inherent toxicity of the digesting solution. Thus, a preliminary study has been carried out to assess the impact of digestion and food on intestinal cells. Indeed, studying the cytotoxicity of digested AgNPs contained in a food matrix implies that treated silver NPs are not incubated alone on the cell model but together with the digesting solution comprised of the food matrix and digestive enzymes. Erasing the potential toxicity of the digesting solution is necessary to avoid biased results and thus, to focus only on the transformations occurring to AgNPs that consequently affect their toxicity. For that, a solution is to dilute digesting solutions so that digestive enzymes and food matrix that are inevitably added on cells with AgNPs are at non-toxic levels.

Experimentally, two treatments, the food matrix model and a HBSS solution (control) have undergone an *in vitro* digestion divided in 3 stages, simulating transformations occurring in the GIT:

- the salivary phase: 10 min incubation with α-amylase at pH 6.9.
- the gastric phase: 2 hours incubation with pepsin under anaerobic conditions at pH 2.0.
- the duodenal phase of digestion: 2 hours incubation with a mix of pancreatic enzymes and bile under anaerobia at pH 7.0.

A third solution containing the food matrix undigested was also prepared. These three treatments, "digested HBSS", "digested food matrix" and "undigested food matrix" were then incubated 3 hours on the Caco-2/HT29-MTX cell model. These were previously diluted 1, 2, 4 and 8X before incubation, in order to find the dilution of the food matrix/digestive enzymes mix that would eliminate the potential harmful effect on the cell lines so that false positive or overestimated results should be prevented. Controls of "undigested HBSS" (positive control) and Triton X-100 (negative control) were also tested simultaneously with the different dilutions. As a final step, the cell viability of the cell model after the incubation with the treatments was tested through the three different assays: CellTiter-Glo®, CellTiter-Blue® and crystal violet.

2.1 Impact of dilution on the cytotoxicity of the digested HBSS control

This first treatment, "digested HBSS", aims at assessing the potential toxicity of digestive enzymes on intestinal cells. Indeed, HBSS is the buffer solution so that only the impact of the digestive enzymes is prospected here. Empirically, the goal is to see if digestive enzymes are toxic undiluted, and if they are, which dilution can cancel their deleterious effect.

Results are shown in Figure 20. They were obtained from four independent repetitions with triplicates performed for each dilution or control. Cell viability was evaluated via the CTG, CTB and CV assays; each

of them testing the following different conditions: dilutions of the *in vitro* digested HBSS (1X, 2X, 4X and 8X), the HBSS positive control and Triton-100 negative control.

Regarding Figure 18, a common observation can be found in the three assays: the positive control and the undiluted digested HBSS were significantly different from the control, meaning that digested enzymes are highly cytotoxic if undiluted. In CTG and CTB assays, dilution 8X became also significantly different form the control. This observation, however, is not consistent, especially when results showed that lower dilutions (2X and 4X) were non-toxic in all assays. As a general first outcome, we can speculate that diluting two times should be enough to reduce substantially the toxic effect of digestive enzymes.

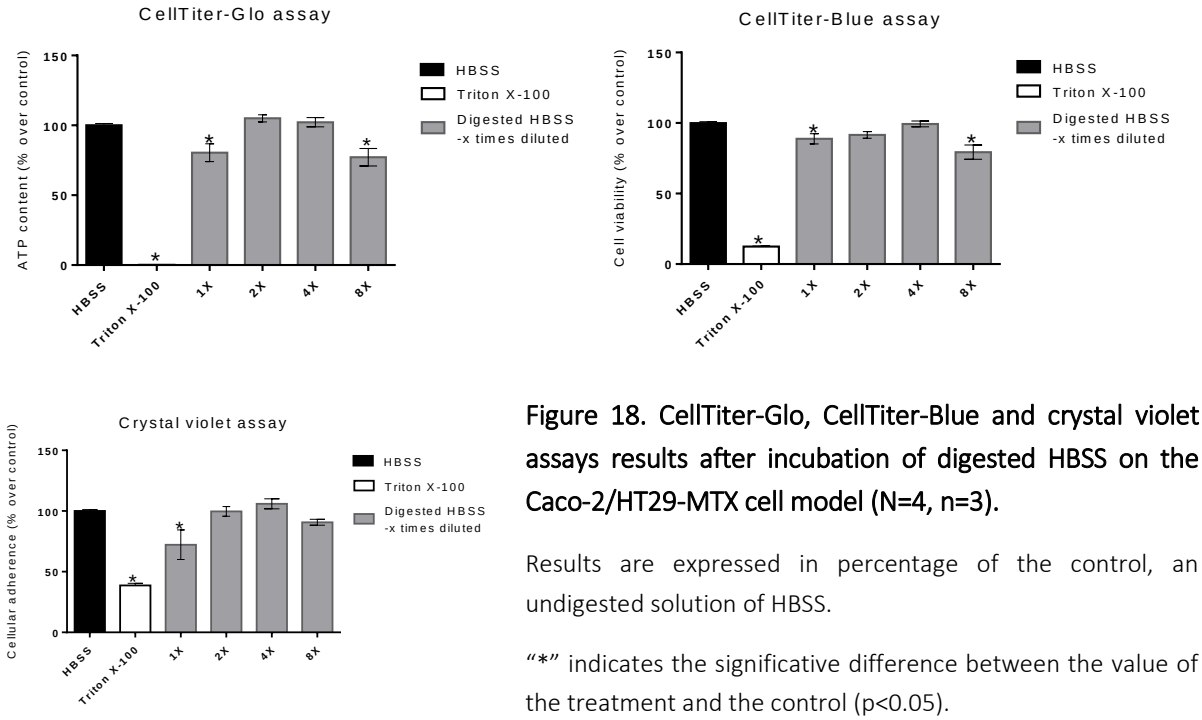

Figure 18. CellTiter-Glo, CellTiter-Blue and crystal violet assays results after incubation of digested HBSS on the Caco-2/HT29-MTX cell model (N=4, n=3).

Results are expressed in percentage of the control, an undigested solution of HBSS.

"*" indicates the significative difference between the value of the treatment and the control ($p<0.05$).

2.2 Impact of dilution on the cytotoxicity of the undigested food matrix

Once the toxicity of the digestive enzymes assessed, we evaluated the cytotoxicity of the food matrix, first without being primary digested and then, after an *in vitro* digestion. As before, Triton X-100 and HBSS were the controls and the same dilutions of the food matrix were prepared before incubation on the cell model (1X, 2X, 4X and 8X). Results of the cytotoxicity assays are shown in Figure 19. They were obtained from four independent repetitions with triplicates performed for each dilution of the undigested food matrix or control.

Regarding results of the CTG assay, a slight reduction of ATP content can be observed when the undiluted food matrix was added: this effect is significantly different from the control and suggests a toxicity of the food matrix that is not demonstrated by the other assays. Nevertheless, ATP content rose as the dilution increased (2X and 4X), except for the last dilution where ATP content dropped but was still non-significantly different from the control. For the CTB assay, undiluted food matrix was not toxic whereas diluted 2X was significantly different from the control, which is not consistent. Regarding the effect on cellular adherence, the positive control was the only one showing substantial toxicity. No reduction of the cellular adherence was observed at any dilution. However, in CTB and CTG, a slight

reduction of the viability was observed for all dilutions suggesting that food matrix had a potential slight toxic effect.

For this case, since the three cytotoxicity assays tend to show divergent results, concluding on the necessity of diluting the undigested food matrix is delicate. Of course, these results must be moderated with those obtained when the digestion effect is taken in account as presented on Figure 22.

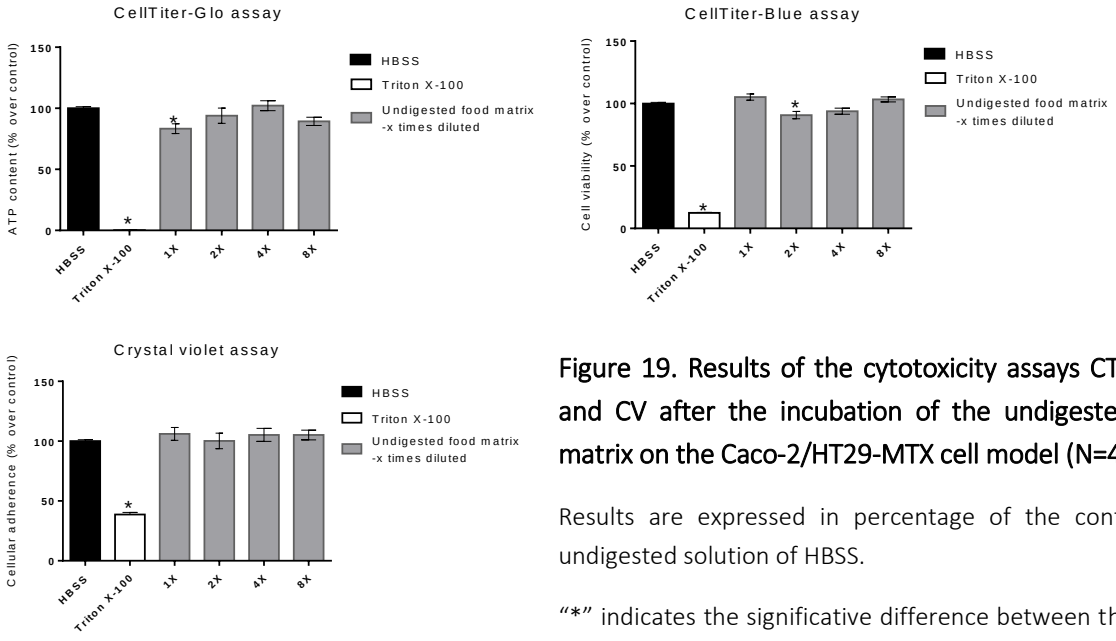

Figure 19. Results of the cytotoxicity assays CTG, CTB and CV after the incubation of the undigested food matrix on the Caco-2/HT29-MTX cell model (N=4, n=3).

Results are expressed in percentage of the control, an undigested solution of HBSS.

"*" indicates the significative difference between the value of the treatment and the control ($p<0.05$).

2.3 Impact of dilution on the cytotoxicity of the digested food matrix

As a final step of this preliminary study, both effects, *i.e.* digestion and food matrix, were assessed together on the Caco-2/HT29-MTX cell model. The food matrix model comprised of BSA, starch and triolein went through an *in vitro* digestion and was incubated on cells after being diluted as previously (1X, 2X,4X and 8X). Same controls as previous were used, and same cytotoxicity assays were performed as well. Presented in Figure 20, results came from four independent repetitions with triplicates performed for each dilution of the digested food matrix or control.

If undiluted, the digested food matrix induced a significant toxicity on ATP content and number of adherent cells; a significant difference from the control was observed for the CTG and CV assays. Diluting the digested food matrix (2X) helped to recover ATP content and cellular adherence values similar to the control.

CTB assays showed no significant toxicity of the undiluted treatment even if there was a more important reduction of cell viability observed for the undiluted treatment than the other dilutions. It can be explained by the large standard deviation of the 1X bar. Besides, 80 % of viable cells were measured after incubation with digested food matrix (1X) while the undigested food matrix (1X) could keep the cell viability to 100 %. This highlights the toxic effect induced by the digestive enzymes, that can also be demonstrated if CV graphs of undigested and digested food matrix are compared.

Regarding all results, the digested food matrix is considered toxic for intestinal cells as it strongly impairs ATP content and cellular adherence (cell viability was also reduced but in a non-significative way). Therefore, diluting 2X the digested food matrix can bring back to a decent cell viability.

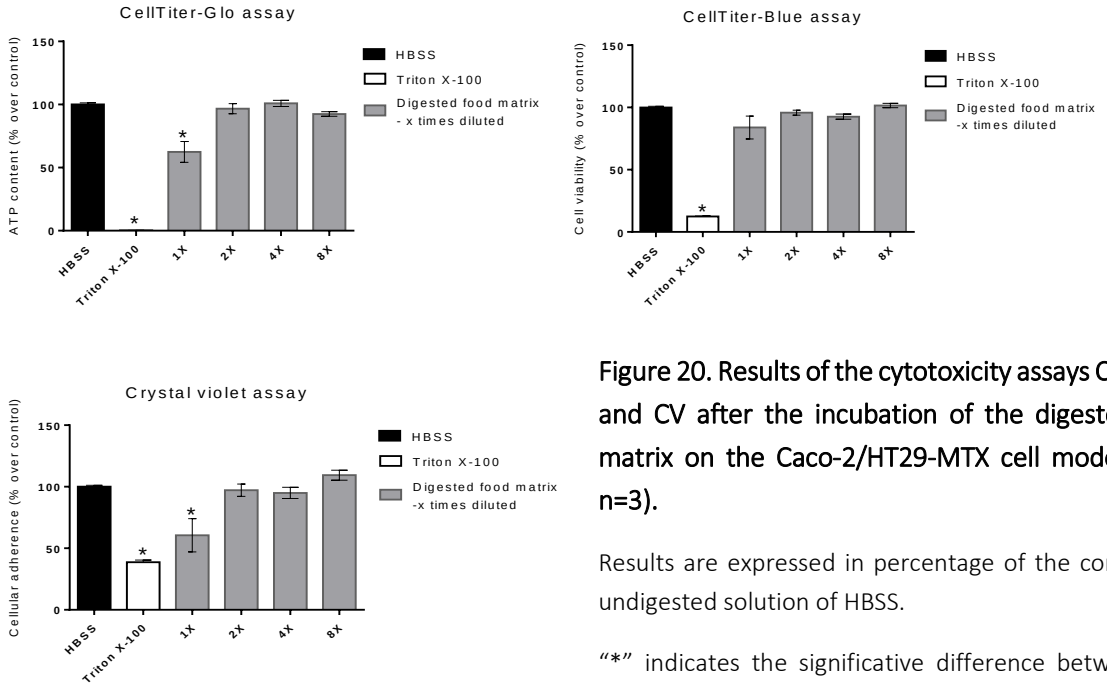

Figure 20. Results of the cytotoxicity assays CTG, CTB and CV after the incubation of the digested food matrix on the Caco-2/HT29-MTX cell model (N=4, n=3).

Results are expressed in percentage of the control, an undigested solution of HBSS.

"*" indicates the significative difference between the value of the treatment and the control ($p<0.05$).

As a general outcome of those results, a dilution 2X appears necessary to avoid digestive enzymes toxicity whether included in HBSS solution or in the food matrix. Results concerning the toxicity of the undigested food matrix were not convergent, so the need of a dilution could not be demonstrated. However, the CTG showed a significant reduction of ATP level for the undiluted food matrix compared to the control and a recovery of nontoxic values after diluting 2 times. Therefore, a dilution 2X of all treatments before their incubation on intestinal model will be carried out in order to put all treatments under the same conditions. Experimentally, choosing this dilution over the higher ones is more realistic but also practical and economical.

2.4 Discussion

Our results showed that digestive enzymes were cytotoxic if used undiluted on the coculture model Caco-2/HT29-MTX. The undiluted food matrix, which was considered as not harmful for the intestinal cells, became toxic after going through the *in vitro* digestion process. Therefore, it is supposed that the toxicity of the digestates is mainly attributable to the digestive enzymes. Since the digestating solution will be incubated along with AgNPs, its toxicity needs to be eliminated in order to show only the impact of transformed AgNPs on intestinal cells. To this end, different dilutions of the digesting solutions were tested. According to our results, a two times dilution seems to be enough to eliminate the inherent toxicity of the digesting solution.

In the present work, we choose to dilute the digesting solutions in order to remove their toxicity, but alternative techniques exist and were used in many studies. To cite one, Markell *et al.* (2017) studied the impact of exposure of innocuous dietary proteins or hazardous proteins untreated or exposed to digestive enzymes on Caco-2 cell monolayers. Proteins were exposed to a simulated gastric fluid

containing pepsin, followed by the exposure to a simulated intestinal fluid containing pancreatic enzymes. Before application on Caco-2 cells, digestive fluids were inactivated to ensure that the enzymes activities would not alter viability of monolayers: pH of digestate was raised to inactivate pepsin while pancreatin was heat-inactivated.

In our case, pepsin is already inactivated during the *in vitro* digestion process. Indeed, the pH rises from 2.0 to 7.0 between the gastric and the intestinal step. So, the final digestate contains an inactivated pepsin but an active pancreatin. However, using heat inactivation for pancreatic enzymes would not be applicable to our experiment. Indeed, heat inactivation has already been tested previously in the lab and impaired strongly AgNPs properties. The AgNPs solution, which was yellow colored at the end of the digestion changed to red after heating (personal communication). This is in line with Yeshchenko *et al.* (2012) observations. They increased the temperature from 0 to 204 °C of samples containing AgNPs of 11 nm size and observed that the surface plasmon resonance shifted to red. They explained that the increase of the temperature leads to the thermal expansion of the NPs, increasing the volume of NPs but decreasing the density of free electrons, which have subsequently lead to the red shift.

Another possible technique to inactivate digestive enzymes is the addition of serum after the digestion of the treatments. Serum is indeed effective to inhibit enzyme's activity thanks to the presence of trypsin inhibitors. In her master thesis, in our lab, L. Laloux (2013) added 10 % (v/v) FBS on samples after the *in vitro* digestion of AgNPs solutions and controls to inhibit enzymatic activity. However, the toxic effect of AgNPs appeared to be modified in the presence of serum. Indeed, the major constituents of FBS are globular proteins, bovine serum albumins that could potentially impair AgNPs properties. Indeed, Yi *et al*. (2016) study indicated that BSA changed the diameter, zeta potential and Ag^+ dissolution of citrate-stabilized AgNPs and concluded that BSA attenuated AgNPs toxicity on the white-rot fungus, *Phanerocaete chrysosporium*.

Given these considerations, the dilution method should be the most appropriate. The general outcome of this preliminary study was the need of diluting two times digesting solutions for them to prevent a toxic effect on the coculture model. This result is in line with the previous master thesis completed in the lab. In 2016, L. Mignard assessed the impact of *in vitro* digestion on AgNPs toxicity on the same coculture model of the intestinal barrier as used in this thesis. Inherent toxicity of digestive enzymes was demonstrated using two permeability assays (TEER and lucifer yellow) and assessment of ATP content. Just as concluded in this thesis, a dilution of 50 % of the digestive enzymes showed no toxicity to intestinal cells.

Lichtenstein *et al.* (2015) compared the cytotoxicity of undigested AgNPs, digested AgNPs and digested AgNPs with food components on Caco-2 cells with CellTiter-Blue assay. The digestion fluids alone were also tested but the food components alone were not. The *in vitro* digestion process was comparable to ours such as food components (olive oil, starch and milk powder from consumer products). They observed a strong cytotoxicity of the digestive fluids if used undiluted. So, they proceeded to a dilution in cell culture medium containing serum of 10-, 20-, 33-, 35- and 40 times (along with the dilution of the digested stock AgNPs solution, initially at 1mg/ml). Their digestion control did not reduce cell viability significantly at any dilution and therefore was considered not toxic (viability was not significantly reduced to 87 % for the 10X dilution). This is in line with our results as the need of a dilution could be demonstrated and reduced significantly toxicity of digestive enzymes. However, the concentration of

the enzymes in their 10X diluted treatment correspond to our undiluted digesting solution and while theirs was not toxic, ours induced significant reduction of cell viability. This could be explained by differences in experiment protocols: digesting solutions, previously diluted in cell culture medium with serum were incubated 24h on cells. Since serum contains trypsin inhibitors, the toxicity of digesting solution could be reduced. However, the digestion fluid mixture with food components was toxic when diluted 10 times but did not induce significant reduction for higher dilutions. Considering that enzyme concentrations used in this thesis for the undiluted treatments were similar to their dilution 10X, results of Lichtenstein are in line with ours, as CTG and CV clearly showed a toxicity of the undiluted digested food matrix and recovery of nontoxic values after diluting 2X. This corresponds to the absence of toxic effect if the digestion control + food matrix is digested 20 X.

Böhmert *et al.* (2014), made a similar study: they proceeded to an *in vitro* digestion of AgNPs (14 nm diameter) and looked at the impact on toxicity for human intestinal cells (Caco-2 cells). A control, consisting of the complete digestion fluid mixture after the artificial digestion without AgNPs was also tested and had a strong toxic effect on cells regarding CTB results, which impaired results interpretation. Lichtenstein 's *in vitro* digestion was replicated from Böhmert's study, meaning that initial concentrations of digestive enzymes used in both protocols were the same. When Lichtenstein proceeded to dilutions of the treatment to avoid enzymes toxicity before incubation on cells, Böhmert did not proceed to further processing of the samples after digestion, which explains their toxic results and suggests the dilutions carried out by Lichtenstein one year later.

These two previous studies highlight the fact that considering the impact of digestive enzymes and looking for their toxic effect beforehand is important in toxicological studies such as ours.

3. Impact of the digestive enzymes and food components on AgNPs toxicity on intestinal cells

Silver nanoparticles have become increasingly prevalent as antibacterial agents: they are found in the highest number of consumer products (Vance *et al.*, 2015). Such a widespread use leads to a higher human and environmental exposure and arise great concerns about their potential undesirable side effects. Many studies have been carried out and indicated the harmful effect of AgNPs in both *in vitro* and *in vivo,* mammalian and human models. These toxicological studies about AgNPs have only been performed and published in the past 15 years while the intensive use of AgNPS dates back to the 80's and the current number of applications incorporating AgNPs is growing exponentially (Stensberg *et al.*, 2011; Syafiuddin *et al*. ,2017)

Over the past few years, the use of AgNPs in food products has soared to a such extent that ingestion is currently considered as the one of the biggest sources of human exposure (Bove *et al.*, 2017). Therefore, toxicological studies should investigate the toxicity of orally ingested AgNPs. However, consumer protection research does not always keep up with the rate of industrial progress. Indeed, only few studies that took in account the physicochemical transformations occurring to AgNPs before they reach the intestinal cells and the interactions with food components, are available. They are recent (e.g. Lichtenstein *et al.*, 2015) but already could demonstrate changes in AgNPs behavior, size, stability, dissociation and aggregation throughout human digestion resulting from the strong shifts of pH, temperature, and concentration of enzymes and salts. Indeed, AgNPs are known for agglomerating as

the pH decreases, adsorbing enzymes and proteins on their surface, forming a protein corona when they are in contact with biological fluids and tending to have a higher dissolution in high ionic strength solutions. All these phenomena occur during the digestion and can modulate AgNPs toxicity; they must therefore be considered seriously in toxicological studies in order to obtain conclusive and realistic results. The purpose of this thesis is in line with these considerations as its subject is the study of the impact of digestive enzymes and food matrix on AgNPs toxicity.

To reproduce a realistic human ingestion scenario that reproduces conditions to which ingested AgNPs are subjected through the GI tract, an *in vitro* digestion including food components was carried out during this thesis. Different concentrations of AgNPs (0, 11.25, 33.75 and 101.25 µg/ml) were tested either in a control solution of HBSS or in a modelized food matrix containing bovine serum albumin, wheat starch and triolein, aiming at mimicking proteins, carbohydrates and fats respectively. Then, AgNPs were digested *in vitro*. The process we used recreated the three main precolonic digestive stages (salivary, gastric and intestinal) by adjusting pH, digestive enzymes and duration of incubation. While AgNPs were at 37 °C and under stirring during the whole digestion, they went through different conditions for each step:

- Salivary: pH 6.9, α-amylase, 10 min.
- Gastric: pH 2.0, pepsin, 2 hours, N_2 saturation.
- Intestinal: pH 7.0, bile and pancreatin, 2 hours, N_2 saturation.

Treated AgNPs and their undigested controls (all diluted two times) were then incubated for 3 hours in an *in vitro* model of the intestinal epithelium, the co-culture model Caco-2/HT29-MTX modelling enterocytes and goblet cells. In total, four different treatments were compared among each other: undigested AgNPs without food matrix, undigested AgNPs with food matrix, digested AgNPs without food matrix and digested AgNPs with food matrix. As a final step, solutions were removed, cell lines washed, and cell viability estimated through three assays: CellTiter-Blue®, CellTiter-Glo® and Crystal violet. These three assays are typically used for cytotoxicity testing; they assess the metabolic activity, intracellular energy and cell death with the number of adherent cells.

3.1 Interference

Due to their high surface activity, AgNPs can interact with a multitude of compounds and substances including assay reagents of the cytotoxicity assays. Such problematic interactions could lead to false-positive or false-negative results, which will ultimately lead to a misinterpretation of AgNPs toxicity. To confirm the validity of results obtained, these potential interactions between AgNPs and assay reagents have to be verified.

To this end, interference assays were carried out. The methods and results of these interference assays can be found in the appendix. Each interference test has two independent repetitions; each concentration having three replicates (N=2, n=3). A statistical analysis was not performed but yet, the six replicates were reliable enough to prove clear results about AgNPs interferences.

Regarding results obtained, no interference was concluded between AgNPs and assay's reagents. Silver nanoparticles showed no interferences with the CTB and CV assays but if high concentrations of AgNPs are in contact with CTG assay, they induce a strong interference, reducing highly the response of the assay.

However, when the different treatments of AgNPs in HBSS buffer or included in a food matrix were incubated on cell lines, a removal of the solutions after the incubation and a washing step with a buffer (PBS) were actually carried out. The remaining potential AgNPs quantities were thus not great enough to interfere with the fluorescent or luminescent signal or mask the assays product signal (resorufin, oxyluciferin or crystal violet).

3.2 Cytotoxicity assays

In order to assess the impact of digestive enzymes and food components on the toxicity of AgNPs, three different assays were used: CellTiter-Glo, CellTiter-Blue and crystal violet.

The CellTiter-Glo kit determines the proportion of viable cells by measuring the amount of ATP left in the cells after incubation with toxic compounds. Luciferase present in the assay solution, uses ATP to convert luciferin into oxyluciferin, a reaction emitting light. The luminescence measured can then be converted into amount of metabolically active cells.

The measurement of the ATP content by CTG assay assess a very important marker of cell viability: the production of intracellular energy, a parameter highly sensitive to stressful situations. CellTiter-Glo assay provides therefore more sensitive results than CTB or CV. Besides, since ATP is produced through the action of enzymes located in the mitochondria, if its release is reduced, this test reveals, among other things, the mitochondrial toxicity of AgNPs.

The CellTiter-Blue assay gives a general overview of the oxidative metabolism of viable cells trough the conversion of resazurin, a redox dye into a fluorescent end-product, resorufin. If cells are non-viable, their metabolic activity is rapidly lost, so a fluorescent signal will not be generated. CTB has, however, a specific effect of exhibiting the presence of viable reducing proteins. Asharani *et al.* (2009), indicated that mitochondrial damage could also be exhibited by a reduced dehydrogenase activity with the conversion of resazurin to resorufin of the CTB assay.

Crystal violet assay gives a complementary information about cell viability, assessing the number of cells still adherent in the wells. The dye crystal violet can indeed bind to the DNA of adherent cells. Absorbance of the bounded CV is then measured and indicates the proportion of adherent cells.

Figure 21 shows the results of the three assays explained formerly: (1) CellTiter-Glo (2) CellTiter-Blue, (3) Crystal violet. For each assay, results were obtained from 4 independent repetitions with triplicates for each tested concentration: 0, 11.25, 33.75 and 101.25 µg AgNPs/ml. Results of ATP content, cell viability and adherent cells after incubation with the 4 different treatments are represented in percentage of the respective controls. Dots correspond to the experimental values while plain curves are obtained with the log-logistic prediction model.

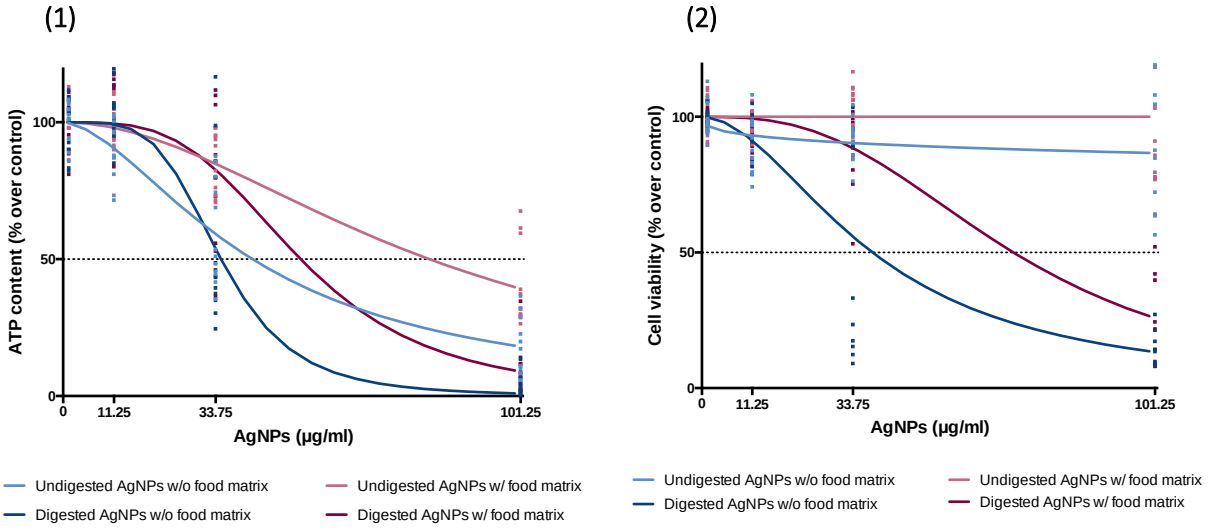

Figure 21. Results of the CellTiter-Glo assay (1) CellTiter-Blue (2) Crystal violet (3) assays after exposition on the Caco-2/HT29-MTX of the following treatments: undigested AgNPs without food matrix (light blue) and with food matrix (light red) and digested AgNPs without food matrix (dark blue) and with food matrix (dark red) (N=4, n=3).

Curves are expressed in percent of the respective controls corresponding to solutions without AgNPs. Dots correspond to the experimental values while plain curves are obtained with the log-logistic prediction model.

Table 3 shows the parameters of the curves modelized by the log-logistic model: EC50 and b parameter. "N.D" is indicated when parameters could not be estimated because the data could not be modelized by a log-logistic model in the range of concentrations tested. Statistical analysis of EC50 differences is also indicated with letters in exponent.

	CTG		CTB		CV	
	EC 50	b parameter	EC 50	b parameter	EC 50	b parameter
1 Undigested AgNPs w/o FM	41.93 ± 2.91$^{a, b}$	1.71 ± 0.19	N. D	N. D	N. D	N. D
2 Digested AgNPs w/o FM	34.97 ± 1.79^{a}	4.37 ± 3.60	38.13 ± 4.04 ^{a}	1.92 ± 0.38	24.87 ± 2.38 ^{a}	1.89 ± 0.31
3 Undigested AgNPs w/ FM	81.07 ± 4.42^{c}	1.97 ± 0.22	N. D	N. D	N. D	N. D
4 Digested AgNPs w/ FM	52.56 ± 4.47^{b}	3.54 ± 0.60	69.62 ± 4.80 ^{b}	2.82 ± 0.41	61.07 ± 6.93 ^{b}	4.2 ± 0.88

Table 3. Estimates parameters from Loglogistic model for each cytotoxicity assay: CellTiter-Glo (CTG), CellTiter-Blue (CTB) Crystal violet (CV). EC50 refers to the concentration of AgNPs that induces a response halfway between the baseline and the maximum while b parameter represents the slope of the curves. "N.D" is indicated when parameters could not be estimated because the data could not be modelized by a loglogistic in the range of concentrations tested. For the CTG assay, treatments not connected with the same letter have EC50s significantly different from each other (Wheeler ratio test, $p < 0.0085$ due to Bonferroni-Sidak correction). For the CTB and CV assays, treatments 2 and 4 only were compared since treatments 1 and 3 could not be modelized.

Treatments not connected with the same letter have EC50s significantly different from each other (Wheeler ratio test, $p < 0.05$).

3.3 Results analysis

As this study is assessing the effect of two parameters (digestives enzymes and food components) on AgNPs toxicity, results will be examined by looking at both effects first separately and then conjointly.

First the effect of the food matrix can be analyzed by comparing undigested treatments between them (light blue curve = without food, light red curve = with food).
Regarding the CTG graph, ATP is highly reduced with pristine AgNPs (meaning here that they were not digested and not included in a food matrix): only 20 % of ATP remained with the highest concentrations. If the food matrix is added (light red curve), ATP content is higher for all concentrations, with twice more ATP measured (40 %) at the 101.25 µg AgNPs/ml. The food matrix seems to significantly buffer the toxic effect of undigested AgNPs. EC50 of the light blue curve is 42 µg/ml and is increased significantly to 81 µg/ml upon the addition of the food matrix.

Regarding CTB and CV graphs, comparing statistically these two curves is impossible since parameters of the curves could not be estimated by the loglogistic model. Even if the light red curve is above the light blue one, concluding that the food matrix inhibit AgNPs toxicity is not possible because the treatment of AgNPs w/o food matrix is already not toxic in the range of concentration tested.

Secondly, the effect of digestive enzymes on AgNPs was analyzed by comparing curves without food components between them (light blue = undigested AgNPs, dark blue= digested AgNPs). Looking at the three assays, a general observation can be drawn: the digested curve suggests an increased toxicity compared to the undigested one. Besides, the dark blue one was systematically the most toxic among all curves. For the CTG assay, the reduction of ATP content was higher for the digested treatment from an AgNPs concentration of 30 µg/ml than for undigested AgNPs. EC50 was slightly reduced from 42 to 35 µg/ml, but the difference is not significative. Nevertheless, b parameter, which is the slope of the curve was increased if digestive enzymes were added: jumping from 1.7 to 4.4. Pristine AgNPs being already toxic to cells and reducing severely the ATP content, the toxic effect of digestive enzymes cannot be demonstrated clearly with CTG assay.

In contrast, the effect of digestion was more apparent and obvious in CTB and CV assays even if statistics could not be carried out. Cell viability and cellular adherence were drastically reduced when digestive enzymes were added. During the experiments, a clear detachment of the cell monolayer was observed after the incubation with digested AgNPs in the absence of food matrix.

The combined effect of digestive enzymes and food components can be examined by comparing the digested curves among them (dark blue curve= digested AgNPs w/o food matrix, dark red curve= digested AgNPs with food matrix). In all assays, the dark red curve suggests a lower viability reduction than the dark blue one. The addition of the food matrix decreased significantly the negative impact that digestive enzymes induced on AgNPs toxicity. EC50 was significantly higher with food matrix in three assays. However, as AgNPs concentration increased, the buffering effect of the matrix decreased and both curves are almost equally cytotoxic at 101.25 µg/ml.

Also, the food matrix was not fully effective against the effect of digestive enzymes since the dark red curve was not the same as the light blue one, representing pristine AgNPs. While these two curves were not different with CTG assay, they are considered different for the CTB and CV assays. Therefore, taking in account the presence of food components and the effect of digestives enzyme on AgNPs is primordial in toxicological studies.

To summarize results:

- Food components alone tend to decrease AgNPs toxicity. ATP content was significantly increased if pristine AgNPs are included in a food matrix.
- Digestive enzymes reduce drastically cell viability and number of adherent cells. The effect is therefore to increase toxicity of AgNPs
- Combined, digestive enzymes and food components tend to increase AgNPs toxicity regarding cell viability and cellular adherence despite the fact that digested AgNPs + food components were significantly less toxic than digested AgNPs in the absence of the food matrix. The food matrix could not totally protect AgNPs from digestive enzymes.
- Digestion and food components are two parameters that need to be modelled when assessing the toxicity of AgNPs, highly susceptible to be orally ingested.

3.4 Discussion

Only a small amount of studies that examined the impact of digestive enzymes and food component on the toxicity of AgNPs could be found in the literature. Regarding results obtained in this thesis, both parameters induce changes in AgNPs cytotoxicity.

3.4.1 Effect of the food matrix

First, we assessed the effect of the food matrix alone. In the light of our results, we observed that toxicity of pristine AgNPs is reduced upon addition of the food matrix, which was comprised of bovine serum albumin (BSA), wheat starch and triolein, three standard compounds chosen to represent the three main macronutrients: proteins, carbohydrates and fats.

The presence of BSA in the food matrix could be responsible of the positive effect of the food matrix on the AgNPs toxicity. Bovine serum albumin is a globular protein consisting of 583 amino acids and having no enzymatic activity. BSA is a typical model protein used in many studies either as stabilizer, blocking reagent, as standard to quantify other proteins or nutrient in cell culture. Albumins are indeed the proteins the most prevalent in serum, *ca.* 20 – 40 mg/ml; BSA being the one found in bovine serum (Rockland, 2018).

Many studies proved that BSA can alter AgNPs properties. Ravindran *et al.* (2010) looked at the spectral, morphological and surface structural changes of Ag nanoparticles induced by BSA. BSA was observed to induce a shift in the plasmon peak of AgNPs. With FT-IR spectroscopy, they also concluded on the complete coating of nanoparticles by BSA as no characteristic peak of AgNPs could be observed. Another *in vivo* study conducted by Gnanadhas *et al.* (2013) showed that uncapped AgNPs loose their antibacterial properties if they are in the presence of serum proteins, due to the interactions with BSA.

Concerning cytotoxicity, most studies agree that BSA reduce cytotoxicity of AgNPs. Indeed, Kittler *et al.* (2010) demonstrated that AgNPs and Ag^+ had a lower toxic effect on cells in the presence of BSA than

in its absence. They dispersed 50 nm AgNPs in different cell culture media, one of them containing 10% BSA and looked at the biological effect on human mesenchymal stem cells (hMSC). Cell viability was assessed with calcein-AM fluorescent staining and toxic concentration of AgNPs were tested. Cell viability was clearly enhanced when BSA was added to the culture medium; the protecting effect was very pronounced for silver ions where cell viability rose to 80 % in most conditions (% of BSA added ranges from 0.001% to 10%). For Ag nanoparticles, cell viability increased only to about 20 % when BSA was added but still, the difference was significant from the control. These results corroborate our observation about of the protecting effect of the food matrix.

As observed in Ravindran *et al.* (2010), AgNPs were fully coated with BSA, which suggests that AgNPs in contact with the food matrix, adsorb protein on their surface forming a well-known protein corona. Indeed, a considerable number of studies reported the formation of a protein corona around AgNPs when they are in contact with a biological fluid (Monopoli *et al.*, 2013; Lundqvist *et al.*, 2008) and pointed out the impairment of AgNPs interactions with cells because of the presence of the protein corona.

A recent study of 2016 provided very interesting results as they could quantify the number of BSA molecules attached per silver nanoparticle, which corroborates the formation of a coating of BSA around AgNPs observed in Ravindran's study. Dasgupta *et al.* (2016) looked at the disruptions of proteins when these are in contact with NPs. The interaction between BSA and silver nanoparticles was investigated at different concentration and BSA changes were monitored with UV-vis spectrometry, DLS, FT-IR spectroscopy and fluorescence quenching. Among the results, they estimated the theoretical amount of BSA proteins adsorbed on the surface of Ag nanoparticles to be ~ 2.7 protein molecules (R_{AgNPs} =30 nm and hydrodynamic radius of BSA= 27 nm) while experimentally only 1-2 BSA molecules are attached.

Among studies revealing the impact of the protein corona on AgNPs behaviour, very recently, the Barbalinardo *et al.* (2018) study indicated that the protein corona mediated and could even promote the uptake and cytotoxicity of AgNPs. They reported the effect of surface coating of AgNPs on the adsorption of serum proteins and the consequences on the uptake and cytotoxicity (MTT assay) in mouse embryo fibroblasts. Citrate-coated AgNPs alone or coated with EG_6OH (11-mercaptoundecyl) hexa(ethylene glycol) were incubated in DMEM containing 10% FBS at 37 °C overnight and then tested on cells cultured in serum-free medium. Stability of citrate-AgNPs was improved with serum proteins adsorption on their surface while the passivated AgNPs were more resistant to proteins adsorption. Results showed that the uptake of citrate-AgNPs took only took place in the presence of a protein coating and cell viability was drastically reduced when citrate-AgNPs were coated with serum proteins while it was not affected without protein coating. They concluded therefore that only AgNPs with a protein corona are internalized and thus induce cytotoxic effect on cells. A proper functionalization of the surface that can hinder protein adsorption can reduce the toxicity of AgNPs. This study tends to show opposite results than ours, indicating that a corona of serum proteins increases AgNPs toxicity. This can be explained by the coating of AgNPs that can influence AgNPs toxicity and interactions with proteins. Indeed, Treuel *et al.* (2012) concluded that the affinity of protein adsorption on AuNPs and AgNPs is strongly affected by their coating surface as PVP-coated NPs showed lower affinities for serums proteins than citrate-NPs.

The study of Monteiro-Riviere *et al.* (2013) showed also divergent results depending on the coating of AgNPs. Cellular uptake was studied for citrate coated AgNPs (20 and 110 nm) and silica-AgNPs (40 and 120 nm) in HEK cells (human epidermal keratinocyte). AgNPs were treated or not with albumin, transferrin and IgG to form protein-complexed NPs. When citrate coated AgNPs were incubated with protein, cellular uptake was reduced, especially for the 110 nm but the greatest uptake was observed for 20 nm silica AgNPs and a mixed-effect for 120 nm. Their results about citrate-AgNPs are even in opposition with Barbalinardo *et al.* study.

Other studies rather associated NPs incubation with serum proteins with a reduction of the uptake into cells such a decreased cytotoxicity. As an example, Zhu *et al.* (2009) look at the effect of carbon nanoparticles (CNP) with and without adsorption of serum proteins in culture medium on cellular uptake and cytotoxicity. They performed MTT assay after 2h incubation on HeLa cells. The uptake of CNPs was 3-4 times higher for the CNPs in a serum-free culture medium. TEM images confirm that serum proteins greatly reduced intracellular uptake of CNPs. Concerning MTT assay results, they observed that cytotoxicity of cells in serum-free medium was higher than in a medium with serum. They even correlated the attenuation in cytotoxicity with the amount of serum proteins adsorbed on CNPs (mg/mg): the higher the adsorption of proteins, the greater the attenuation of cytotoxicity.

Ravindran (2016), Zhu (2009), Kittler (2010) and Dasgupta (2016) studies tend to show that a protein corona containing BSA can be formed around nanoparticles (AgNPs and other NPs like CNPs) and additionally, reduce their toxicity. Therefore, proving its presence on AgNPs surface is the first step to explain our results about the effect of the food matrix. To this end, a quantification assay of the proteins adsorbed on AgNPs when they were in contact with the food matrix was performed as a final experiment of this master thesis. Results and Discussion can be found in section 4.

The effect of BSA on AgNPs was vastly investigated but our food matrix was also comprised of triolein and starch that could also impair AgNPs properties. Go *et al.* (2017) investigated the interactions between food additives silica-NPs and different food matrices: saccharides, proteins, lipids, and minerals. In honey, SiO_2-NPs had less negative charge and a higher hydrodynamic radius (4 times bigger) while no change in zeta potential and a decrease of the hydrodynamic radius were observed in a sugar mixture with similar amounts of monosaccharides. Stronger interactions with fructose and glucose could however be demonstrated. Kästner *et al.* (2017) looked at the stability of AgNPs during digestion in the absence or presence of food components (oil, starch and milk powder). When starch is added, the mean radii of the particles and the aggregates is not affected during all stages of digestion. Same observation when AgNPs were digested in oil. Concerning interactions with lipids, Go *et al.* (2017) could not perform measures of zeta potential and hydrodynamic diameter because of the high viscosity of olive oil but since SiO_2-NPs have a hydrophilic surface, they presumed that fatty acids slightly bound would easily detach with washing with organic solvents.

Regarding Go *et al.* (2017) and Kastner *et al.* (2017), carbohydrates and lipids seem to only slightly interact with AgNPs. Focusing on the interactions between proteins and AgNPs seems therefore more relevant.

3.4.2 Effect of digestive enzymes

According to our results, digestive enzymes have a clear effect of increasing AgNPs toxicity and reducing drastically cell viability (CTB assay) and the number of adherent cells (CV assay). The deleterious effect

of digestives enzymes was not evident with CTG assay, the difference between the two curves was indeed not significantly different even if a reduction of the EC50 was induced. Similar studies found on the literature tend to show opposite results; the digestive enzymes having no impact on AgNPs toxicity.

Böhmert *et al.* (2014) assessed the impact of *in vitro* digestion on AgNPs (14 nm diameter) toxicity in Caco-2 cell monolayers. They compared effects of digested and undigested AgNPs with the CTB assay. Outcomes were a decrease of cell viability in a concentration-dependent manner and no significant differences between digested and undigested NPs except for the highest concentration (100 µg AgNPs /ml) where the digested treatment was clearly more toxic than undigested material. Our results of the cell detachment assessment (CV assay), highlighting the higher toxicity of digested AgNPs, are in line with their observation for the highest concentration of AgNPs. They used DAPI staining to quantify the number of remaining cells. DAPI is a DNA fluorescent stain that correlates the fluorescent signal to the quantity of DNA. Number of cells starts to decrease remarkably because of digestion when AgNPs have a concentration of 100 µg/ml. While 30 % of cells remained with pristine AgNPs, only 5 % was measured when AgNPs are digested. Even if our drop of adherent cells is bigger at the highest concentration (90 % to 15%), the effect of digestive enzymes on the number of adherent cells is demonstrated.

Since they saw significant differences only at the highest concentration, they concluded on the minor influence of the artificial digestion to the toxicity of AgNPs whereas changes in aggregation state and morphology could be monitored during the *in vitro* digestion process. However, these results should be taken with caution considering the fact that their digestion control was also toxic. Discriminate between the effect of digestive enzymes on cells or their effect on AgNPs is therefore almost impossible. Some difference exists also between our experiment and theirs. First, they incubated AgNPs treatments on cells during 24h while we performed an incubation of only 3h. The 24h incubation implies that cells need culture medium and as the medium they used contains serum, serum proteins like BSA can interact with AgNPs. Moreover, they obtained the final AgNPs concentrations by diluting a stock solution after the *in vitro* digestion. This means that in all concentrations tested, digestive enzymes are diluted the same way. In our protocol, different concentration of AgNPs went simultaneously through the digestion, therefore the concentration of digesting solutions is the same in each condition and the effect of only AgNPs can be revealed.

Based on Böhmert's study, Lichtenstein *et al.* (2015) obtained similar results. They investigated the effect of pristine AgNPs, digested AgNPs and digested AgNPs with food components on cell viability with CellTiter Blue assay. After an *in vitro* digestion of 7 nm coated-AgNPs, they put the different treatments in contact with Caco-2 cells monolayer and examined cell viability. After 24h exposure, digestive enzymes did not remarkably affect the toxicity of AgNPs. Both treatments, digested and undigested AgNPs were equally cytotoxic, their respective curves looking the same on the CTB graph. Again, comparing these results with ours is delicate since they incubated treatments during 24 h on cells, and as Böhmert *et al.*, they diluted digestates after the *in vitro* digestion. Furthermore, they used smaller nanoparticles (7nm diameter) than ours (around 15 nm uncoated).

Even if results of the two previous studies are different from those in the present work, they can relate to the results of our CTG assay. Indeed, no effect of the digestive enzymes could be demonstrated since pristine AgNPs were very toxic and induced a substantial drop in ATP content, even with small concentrations. Therefore, this interpretation could also be applied to Böhmert and Lichtenstein's

results; no digestion effect could be observed on AgNPs toxicity since they are already extremely toxic, which turns out to be true. The smaller size of AgNPs tested (7 nm in Lichtenstein) and the longer duration of incubation of AgNPs on cells (24h) could indeed explain their higher toxicity.

Pindakova *et al*. (2017) subjected AgNPs to the action of simulated saliva, gastric and intestinal fluids (SSF, SGF and SIF) added with pepsin and pancreatin. They performed DLS and TEM microscopy and look at the toxicity and the ability to induce inflammation in a human cell-based 3D model. The EpiIntestinal tissue showed great resistance against treatments. After 24h incubation of the different digestive fluids with and without AgNPs, the viability of the tissue was only slightly decreased and the differences between AgNPs with and without enzymes were not observed suggesting that digestive enzymes do not influence AgNPs toxicity. However, their protocol is very different from ours. First, they did not proceed to a continuous digestion, but put AgNPs in contact with digestive fluids separately. Second, the model used was human reconstructed tissues of the oral cavity, the stomach and intestine (3D models EpiOral, EpiGingival and EpiIntestinal) which are very different from the co-culture monolayer used in our study.

Even if no study corroborating the negative effect of digesting enzymes on AgNPs cytotoxicity could be according to our literature review, explanations can be hypothesized.

The higher toxicity of digested AgNPs could be explained by an increase of the Ag^+ release during the digestion (Mwilu *et al.*, 2013; Bove *et al.*,2017) or changes in physico-chemical properties such as morphology or aggregation state, which could potentially worsen the toxic properties of AgNPs (Pindakova *et al.*, 2017, Ault *et al.*, 2016).

Mwilu *et al.* (2013) exposed AgNPs of different sizes and capping agents to human stomach synthetic fluids (SSF) and looked at changes in morphology, size, and chemical composition. Exposed to SSF, AgNPs were found to aggregate significantly and release ionic silver that react with chloride in the aggregates. They suggested that in acidic environment, AgNPs first rapidly aggregate. Then Ag^+ is released through oxidation processes and chloride present in solution react with silver ion to produce insoluble AgCl. Even if they did not determine the degree of Ag^+ ion release, the presence of AgCl confirm that AgNPs indeed release ions when in contact with digestive enzymes.

An increased dissolution of AgNPs (NM-300K, 20 nm diameter) was also monitored by Bove *et al.*, (2017) along an *in vitro* digestion process, especially at the gastric step where 20 % of free ions could be measured. After the salivary step, AgNPs were partially agglomerated and almost totally dissolved in the stomach compartment. At the intestinal level, 2% of ions were measured.

Ault *et al.* (2016) look at the effect of simulated gastric fluid containing pepsin to AgNPs of different size and coatings (citrate-AgNPs 20 and 110 nm and PVP-AgNPs 20 and 110 nm). They observed a rapid increase of all AgNPs size with SGF, which was higher with pepsin addition. 20nm NPs double size while the increase was lower with bigger molecules. In addition, agglomerates were formed when pepsin was added. While the particle size of larger NPs (110nm) changed, smaller NPs (20 nm) did not change their size within the agglomerates, which suggest only a small dissolution into Ag^+. Inversely, AgNPs could also have an impact on digestives enzymes. Therefore, toxicity of digested AgNPs could be explained by an increased activity of digestives enzymes due to AgNPs interactions. In Ault *et al.* (2016), as previously explained, the effect of AgNPs on protein catalytic activity of pepsin and conformational structure was

also assessed. While changes in secondary structure of pepsin could not be observed, a decrease in catalytic activity of pepsin in a dose-dependent manner could be demonstrated after 10 minutes incubation with the different AgNPs (citrate-AgNPs 20 and 110 nm and PVP-AgNPs 20 and 110 nm). Pepsin is inactivated in our case due to the alkaline pH of the intestinal step but the mix of bile-pancreatin is still active at the end of the digestion processing. AgNPs could therefore impair the activity of trypsin and lipase contained in pancreatin and potentially increase it. More research is needed to be done about the interaction of AgNPs and digestive enzymes, especially trypsin and lipase in order to clarify this hypothesis.

3.4.3 Joint effect of digestive enzymes and food matrix

As a final result, we observed that digested AgNPs in the presence of food matrix were more toxic than pristine AgNPs. However, compared to digested AgNPs without matrix, the addition of the food matrix was significantly less toxic meaning that food matrix could protect AgNPs against the negative effect of digestive enzymes but not totally since they were still more toxic than pristine AgNPs.

In Lichtenstein *et al.* (2015), pristine AgNPs, digested AgNPs and digested AgNPs with food components were incubated on Caco-2 cells for 24 hours and cell viability was assessed with CTB. Results showed that three treatments were equally cytotoxic meaning that digested AgNPs were not less toxic upon addition of food components and that digested AgNPs without food components were not more toxic than pristine AgNPs, which is in complete opposition with our results. Again, differences in protocols explained previously prevent a valid comparison with our results. They also monitored the properties of AgNPs during digestion and they observed that size and size distribution of undigested NPs and digested NPs with food components were similar suggesting that AgNPs keep the same size throughout digestion and therefore keep their initial characteristics and consequently their toxicity. However, they observed that aggregates usually formed during digestion of AgNPs were not formed when food supplements were added before digestion. They emitted the possibility that food supplements act as colloidal stabilizers.

The study of Kästner *et al.* (2017) observed a similar stabilization and provides part of the answer of the beneficial effect of the food matrix on digested AgNPs. They reported the impact of an *in vitro* digestion of AgNPs in the presence or absence of food by characterizing 3 nm radius coated AgNPs with small-angle X-ray scattering (SAXS). Digestion of the NPs was repeated in the presence of oil, starch, skimmed milk and a mixture thereof such as in the absence of food component. Radii of AgNPs were measured after each digestive step. They found out that all food components have a strong colloidal stabilizing effect compared to the situation in their absence. While the radii decreased in the stomach in the absence of food from 3.1 to 2.2 nm, it remained at 3.1 nm during the whole digestion upon addition of milk (radii decreased with oil and starch). They attributed these findings to the strong stabilizing properties of milk proteins. Indeed, no silver aggregates were found in food mixture and milk while they were found in all other treatments (none, oil and starch). This suggested that proteins especially, prevent AgNPs against changes during the digestion. Considering the fact that BSA is the protein representant in our food matrix, its effect on digested AgNPs should be looked more closely.

Tai *et al.* (2014) studied AgNPs under acidic environments and investigated the impact of protein interactions (BSA) to the stability of AgNPs. Unconjugated AgNPs showed an increase of aggregation and average particle size as acidity increases. AgNPs treated with BSA exhibited an improved stability,

both dissolution and aggregation of AgNPs was negligible. They concluded that the formation of BSA corona suppressed both dissolution and aggregation under acidic environments. Since pH of the stomach is acid, these results suggested that aggregation of nanoparticles could be prevented with the formation of a protein corona of BSA. However, our results with UV-visible spectroscopy during the gastric phase (section) showed an aggregation of the AgNPs even if the food matrix is added. Knowing that pepsin was added during the gastric phase in our protocol, this could explain our results. Further investigations should prospect the presence of digestives enzymes on the corona when AgNPs are digested and the interactions with BSA.

Ramos *et al.* (2017) performed an *in vitro* digestion (including saliva, gastric and intestinal steps) of a chicken meat containing AgNPs and of 40 nm AgNPs alone. The purpose was to measure the amount of dissolved AgNPs with ICP-MS from the initial matrix after the digestion. While 81 % of the initial AgNPs in the standard solution would reach the intestinal compartment, 13 % only were measured in the case of the spiked meat, the rest being in dissolved silver species. This suggest a higher dissolution of AgNPs when these are contained in a food matrix. This study highlights again the fact that AgNPs act differently during the digestion if they are included in a food matrix, corroborating our results.

Just as shown in our study, as well as in Ramos *et al.* (2017) and Kästner *et al.* (2017), the addition of food components can strongly affect properties of AgNPs during the digestion process. Considering both impact of digestive enzymes and food components in toxicological studies of AgNPs is primordial to draw realistic conclusions.

Since the positive effect of food matrix on digested AgNPs shown in our study could not found clear explanations in other similar studies, a characterization of AgNPs during the *in vitro* digestion in a control solution (HBSS) and in a modelized food matrix was performed. Changes in aggregation state could maybe be exhibited. Results of UV-visible spectroscopy of samples during the *in vitro* digestion are shown and discussed in point 3.

4. Characterization of AgNPs included in a food matrix during in vitro digestion

Oral ingestion is an important route of exposure for silver nanoparticles (AgNPs), but their fate during gastrointestinal digestion is poorly understood such as the interactions with food components. When AgNPs are ingested and pass through the GIT, they do not maintain their primary properties (Bove *et al.*, 2017). In addition to be subjected to different temperatures, pH and oxygen conditions, they interact with food components and digestive enzymes, which can substantially impact their toxicity, biokinetic behavior, dissolution rate, surface characteristics and aggregation state (Kästner *et al*, 2017; Martirosyan *et al.*, 2013; Walczak *et al.*, 2012). These changes can be indirectly monitored after each stages of the *in vitro* digestion through UV-visible spectroscopy.

A typical nanosilver suspension at the free state (diameter < 20 nm) is yellow colored. Since, the color of AgNPs solutions depends on the extinction of the selected portions of visible light, the typical yellow color appears with absorption of the blue-purple light (Mendis *et al.*, 2013). Metal NPs have indeed the particularity of exhibiting a surface plasmon resonance (SPR) phenomenon, induced by the collective oscillation of the conduction electrons in resonance with a precise lightwave (Das *et al.*, 2010).

Regarding AgNPs, this collective oscillation, commonly called the SPR peak, happens between 400 and 420 nm and is responsible for the typical yellow color. The color of silver solution is in fact attributed to the surface plasmon resonance (Mendis *et al*, 2013).

Measured by UV-visible spectroscopy, the SPR peak's position and intensity depends on surface morphology like size and shape, just as the dielectric properties of the surrounding environment (Li *et al.*, 2016). It is known that low pH, high temperatures and high ionic strength increase AgNPs dissolution, which can lead to the formation of agglomerates as shown in the Walczak *et al*. (2013) study.

Any change in AgNPs aggregation or dissolution state is therefore reflected at a large scale by a change in the color solution, which can be confirmed by examining absorbance spectrum and SPR peaks. Macroscopic observations of the solutions such as UV-visible spectra have been therefore carried out before the digestion and after each digestive stage in order to monitor AgNPs alterations through the GI tract.

As a reminder, digesting bottles (containing AgNPs concentrations of 0, 22.5, 67.5, and 202.5 µg/ml either in HBSS or in the food matrix solution) were maintained at 37° C and under constant agitation (350 rpm) throughout the whole *in vitro* digestion process. For the salivary stage, pH was adjusted at 6.9 and solutions were incubated for 10 minutes with α-amylase. For the gastric stage, pepsin was incubated for 2 hours under anaerobic conditions at pH 2.0; and for the intestinal stage, digesting solutions were incubated for 2 hours with a mix of bile and pancreatin still under anaerobic conditions at pH 7.0.

Pictures of samples and UV-visible measurement were performed before the *in vitro* digestion process and after each step. UV-visible measurements were taken during the four independent measurements but only the results of one repetition are shown as representative's ones.

4.1 Macroscopic observations

Figure 22. Samples of undigested AgNPs in HBSS (left) and included in a food matrix (right). The following concentrations were tested in the samples: 0, 22.5, 67.5, and 202.5 µg AgNPs/ml.

Figure 23. Samples collected after the salivary stage: AgNPs in HBSS (left) and in the presence of food matrix (right). The following concentrations were tested in the samples: 0, 22.5, 67.5, and 202.5 µg AgNPs/ml.

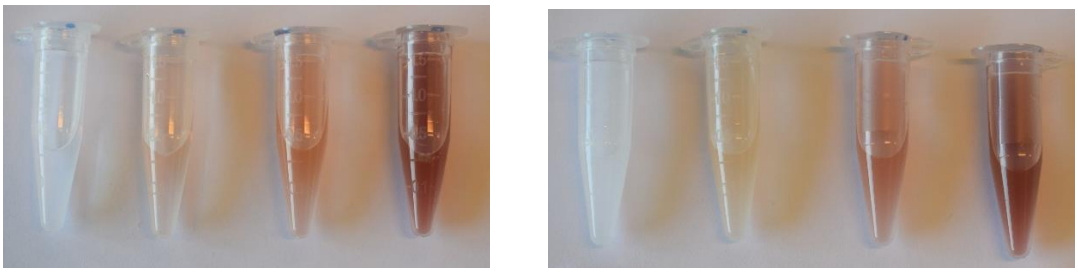

Figure 24. Samples collected after the gastric stage: AgNPs in HBSS (left) and included in the food matrix (right). The following concentrations were tested in the samples: 0, 22.5, 67.5, and 202.5 µg AgNPs/ml.

Figure 25. Samples collected after the intestinal stage: AgNPs in HBSS (left) and in the food matrix (right). The following concentrations were tested in the samples: 0, 22.5, 67.5, and 202.5 µg AgNPs/ml.

During the *in vitro* digestion, samples of the AgNPs solutions were collected after each step in order to analyze them by UV-visible spectroscopy. Figure 22 to 25 show the appearance of the samples, giving us an insight of the macroscopic transformations of AgNPs through the digestion.

Figure 22 shows the samples before going through the digestion process. AgNPs in HBSS samples display the typical yellow color, with an intensity being stronger as the concentration increases. Compared to samples to which the food matrix was added, difference is not visible on the picture, but samples were more trouble because of the food matrix and more importantly the presence of starch.

After the salivary step where α-amylase was incubated for 10 min in the digesting bottles, the color of the solutions was unchanged in both HBSS and food matrix treatments. However, after the gastric stage, solution's color changed drastically. After incubation in anaerobic conditions with pepsin for 2 hours, solutions appeared red, with a color spectrum ranging from beige for the smallest concentration of 22.5 µg/ml to deep red for the highest. Once the final intestinal stage completed, solutions return to their initial yellow color.

Regarding these observations, we can say that the digestion has a visible impact on AgNPs solutions especially during the gastric phase where a clear change in color is exhibited. These macroscopic observations could be explained partially by looking at the curves obtained from UV-visible spectroscopy.

4.2 UV-visible spectroscopy

UV-visible absorbance spectra displayed on Figure 29 are considered as representative ones for the four repetitions. Absorbance of the AgNPs solutions was measured at different concentrations (22.5, 67.5 and 202.5 µg/ml) in suspension in HBSS for the left column and in the food matrix model in the right column. Two controls containing the HBSS and the food matrix alone, *i.e.* in the absence of silver nanoparticles, were also tested.

For each graph, the four curves represent the spectra of the control and AgNPs treatments before and after each steps of the *in vitro* digestion: the orange curve stands for the absorbance's solution before the digestion process, the red curve after the salivary step, the blue one after the gastric step and the green curve after the intestinal step.

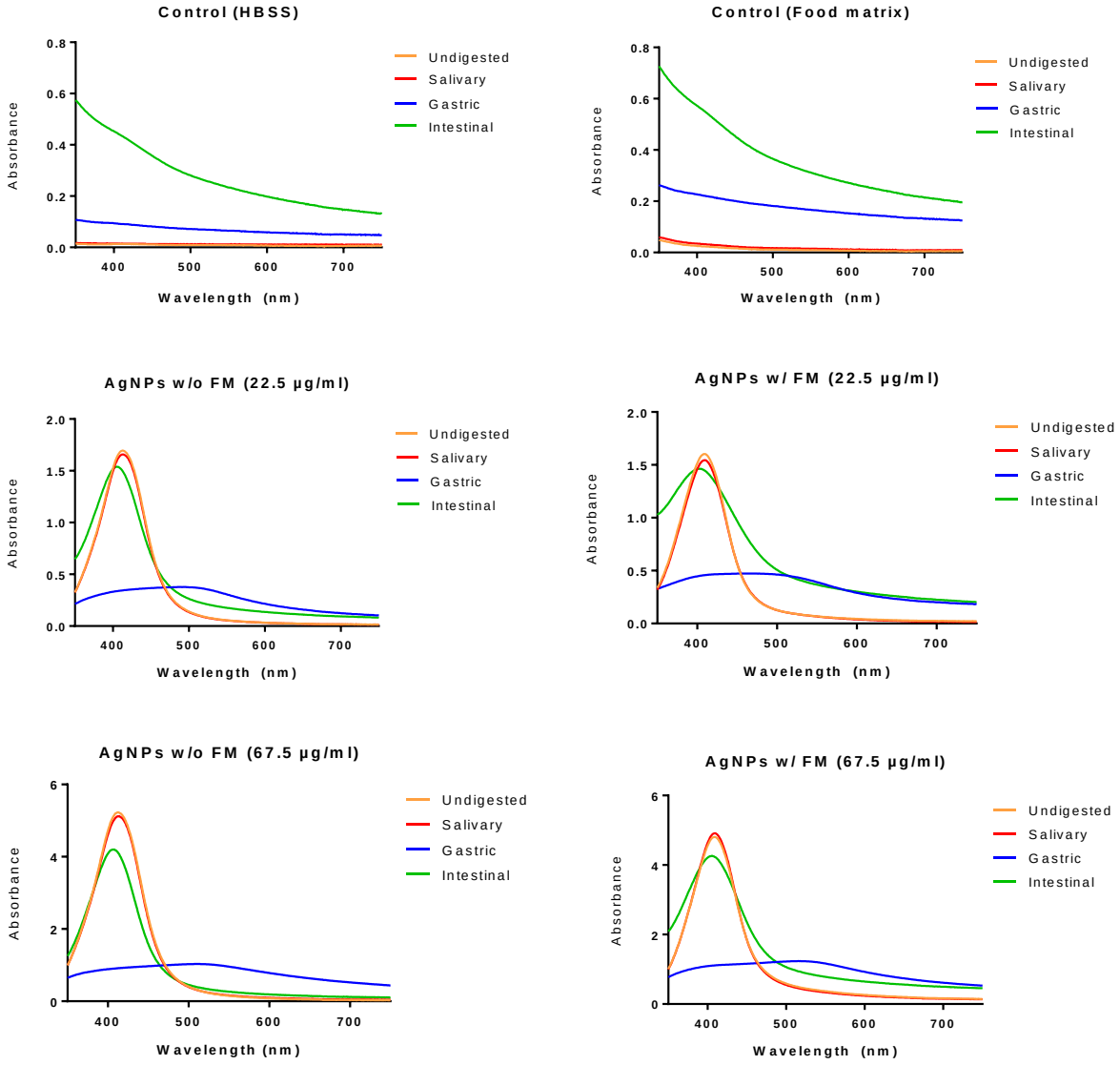

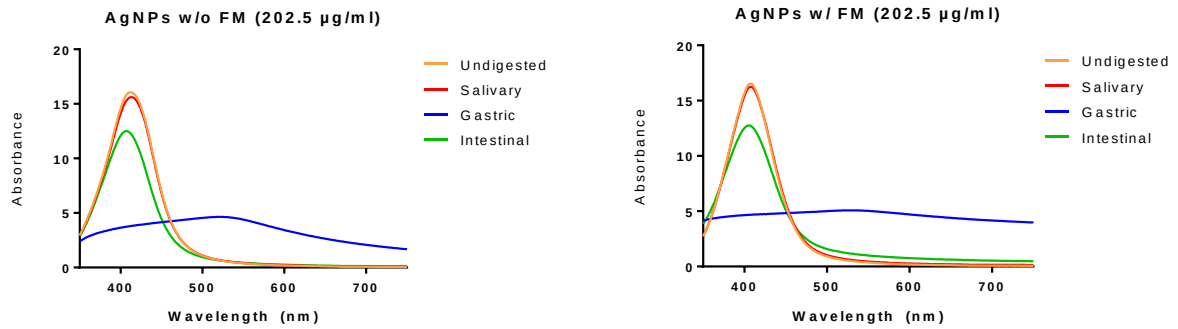

Figure 26. UV-visible absorbance spectra of AgNPs at different concentrations (0, 22.5, 67.5, 202.5 µg/ml) after each stage of *in vitro* digestion either diluted in HBSS (left column) or in the food matrix model (right column). The orange curve indicates the absorbance of the samples before the *in vitro* digestion, the red is for the salivary step, the blue for the gastric step and the green for the intestinal step.

Table 4. presents the values of maximum wavelength λ_{max} and maximum intensity I_{max} of each curve presented in the UV-visible spectra above.

Ag conc. (µg/ml)		Before digestion		Salivary stage		Gastric stage		Intestinal stage	
		w/o FM	w/ FM	w/o FM	w/ FM	w/o FM	w/ FM	w/o FM	w/ FM
0	I_{max}	0.01	0.05	0.02	0.06	0.1	0.26	0.57	0.73
	λ_{max}	(350 nm)	350 nm	350 nm	350 nm	350 nm	350 nm	350 nm	350 nm
22.5	I_{max}	1.7	1.6	1.65	1.54	0.37	0.47	1.54	1.46
	λ_{max}	413 nm	409 nm	413 nm	409 nm	485 nm	459 nm	405 nm	402 nm
67.5	I_{max}	5.2	4.8	5.1	4.9	1.03	1.24	4.2	4.26
	λ_{max}	412 nm	409 nm	414 nm	409 nm	507 nm	515 nm	406 nm	405 nm
202.5	I_{max}	16.1	16.5	15.6	16.2	4.6	5.1	12.5	12.6
	λ_{max}	412 nm	407 nm	412 nm	407 nm	518 nm	531 nm	407 nm	405 nm

Table 4. Values of SPR peaks (maximum wavelength λ_{max} and maximum intensity I_{max}) of the absorbance spectrum obtained after each digestive step of the *in vitro* digestion in the presence or absence of the food matrix for different AgNPs concentrations.

4.3 Results Analysis

As a general observation, we can point out the effect of the AgNPs concentration. Indeed, the peak intensities increase proportionally to the AgNPs concentration. When AgNPs concentration rose from 22.5 µg/ml to 202.5 µg/ml, peak's intensity measured was 10 times higher, passing from 1.5 to 15. A higher concentration means a higher number of particles capable of absorbing light, which is correlated with a higher absorbance according to Lambert-beer's law.

Regarding the HBSS control, we see that the digestives enzymes had a very slight absorbance on their one, especially the bile salts and pancreatin enzymes which display an inherent absorbance of ~ 0.6.

Adding the food matrix, has only a negligible effect on the inherent absorbance of the digestive enzymes; values being practically the same.

Comparing the curves of AgNPs solutions in HBSS or in food matrix, the effect of the food matrix was not clear since they looked the same. Nevertheless, a slight shift was induced with the food matrix when looking at SPR peaks (Table 4). Before digestion, we see that the peaks occurred systematically at lower wavelengths when the food matrix was added. For example, at the concentration of 67.5 µg/ml, the peaks decreased from 412 to 409 nm. This slight shift towards lower wavelengths (blue shift) reveals the interactions between AgNPs and the components of the food matrix.

Eventually, we see that spectral curves display the same trends throughout the digestion whether the food matrix was included or not.

- After the salivary stage, the curve did not change from before undergoing a digestion process, exhibiting the typical single peak around 412 nm, a sign of the free individual state of the particles. This corresponds to the samples remaining yellow after the salivary step as observed macroscopically.
- After the gastric stage, the curve got wider and SPR peaks shifted towards higher wavelengths simultaneously. This effect known as red-shifting is a sign of an increase in size particle and formation of agglomerates (Sigma Aldrich, 2011). Macroscopically, the AgNPs solution appeared red.
- After the intestinal step, a similar peak as before digestion was observed. This corroborates the return of the yellow color. However, SPR peaks were less intense and slightly shifted towards lower wavelengths. At 202.5 µg/ml, the peak appeared at 407 nm (12.5 of absorbance) after the intestinal stage while it was 412 nm (15.6 of absorbance) after the salivary stage without food matrix. The decrease of the absorbance can be explained by the dilution of the AgNPs solutions. Indeed, digestives enzymes and solutions to modulate pH were added throughout the digestion and therefore dilute the initial AgNPs solutions. Final concentrations are therefore less concentrated than initially. The blue shift reveals interactions of AgNPs with the digestive enzymes.

4.4 Discussion

Both digestive enzymes and food components appeared to induce changes in the cytotoxicity of AgNPs. Therefore, characterizing AgNPs during digestion whether included in a food matrix or not is necessary to explain previous results. Since optical properties of AgNPs are very sensitive to interactions with proteins (Argentiere *et al.*, 2016), UV-visible spectroscopy was performed in order to visualize plasmon bands of AgNPs and changes induced by digestive enzymes and food components.

First, regarding our controls, we saw that digestive enzymes of the intestinal compartment had a slight inherent absorption. The mix of bile-pancreatin had indeed a slight yellow color that can explain the inherent absorbance observed after the intestinal step.

Secondly, an effect of the food matrix could be pointed out, looking at the results before digestion. Indeed, a shift of ~ 4 nm of the absorption peak toward lower wavelength, called a blue shift, is induced upon addition of the food matrix.

Similar results were also observed in Ravindran's study. Ravindran *et al.* (2010) studied the interaction of BSA (0.05-0.85%) with AgNPs through UV-visible spectral, structural and morphological changes. At pH 7.0, they observed that as BSA % increased, absorbance decreased and a blue shift in the plasmon band from 425 to 410 nm appeared from 0.45 % BSA (Figure 27 left graph). The blue shift went further to 400 nm at pH 12.0 (Figure 27. Right graph). They suggested two different hypotheses for the blue shift with increasing BSA concentration: either AgNPs with adsorbed layers would repel each other, enhancing the stabilization as the flocculation is prevented (blue shift would be a size-dependent phenomenon) or surface charge density of the AgNPs would increase with BSA. The isoelectric point of BSA being at 4.5 -4.9, at the pH 7.0 of the experiment, BSA had a significant number of negatively charged functional groups, which could restrict free electrons of AgNPs within a smaller volume, leading to an increased free electron density, thus a higher plasmon frequency (thus lower wavelength). With X-ray diffraction, they could also exhibit the full coverage of BSA on AgNPs surface. However, morphology and size stayed the same after incubation with BSA, proving, according to the authors that BSA coating prevents aggregation.

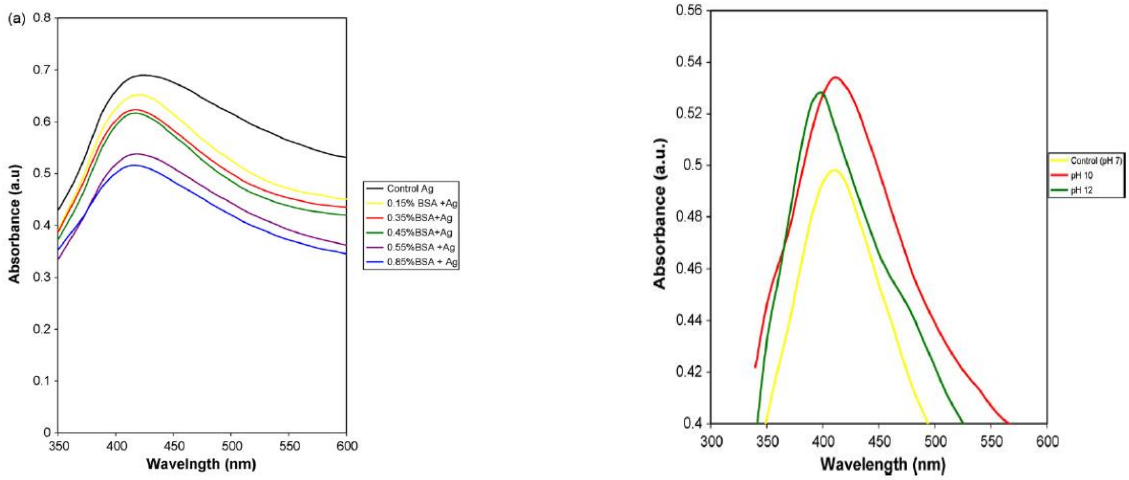

Figure 27. UV–vis spectra recorded in the range of 350–600nm as a function of interaction of different concentrations of BSA (0.15%, 0.35%, 0.45%, 0.55%, 0.85%) with Ag nanoparticles (50 ppm) for 4 h (Left). UV-vis spectra of BSA coated AgNPs (0.85 % BSA with 50 ppm Ag) recorded as a function of pH (Right).
Source: Ravindran *et al.*, 2010.

Wang *et al.* (2017) probed the interaction between BSA and AgNPs (40 nm) using multiple spectroscopic techniques. Results showed that BSA interacts with AgNPs to form stable BSA-AgNPs complex. One of their experiment was the monitoring of the absorbance of AgNPs with increasing concentrations of BSA. As BSA concentration increased, the absorbance peak at 416 nm was first slightly red shifted and then increasingly blue shifted as the BSA concentration increased. The intensity of the peak decreased gradually upon addition of BSA. These results about the blue shift are in line with Ravindran's study. With these results, they concluded that the surface was indeed coated with BSA and that the addition of BSA tends to stabilize the absorption, indicating that the binding would reach a saturation at a certain point.

However, Argentiere *et al.* (2016) showed opposite results. They incubated citrate- and PVP-coated AgNPs (10, 40 and 100 nm) in cell culture media with 10 or 100 % FBS and compared spectral curves.

After incubation in 10 or 100% FBS, the spectral position of the SPR peak of all AgNPs shift towards higher wavelength values. The red-shift was bigger for citrate-AgNPs than PVP-AgNPs while no trend with increasing diameter size could be demonstrated. They explained that "*In general, the increase in the λ max (maximum wavelength) (namely a red-shift) along with the reduction of the H max (maximum absorbance) value with respect to the control sample is associated with the protein corona formation, thus indicating that nanoparticles are well suspended in the tested medium* ". This results and interpretations are in opposition with ours, and Wang's and Ravindran's results. This can be explained by the presence of the coating that highly influences the binding of proteins and proteins corona formation as demonstrated by Treuel *et al.* (2012). Moreover, Argentiere *et al.* used FBS, a more complex medium than BSA alone. The other proteins present in the medium could therefore adsorb on the surface and modify the spectrum in another manner.

In the light of Ravindran and Wang's studies, the blue shift observed in this work could be explained by the formation of a BSA corona around AgNPs even if studies do not agree on the explanation of the blue shift. According Wang *et al.* (2017), the interaction between BSA and AgNPs results in stable complex, which explains the decreasing intensities of the plasmon peak. Slightly lower intensities are also observed in our results upon addition of the food matrix but only with the two first AgNPs concentration (At 22.5 µg/ml, peak at 1.7 decreased to 1.6 and at 67.5 µg/ml, peak at 5.2 decreased to 4.8).

The changes in spectral curves of AgNPs coated with lipids and carbohydrates were also found in literature but their results were not in line with ours and tend to show a red-shift when AgNPs are lipid coated (Munjar & Gilbert, 2017) and no changes with starch coated-AgNPs (Jung *et al.*, 2018).

Munjar & Gilbert (2017), investigated through UV-visible spectroscopy different functionalizations (citrate; PAH, and lipids) on Au-NPs and AgNPs. Unfunctionalized AgNPs showed a peak at 399.5 nm while lipid coated AgNPs had a peak at 407 nm. The coating of lipids induced a red shift and could be demonstrated by increased diameter size of the particles to 139 nm while their initial diameter size was 54 nm. Their results can however hardly be compared to ours as the lipids used are different such as the volumes added. They used a mix POPS and LPC in a ratio 1:1 (1-palmitoyl-2-oleoyl-sn-glycero-3-phospho-L-serine POPs and lysophosphatidylcholine LPC) as a lipid solution while we used triolein. Furthermore, bigger volumes of lipids solution were added so that a complete lipid corona could form around AgNPs while we only put very small quantities of triolein, most likely not forming such a corona.

Jung *et al.* (2018) prepared starch-AgNPs in a single step by ultrasonicating a mixture of starch, silver nitrate and distilled water. They characterize them with UV-vis spectroscopy and TEM. Starch-AgNPs were synthesized with increasing concentrations of starch but all showed the characteristic peak near 427 nm. However, as starch concentration increased, the intensity of the 427 nm band increased too. This suggests that starch coating does not induce a shift but can stabilize AgNPs as they prevent their aggregation.

In general, our results showed great changes during the digestion of AgNPs regardless of the presence of the food matrix. Indeed, curves and plasmon peak values showed same trends in both cases. Spectral curves were not changed after the salivary step (peak around 412 nm) and the color of the samples stayed yellow, the initial color of AgNPs. After the gastric step, color changed to red and plasmon peaks were broadened and red-shifted to ~ 500 nm. The color returned to yellow after the intestinal step.

After the digestion, intensities of the SPR peak were decreased due to the dilution of the AgNPs within the digesting solution and a slight blue shift appeared.

Same changes along the digestion, and during the gastric step especially, were reported in many other studies (Bove *et al.*, 2017; Kästner *et al.* 2017) and are explained by the formation of aggregates in the stomach. Indeed, as the diameter of AgNPs increases, the SPR peak shifts toward higher wavelength and widens. When AgNPs aggregate, NPs are electronically coupled, which decreases the surface electron density. Thus, the SPR peak of multi-nanoparticle aggregate will be red-shifted to longer wavelengths (Sigma-Aldrich, 2011). Therefore, the red-shift observed in the gastric step indicates that AgNPs were in an aggregate form, hence the red color of the solution.

Bove *et al.* (2017) studied the dissolution of AgNPs (NM-300K, 20 nm diameter) during an *in vitro* human digestion. Nanoparticles were characterized in the different phases with different techniques: UF/ICP-AES, DLS, TEM, zeta potential and UV-vis spectroscopy. The initial size of 20 nm was found in the control and in the saliva compartment, even if a low level of dissolution and formation of agglomerates could be observed. During the passage in the stomach, TEM analysis showed a high degree of dissolution, with the presence of NPs below 5 nm together with aggregates. The UCP/ICP-AES measured 20 % of free Ag ions. In the intestine, the dissolved fraction reduced to 2 %, some aggregates and particles of 20 nm were observed. A small aggregation in the saliva was reported with DLS and confirmed with UV-visible spectroscopy. The UV-visible confirmed the presence of two peaks, the first as the typical absorption peak at 412 nm indicating the presence of nanoparticles, and the second was a broad band in the red region (550 – 650 nm), the typical indicator of agglomerates. In the gastric and intestinal compartment, big agglomerates (700-740 nm) were detected with DLS whereas UV-vis displayed the absence of the peak at 412 nm, confirming the NP dissolution. However, no data of the wavelength position were displayed. They concluded that NPs begin to partially agglomerate in the salivary compartment and quite totally dissolve in the stomach. Similarities and differences with our results can be highlighted. Like us, they showed big agglomerates in the stomach, but values of SPR peaks were not indicated. They saw a small amount of agglomerates in the salivary and the intestinal compartments while our results suggest no agglomerates formation in both stages. First, the pH in their intestinal step was at 6.5, which is lower than in our intestinal step (7.0) and agglomeration of AgNPs was enhanced with acidic pH as showed by Lau *et al.*, 2016.

In Kästner 'study as explained before, they also characterized AgNPs during their digestion. In the absence of food, NPs with an initial size of 3 nm begin to agglomerate in the salivary step into small aggregates of 8 nm. After the gastric step, the initial size decreased (2.2 nm), which indicates their dissolution and agglomerates of 9 nm were formed. After the intestinal stage, the size stayed lower than initially (2.6 nm) and aggregates of 9 nm were still present. These results corroborate Bove 's findings about the beginning of the agglomeration at the salivary step and the presence of aggregates till the intestinal phase.

However, in other studies like Walczak *et al.*, (2013), similar results to ours were obtained for the salivary and intestinal stages. They performed an *in vitro* digestion of 60 nm nanoparticles (with and without enzymes) and characterized samples after each stage. Size and number of AgNPs stayed the same after the salivary step, but after gastric stage the number decreased dramatically by 90% and the size decreased from 50-60 nm to 20-30 nm. The values return to the original ones after the intestinal

digestion. These results in the salivary and intestinal stages are in line with our observations as the color stayed yellow in both compartments. They explained the reduction in number particles in the stomach by their clustering. Indeed, presence of agglomerates of 200 - 500 nm in the gastric step could be revealed. These aggregates seemed to break down in the intestinal step as only 60 nm NPs and dispersed were in solution. Moreover, they digested $AgNO_3$ in the presence of proteins and could demonstrate formation of new particles (20 -30 nm) composed of silver, sulphur and chlorine. The authors concluded that AgNPs in the presence of proteins, survived the extreme digestive conditions and thus reached the intestine with minimal changes in size.

In the light of Bove *et al.* (2017), Walczak *et al.* (2013) and Kästner *et al.* (2017) studies, we can explain the red-shift in the gastric phase and color changing from yellow to red by the agglomeration of nanoparticles. As demonstrated by Walczak, the agglomerates disaggregate during the intestinal step, which can explain why samples color return to yellow. The return to particulate form of AgNPs after the intestinal stage can be explained by the stabilizing properties of bile salts. Indeed, bile salts have powerful detergent properties, which are important during digestion to stabilize bile that is in a supersaturated state (Heaton, 1969). The interactions between AgNPs and bile salts could be responsible for the slight blue shift after the intestinal step as AgNPs would be maybe more stable.

A study of Winuprasith *et al.* (2014) looked at the alterations of the protein corona of bLg(betalactoglobuline)-coated Au-NPs by biological surfactants like bile salts. They could demonstrate the presence of bile salts in the corona and that the protein coating was not fully displaced by bile salts. The effect of bile salts was described as "orogenic": the mixed corona was formed "*of islands of aggregated proteins surrounded by a sea of bile salts".* They could also reveal spectral changes due to bile salts. The spectral position of the surface plasmon resonance band of the bLg-coated GNPs redshifted from 582 nm to 580 when bile salts were added. This study indeed revealed the interaction of bile salts with the protein corona of NPs, which can explain the changes in spectral curve after the intestinal step showed in our study.

5. Quantification of the protein corona

According to the results of cytotoxicity assays, silver nanoparticles included in a food matrix were considered less toxic than pristine AgNPs. Results of the CellTiter-Glo assay showed that ATP content was significantly increased and EC50 would even double when the food matrix was added (42 µg/ml for pristine AgNPs and 81 µg/ml when added with the food matrix). The "food matrix effect" on AgNPs can therefore be described as protective against AgNPs toxicity. The characterization with UV-visible of AgNPs during the digestion could also reveal an effect of the food matrix. Indeed, a blue shift of the plasmon peak was observed when AgNPs are added with food matrix. Both results have led to the same interpretation: when AgNPs are in contact with the modelized food matrix, components of the food matrix adsorb on the surface of the nanoparticles and form a corona that can disrupt AgNPs properties. The role and importance of BSA in the effect of the food matrix and the formation of the protein corona has also been brought to light.

As a reminder, the formation of corona around nanoparticles upon contact with a biological fluid e.g. a culture medium or a digesting mixture is reported in many studies (Cerdevall *et al.*,2007; Lundqvist *et al.*, 2008; Monopoli *et al.*, 2011) for a long time. Nanoparticles interact with the proteins, small

molecules and ions adsorbing them on the surface, which creates a "*protein corona*" (Kokkinopoulou *et al.*, 2017).

Providing a new biological identity, the protein corona can be divided into the "hard" corona made of high binding affinity proteins and the "soft" corona, comprised of loosely bounds proteins with a low affinity and high exchange rates (Kokkinopoulou *et al.*, 2017). The formation of a corona around NPs was proven by many studies to alter *in vivo* response by reducing cytotoxicity through the impairment cellular uptake or the modulation of cell membrane damage (Hu *et al.*, 2011). Therefore, proving the presence of a protein corona around AgNPs is the first step to demonstrate its implication on the protecting effect of the food matrix. In order to prove the formation of a protein corona, a "protein corona assay" was performed; separated in two phases: the isolation of the AgNPs- proteins complexes followed by the protein quantification assay microBCA.

First, AgNPs solutions (0, 11.25, 33.75 and 101.25 µg/ml) were either mixed with HBSS or the food matrix and incubated 1 hour under stirring at 25° C in order to induce the adsorption of the proteins on the AgNPs surface. AgNPs-proteins complexes were then isolated by 3 centrifugations with different settings (speed and centrifugation time) that removed loosely and unbound proteins in solution. The amount of proteins adsorbed on AgNPs was then evaluated with the microBCA assay.

5.1 Protein quantification results

The microBCA assay provides a colometric detection of total protein. The principle is based on the reduction of Cu^{2+} to Cu^{+} by proteins in an alkaline environment. Reduced cupper is then chelated with 2 molecules of BCA (bincichoninic acid) into a purple complex. The absorbance is then read at 562 nm and is proportional to the protein concentration. BSA scales were created in order to convert absorbance obtained with microBCA into protein concentration.

Figure 28 shows the results obtained from the microBCA assay. The graph on the left shows the primary results: the protein concentration expressed in µg/ml. Primary values were then divided with the AgNPs concentration in order to obtain values expressed in µg/µg AgNPs showed on the right graph. Values are obtained from four independent repetitions with 3 replicates for concentration tested and reported on the table XX. Statistical analysis was performed comparing all values among themselves (Student test, $p < 0.0085$ due to Bonferroni-Sidak correction for results expressed in µg/ml and $p < 0.0170$ due to Bonferroni-Sidak correction for results expressed in µg/µg AgNPs) and indicated with letters in exponent.

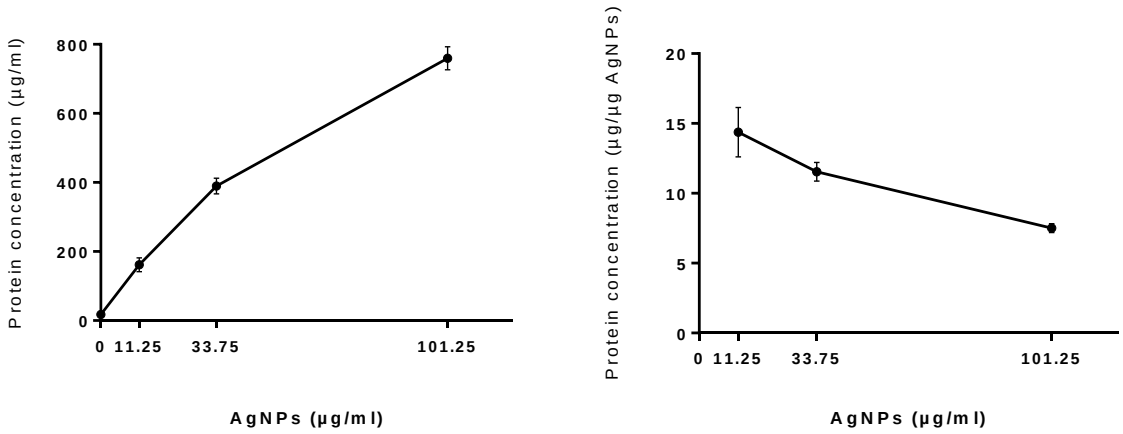

Figure 28. Results of the protein quantification with microBCA assay. Results are expressed in µg protein/ml in the left graph and in µg protein/µg AgNPs in the right graph. Values are obtained from four independent repetitions with three replicates (N=4, n=3).

AgNPs concentration (µg/ml)	Protein concentration (µg/ml)	Protein concentration (µg/µg AgNPs)
0	17 ± 5 [a]	-
11.25	162 ± 20 [b]	14 ± 2 [a]
33.75	389 ± 23 [c]	11.5 ± 0.7 [a]
101.25	759.5 ± 33 [d]	7.5 ± 0.3 [b]

Table 5. Protein concentration values at the different AgNPs concentration tested with microBCA assay. Results (Mean ± SEM) were obtained from four independent repetitions with three replicates (N=4, n=3). Treatments not connected with the same letter have protein corona quantification significantly different from each other (Student test, $p < 0.0085$ due to Bonferroni-Sidak correction for results expressed in µg/ml and $p < 0.0170$ due to Bonferroni-Sidak correction for results expressed in µg/µg AgNPs).

Regarding Figure 28, the left graph shows that the protein concentration rose with the concentration of AgNPs. Since the amount of silver nanoparticles increased, the number of total adsorbed proteins increased but compared to the AgNPs surface, the number of proteins adsorbed decreased as shown in the left graph. Statistically, all values are different from each other. More importantly, the significative difference between 0 and 11.25 values suggests that proteins of the corona's AgNPs were quantified by the assay and not the unbound proteins that may remain in the supernatant. Indeed, 17 µg/ml were initially measured in HBSS (0 µg/ml) whereas 162 µg/ml, 10-times more, were measured with the lowest concentration of AgNPs (11.25µg/ml).

However, protein concentrations must be compared proportionally to the quantity of AgNPs, hence the graph of the right expressing the protein concentration in µg proteins/µg AgNPs. This graph shows that less proteins were quantified proportionally to AgNPs as the concentration of silver increases. 14 µg of proteins per µg AgNPs are measured at the concentration of 11.25 µg/ml while 7.5 µg proteins per µg AgNPs were amounted when concentration was 10 times higher, 101.25 µg/ml. The value at 101.25µg/ml was the only being significantly different from the others. This graph suggest that the amount of proteins is not sufficient to form AgNPs fully coated with proteins. To this end, amount of

proteins in excess should be incubated with AgNPs. Further investigations should therefore focus on finding this amount in order to quantify the maximum amount of proteins that AgNPs can adsorb on their surfaces.

5.2 Discussion

When nanoparticles are incubated in a biological fluid, a protein corona is formed on their surface and can strongly influence their behavior *in vivo*. Many studies showed that AgNPs protein coronas impair biological responses like oxidative stress, endocytosis, cytotoxicity, … (Zhang *et al.*, 2016).

In order to confirm the hypothesis that the protein corona reduces the toxicity of AgNPs, the presence of the corona itself needs to be proved. Our results strongly suggest that proteins quantified by the microBCA were those adsorbed on the surface and that there is indeed a protein corona around AgNPs when they are included in our modelized food matrix. Therefore, the protecting effect of the food matrix could be explained by the formation of a protein corona around AgNPs. Further investigations should focus on characterizing the composition of the protein corona, in order to prove that BSA is indeed responsible for the blue shift shown in UV-visible spectroscopy results.

Our experiment was based on Monopoli *et al.* (2013) study who provides protocols to study nanoparticle protein corona. They suggested the microBCA assay to quantify the adsorbed proteins. Other studies could successfully quantify the protein corona around other NPs. Ho *et al.* (2015) incubated Au-NPs with four different proteins solutions of BSA, IgGn (normal – *i.e.* with unknown specificity - mouse immunoglobulin), FBG (fibrinogen), and Apo-A1 (Apolipoprotein A1) and performed microBCA assay but also Bradford assay and UV-vis spectroscopy. Kelly *et al.* (2015) used also microBCA to investigate the amount of proteins attached to NPs (polystyrene and carboxylated polystyrene NPs) when incubated in human plasma. They also demonstrate that results of the microBCA assay were similar to measurements with other quantification techniques tested: DCS (differential centrifugal sedimentation) and SDS-page; microBCA seems therefore a solid technique to quantify protein corona.

In this work, we therefore quantified the proteins adsorb on AgNPs surface, but other techniques exist and were used in many studies to characterize the protein corona and could give various information about it. Kokkinopoulou *et al.* (2017) used transmission electron microscopy (TEM) and were the first to visualize the morphology of the protein corona and able to provide a 3D model of its structure. Three types of polystyrene nanoparticles (plain, carboxyl-, and amino-functionalized) were incubated in human serum to form an initial corona. For the TEM analysis, proteins were embedded in a thin trehalose film containing heavy metals salts (like uranyl acetate) that provides high contrast samples, suitable for TEM. The protein corona was visualized with this technique and a 3D model reconstruction was used to quantify the amount of adsorb proteins covering the NPS. The soft corona could be estimated at 70-100 nm thick given the initial diameter of the NPs and the non-uniform structure could be pointed out. They also used DLS (dynamic light scattering) to measure the average hydrodynamic size of nanoparticles incubated in human serum and could see a size increase of the hydrodynamic radius, which confirmed TEM images. A separation process made of 3 washing/centrifugation steps was performed to separated loosely bound proteins form the hard corona. They evaluated the amount of proteins adsorbed at ~ 1.200 proteins after the first step and at 400 proteins after the whole process. The thickness was reduced to 15 nm after the last centrifugation.

Sharma *et al.* (2014) incubated gold nanoparticles (Au-NPs) with lysate of CH12.I.X-cell line derived from murine cell lymphoma, model of B-lymphocytes to see if Au-NPs could interact with membrane-bound or intracellular proteins of the CH12.I.X cells. They characterized the protein corona using UV-vis spectroscopy and TEM images. They could see the typical peak at 525 nm for the Au-NPs and peaks at lower wavelengths representing proteins that were absent when analyzing Au-NPs in the absence of cell lysates. Confirmed with TEM images, the formation of a protein corona could be proved with UV-visible spectroscopy.

Experiments performed in Kokkikopoulou's and Sharma's studies should be reproduced for further characterization of the protein corona formed around AgNPs incubated in our food matrix.

CONCLUSION & PERSPECTIVES

The emergence of nanotechnologies during the last decades has revolutionized our societies and industries. The use of engineered nanomaterials (ENMs) increases exponentially thanks to their unique designs and properties. Among metal ENMs, silver nanoparticles gained much attention in recent years thanks to their effective and well-known antibacterial activity. Used in all sectors of industry, they are incorporated in a large number of consumer products, especially in the food sector. Indeed, AgNPs could be found in plastic food containers, kitchenware, cutting boards, baby bottles, sprays for oral hygiene, food packaging's, … However, the leaching of Ag/ Ag^+ from these products has been reported by researchers (Von Goetz *et al.* 2013; Echegoyen & Nerin, 2013) raising great concerns about the exposure of consumers to AgNPs through food ingestion, which seems inevitable.

The toxicity of AgNPs has already been reported in many *in vivo* and *in vitro* studies. Exposed directly to intestinal cells, AgNPs are internalized by endocytosis and can disrupt their permeability, decrease cell viability and induce inflammation mechanisms and oxidative stress. However, AgNPs are ingested before they reach our intestinal cells and their transit through the GIT tract is less likely to be without consequences. They could be highly altered by the digestive enzymes, strong pH shifts and interactions with food components, consequently leading to a disruption of their initial toxicity. To study AgNPs toxicity properly, the use of methods that account for the physico-chemical transformations occurring when they are incorporated into food and during their transit across the GIT is essential to produce realistic outcomes.

In this framework, the first objective of this master thesis was the evaluation of the impact of food components and digestive enzymes on the cytotoxicity of silver nanoparticles in a model of the gut epithelium. The model is a coculture consisting of Caco-2 cells, coming from a human colon carcinoma and differentiating into enterocyte-like cells, mixed in a ratio 3:1 with HT29-MTX cells, also coming from a human colon adenocarcinoma, but treated with methotrexate in order to produce mucins and therefore mimicking human goblet cells. The coculture Caco-2/HT29-MTX represents the two major cell-types found in the human intestinal epithelium.

An *in vitro* digestion process on AgNPs (NM-300K, 15 nm) was performed in the presence or absence of a modelized food matrix to be the as close as possible to the real conditions that orally ingested AgNPs would be subjected to. The food matrix model was comprised of realistic concentrations of triolein, starch, and bovine serum albumin chosen as representants of the three main macronutrients. The *in vitro* digestion is a process separated into 3 steps (the salivary, the gastric and the intestinal) among which the type of digestive enzymes, the duration of incubation and pH were adjusted to reproduce the most realistic digestion. Digested and undigested AgNPs included or not in the food matrix were then incubated on the coculture intestinal model for cytotoxicity assessing.

To carry on such a study, preliminary concerns needed to be clarified. First, the inherent toxicity of the digesting solutions needed to be eliminated. The cytotoxicity of different dilutions was tested on the coculture model Caco-2/HT29-MTX cells. Results showed that indeed, if used undiluted the digestive enzymes were cytotoxic in this cell culture system, but a 2 times dilution was enough to inhibit their toxic effect. Therefore, such a dilution of all the treatments before their incubation on cells was performed so that the effect of treated AgNPs solely appeared.

Secondly, interference assays were performed to make sure that AgNPs would not react with the cytotoxicity assays and bias our results. Our results indicate that a potential interference was less likely

to appear because of the very low concentrations of AgNPs remaining on cells before we performed the cytotoxicity assays.

Then the different treatments previously explained were incubated on cells. The toxicity induced by them was monitored through 3 assays: CellTiter-Glo, CellTiter-Blue and Crystal violet assessing ATP content, cell viability and cellular adherence respectively.

Results showed, on one hand, that pristine AgNPs were less toxic when included in a food matrix: ATP content level was twice higher at the highest AgNPs concentration. According to other studies, the formation of a protein corona around AgNPs is the most likely explanation. On the other hand, we saw that digested AgNPs were more toxic than pristine, according to CTB and CV assays. Studies reporting a similar deleterious effect of digestion on AgNPs toxicity could not be found but our results could be explained by changes in size, aggregation state or dissolution induced by the digestion, as also reported by other studies (Bove *et al.*, 2017; Ault *et al.*, 2017). The hypothesis of the increased enzymatic activity of pancreatic enzymes in the presence of AgNPs was also suggested. Digested AgNPs with food matrix showed less toxicity than without, but still, they were more toxic than pristine AgNPs. Similar and opposite results were found in literature, but the stabilizing properties of the food components were suggested as a redundant explanation and can corroborate our results. However, the fact remains that pristine AgNPs and digested AgNPs included in a food matrix showed significantly different results.

Given our results, we should conclude that the toxicity of AgNPs is strongly influenced by digestive enzymes and food components. Therefore, both parameters should be considered as necessary in the next toxicological studies on AgNPs. Indeed, their absence could produce distorted results and lead to misinterpretations.

The second part of this thesis consisted in searching explanations and complementary information about the results obtained from the cytotoxicity assays. To this end, we first characterized AgNPs throughout the *in vitro* digestion thanks to UV-vis spectroscopy and second, quantified the adsorbed proteins on AgNPs when these were incubated in the food matrix.

First, results of the UV-vis spectra showed indeed that the food matrix has an effect on AgNPs: a blue shift appeared. The hypothesis retained, on the basis of literature data, was the formation of a protein corona, comprised essentially of BSA molecules. After quantifying the amount of proteins adsorbed around AgNPs, we could indeed confirm that when AgNPs are in contact with our modelized food matrix, a protein corona forms around them and therefore can impact their toxicity.

Second, macroscopic and spectral changes during digestion could be observed. While samples kept their initial yellow color and peak wavelength after the salivary step, spectral curves red-shifted and widened after the gastric step; the color of the solution turned to red. Reported in other studies, this effect bears witness the formation of aggregates in the gastric compartment. After the intestinal step, the solution returns to a yellow color, meaning that aggregates were dissolved, and the spectral curves were slightly shifted towards lower wavelength compared to the salivary step. The detergent and stabilizing properties of bile salts were suggested as main explanation for the breakdown of agglomerates such as the blue shift.

This master thesis provides undeniably insights about the effect of the GI tract and food components on AgNPs but also raises the need for further investigations.

The importance of bovine serum albumin in the effect of the food matrix is only suggested in this study and should be further investigated and proved by qualitative characterization of the food matrix. A very popular technique to characterize the composition of the protein corona is SDS-PAGE followed with MS analysis. In the same way, other techniques to characterize the protein corona should be performed like an assessment of the size with DLS, the morphology with TEM and surface charge with zeta potential measurement. Besides, our protocol of the quantitative characterization of the protein corona could be improved by putting enough proteins in solution to form fully coated AgNPs. We could therefore have an assessment of the maximum amount of proteins that AgNPs can adsorb.

Furthermore, characterizing quantitatively and qualitatively the protein corona after each digestive step should provide more information about the joint effect of digestive enzymes and food matrix and the new biological identity acquired by AgNPs. After each digestive step, several samples could be collected and characterized by UV-vis spectroscopy, TEM, DLS, microBCA and the composition of the protein corona could be investigated by gel electrophoresis followed by quantitative mass spectrometry.

Assessing the effect of AgNPs on the activity of pancreatic enzymes should also be interesting in order to give explanations about the higher toxicity of digested AgNPs. Trypsin activity could be measured with a colorimetric assay e.g. using the release of p-nitroaniline or fluorometric one with the hydrolysis of MCA (methylcoumarin-amide) and lipase activity with a colorimetric assay based on the hydrolysis of a triglyceride substrate into glycerol.

BIBLIOGRAPHY

Abbott Chalew, TE. And Schwab, KJ. (2013). "Toxicity of commercially available engineered nanoparticles to Caco-2 and SW480 human intestinal epithelial cells." Cell Biology and Toxicology **29** (2): 101-116.

Agnihotri, S., Mukherji, S., and Mukherji, S. (2014). "Size-controlled silver nanoparticles synthesized over the range 5–100 nm using the same protocol and their antibacterial efficacy." RSC Adv **4**: 3974–3983.

Ajitha, B., Reddy, Y.A.K., and Reddy, P.S. (2015). "Green synthesis and characterization of silver nanoparticles using *Lantana camara* leaf extract", Mater. Sci. Eng **49**: 373-381.

Alagarasi A. (2013). "Introduction to nanomaterials". retrieved from https://www.researchgate.net/publication/259118068_Chapter_-_INTRODUCTION_TO_NANOMATERIALS .

Alzaharna, M. (2016). "Unit II: Bioenergetics and Carbohydrate Metabolism". Retrieved from http://slideplayer.com/slide/10790043/

Argentiere, S., Cella, C., Cesaria, M., Milani, P. and Lenardi, C. (2016). "Silver nanoparticles in complex biological media: assessment of colloidal stability and protein corona formation". Journal of Nanoparticle Research **18** :253.

Arora, S., Jain, J., Rajwade, J.M., Paknikar, K.M. (2008). "Cellular responses induced by silver nanoparticles: *In vitro* studies." Toxicology Letters **179**: 93-100.

Asharani, P.V., Kah Mun, G.L., Hande, M.P. and Valiyaveettil, S. (2009). "Cytotoxicity and genotoxicity of silver nanoparticles in human cells". ACS Nano. **3** (2): 279-290.

Asharani P.V., Wu L.Y., Gong Z. and Valiyaveettil S. (2008). "Toxicity of silver nanoparticles in zebrafish models." Nanotechnology **19**: 1-8.

ASTDR Agency for Toxic Substances & Diseases Registry (2011). "Silver" on Toxic substances portal retrieved from https://www.atsdr.cdc.gov/substances/toxsubstance.asp?toxid=97

Ault, AP, Stark, DI., Asxon, JL., Keeney, JN., Maynard, AD. et al. (2016). "Protein corona-induced modification of silver nanoparticle aggregation in simulated gastric fluid". Environm Sci Nano **3** (6): 1510-1520.

Barbalinardo, M., Caicci, F., Cavallini, M. and Gentili, D. (2018). "Protein corona mediated uptake and cytotoxicity of silver nanoparticles in mouse embryonic fibroblast." Small.

Bellmann, S., Carlander, D., Fasano, A., Momcilovic, D., Scimeca, J.A., Waldman, W.J. et al. (2015). "Mammalian gastrointestinal tract parameters modulating the integrity, surface properties, and absorption of food-relevant nanomaterials". Nanomedicine and Nanobiotechnology **7**: 609-622.

Biowest (2013). " Bovine Serum Albumin 30 % - Technical Data sheet". Retrieved from https://www.biowest.net/media/a0296t__073787700_1349_07012014.pdf .

Böhmert, L., Girod, M., Hansen, U., Maul, R., Knappe, P., Niemann, B. et al. (2014). "Analytically monitored digestion of silver nanoparticles and their toxicity for human intestinal cells". Nanotoxicology **8** (6): 631-642.

Bone, A.J., Colman, B.P., Gondikas, A.P., Newton, K.M., Harrold, K.H., Cory, R.M et al. (2012). "Biotic and abiotic interactions in aquatic microcosms determine fate and toxicity of Ag nanoparticles: Part 2–toxicity and Ag speciation". Environ. Sci. Technol 46 : 6925–6933.

Bornstein, J.C. (2009). "Autonomic nervous system : Gastrointestinal control". In: Squire, L.R. (Ed.), Encyclopedia of Neuroscience. Academic Press, Oxford, pp. 929 -939.

Bott, J., Störmer, A. and Franz, R. (2014)." A comprehensive study into the migration potential of nano silver particles from food contact polyolefins." Chemistry of Food, Food Supplements, and Food Contact Materials: From Production to Plate, pp 51-70.

Boudreau, M.D., Imam, M.S., Paredes, A.M., Bryant, M.S, Cunningham, C.K., Felton, R.P. et al. (2016). "Differential effects of silver nanoparticles and silver ions on tissue accumulation, distribution, and toxicity in the Sprague Dawley rat following daily oral gavage administration for 13 Weeks ", Toxicological Sciences 150 (1): 131–160.

Bouwmeester, H., Poortman, J., Peters, RJ., Wijma, E., Kramer, E. Makama, S. et al. (2011). "Characterization of translocation of silver nanoparticles and effects on whole-genome gene expression using an in vitro intestinal epithelium coculture model." ACS Nano 5 (5): 4091-4103.

Bove, P., Malvindi, M.A. and Sabella, S. (2017). "In vitro human digestion test to monitor the dissolution of silver nanoparticles". Journal of Physics: Conference Series 838 (1).

Calderón-Jiménez, B., Johnson, M. E., Montoro Bustos, A. R., Murphy, K. E., Winchester, M. R., and Vega Baudrit, J. R. (2017). "Silver Nanoparticles: Technological Advances, Societal Impacts, and Metrological Challenges." Frontiers in Chemistry 5 (6).

CE. (2011). "Regulation EU No 1169/2011 of the European parliament and of the council of 25 October 2011, Commission Directive 1999/10/EC, Directive 2000/13/EC of the European Parliament and of the Council, Commission Directives 2002/67/EC and 2008/5/EC and Commission Regulation (EC) No 608/2004". Official Journal of the European Union L304/18.

CE (2011). "Recommendations: Commission recommendation of 18 october 2011 on the definition of nanomaterial (2011/696/EU)". Official Journal of the European Union I. 275/38.

Cerdevall, T., Lynch, I., Lindman, S., Berggård, T., Thulln, E., Nilsson, H., Dawson, K.A. and Llnse, S. (2007). "Understanding the nanoparticle–protein corona using methods to quantify exchange rates and affinities of proteins for nanoparticles". Proceedings of the National Academy of Sciences 104 (7): 2050-2055.

Chen, X. and Schluesener, H.J. (2008). "Nanosilver: A nanoproduct in medical application". Toxicology Letters 176: 1-12.

Chopra, I. (2007). "The increasing use of silver-based products as antimicrobial agents: a useful development or a cause for concern". Journal of antimicrobial chemotherapy 59 (4): 587-59.

Contado, C. (2015). "Nanomaterials in consumer products: a challenging analytical problem". Frontiers in Chemistry 3:48.

Corr, S.C, Gahan, C. G. and Hill, C. (2008).” M-cells: origin, morphology and role in mucosal immunity and microbial pathogenesis “. FEMS Immunol Med Microbiol 52 (1): 2-12.

Das, R., Nath, S.S., Chakdar, D., Gope, G. and Bhattacharjee, R. (2010). “Synthesis of silver nanoparticles and their optical properties”. Journal of Experimental Nanoscience 5 (4).

Dasgupta, N., Ranjan, S., Patra, D., Srivastava, P., Kumar, A. and Ramalingam, C. (2016). “Bovine serum albumin interacts with silver nanoparticles with a “side-on” or “end on” conformation.” Chemico-Biological Interactions 253 : 100-111.

DeLoid, G.M., Wang, Y., Kapronezai, K., Lorente, L.R., Zhang, R., Pyrgiotakis, G. et al. (2017). “An integrated methodology for assessing the impact of food matrix and gastrointestinal effects on the biokinetics and cellular toxicity of ingested engineered nanomaterials.” Particle and Fibre Toxicology 14 (40).

Dhawan, A. and Sharma, V. (2010). “Toxicity assessment of nanomaterials: methods and challenges”. Analytical and Bioanalytical Chemistry 398 (2): 589-605.

Dhingra, D., Michael, M., Rajput H. and Patil R.T. (2012). “Dietary fibre in foods: a review”. Journal of Food Science and Technology 49 (3): 255-266.

Durán, N., Marcato, P.D., De Conti, R., Alves, O.L., Costa, F.T.M., and Brocchi, M. (2010).” Potential use of silver nanoparticles on pathogenic bacteria, their toxicity and possible mechanisms of action.” J Braz Chem Soc 21: 949-959.

Echegoyen, Y. and Nerin, C. (2013). “Nanoparticle release from nano-silver antimicrobial food containers”. Food and Chemical Toxicology 62: 16-22.

Eom, H-J and Choi, J. (2010). “p38 MAPK activation, DNA damage, cell cycle arrest and apoptosis as mechanisms of toxicity of silver nanoparticles in Jurkat T cells.” Environmental Science & Technology 44 (21): 8337-8342.

EU. (2009). “Regulation (EC) No 1223/2009 of the European parliament and of the Council of 30 November 2009 on cosmetic products”. Retrieved from https://ec.europa.eu/health/sites/health/files/endocrine_disruptors/docs/cosmetic_1223_2009_regulation_en.pdf

EU. (2012). “Regulation (EU) No 528/2012 of the European Parliament and of the Council of 22 May 2012 concerning the making available on the market and use of biocidal product.” Retrieved from https://www.echa.europa.eu/documents/10162/17158507/consolidated_bpr_en.pdf

Faure, P. (2012). " Chapitre 3 : Digestion et absorption des glucides ". retrieved from http://unf3s.cerimes.fr/media/paces/Grenoble_1112/faure_patrice/faure_patrice_p03/faure_patrice_p03.pdf

Feher, J. (2017). “Digestion and absorption of the macronutrients “. In: Quantitative Human Physiology: An Introduction. Second edition, Academic Press, Oxford, pp 821-833.

Feoktistova, M., Geserick, P. and Leverkus, M. (2016). “Crystal violet assay for determining viability of cultured cells”. Cold Spring Harbor Protocols 4.

Ferraretto, A., Bottani, M., De Luca, P., Cornaghi, L., Arnaboldi, F., Magglioni, A. et al. (2018). "Morphological properties of a differentiated Caco2/HT-29 co-culture as an in vitro model of human intestinal epithelium". Biosciences Reports **38** (2).

Fleischer, C.C. and Payne, C.K. (2014). "Nanoparticle-cell interactions: molecular structure of the protein corona and cellular outcomes", Acc Chem Res **47** (8): 2651-2659.

Florence, A.T. (2005). "Nanoparticle uptake by the oral route: fulfilling its potential?". Drug Discovery Today: Technologies 2(1): 75-81.

Foldbjerg, R., Jiang, X., Miclăuş, T., Chen, C., Autrup, H. and Beer, C. (2015). "Silver nanoparticles–wolves in sheep's clothing? ". Toxicol. Res. **4** :563–575.

Fröhlich, E. E. and Fröhlich, E. (2016). "Cytotoxicity of nanoparticles contained in food on intestinal cells and the gut microbiota" International Journal of Molecular Sciences **17** (4): 509.

Ganong, F. W. (2003). "Review of Medical Physiology", 21st edition, Mc Graw Hill, pp. 471-516.

Garabedian, E.L., Roberts, L.J.J., McNevin, M.S. and Gordon, J.I. (1997). "Examining the role of Paneth cells in the small intestine by lineage ablation in transgenic mice, The journal of biological chemistry". Journal of Biological Chemistry **272**: 23729-23740.

Giri, K., Shameer, K., Zimmermann, M. T., Saha, S., Chakraborty, P. K., Sharma, A. et al. (2014). "Understanding Protein–Nanoparticle interaction: a new gateway to disease therapeutics". Bioconjugate Chemistry **25** (6): 1078–1090.

Gliga, A.R., Skoglund, S., Wallinder, I.O., Fadeel, B. and Karlsson, H.L. (2014). "Size-dependent cytotoxicity of silver nanoparticles in human lung cells: the role of cellular uptake, agglomeration and Ag release." Particle and Fibre Toxicology **11** (11).

Global Market Insights (2017). "Nanosilver Market Size By Mode of Synthesis (Physical, Biological, Chemical Reduction), By End-user (Electrical & Electronics, Healthcare, Food & Beverages, Textile, Water Treatment), Industry Analysis Report, Regional Outlook (U.S., Canada, Germany, UK, France, Spain, Italy, China, India, Japan, Australia, Indonesia, Malaysia, Brazil, Mexico, South Africa, GCC), Application Growth Potential, Price Trends, Competitive Market Share & Forecast, 2017 – 2024" retrieved from https://www.gminsights.com/pressrelease/nanosilver-market

Gnanadhas, DP., Ben Thomas, M., Thomas, R., Raichur, AM. And Chakravorthy D. (2013). "Interaction of silver nanoparticles with serum proteins affects their antimicrobial activity in vivo." Antimicrobial Agents and Chemotherapy **57** (10): 4945-4955.

Go, MR., Bae, SH., Kim, HJ, Yu, J. and Choi, SJ. (2017). "Interactions between food additives silica nanoparticles and food matrices". Frontiers in Microbiology **8**:1013.

Griffin, S., Masood, M.I., Nasim, M.J., Sarfraz, M, Eboikawe, A.P, et al. (2018). "Natural Nanoparticles: A Particular Matter Inspired by Nature." Antioxidants **7**: 3.

Greulich, C., Diendorf, J., Simon, T., Eggeler, G., Epple, M. and Koller, M. (2011)." Uptake and intracellular distribution of silver nanoparticles in human mesenchymal stem cells". Acta Biomaterialia **7** (1): 347–354.

Guénard, H. (2009). " Physiologie Humaine ", Editions Pradel, pp. 341-382.

Heaton, K.W. (1969). "The importance of keeping bile salts in their place." Gut **10** (10): 857-863.

Histology@Yale, (2018)." GI Tract Lab", retrieved from http://medcell.med.yale.edu/histology/gi_tract_lab.php

Ho, YT., Poinard, B., Yeo, E.L. and Kah, J.C. (2015). "An instantaneous colorimetric protein assay based on spontaneous formation of protein corona on gold nanoparticles". Analyst 140 (4): 1026-1036.

Hogben, C.A.M., Schanker, L.S., Tocco, D.J. and Brodie, B.B. (1957). "Absorption of drugs from the stomach. II. The human". Journal of Pharmacology and Experimental Therapeutics **120** (4): 540-545.

Hollebeeck, S., Borlon, F., Schneider, YJ., Larondelle, Y., and Rogez, H. (2012). "Development of a standardized human *in vitro* digestion protocol based on macronutrient digestion using response surface methodology", Food chemistry **138** (2-3): 1936-1944.

Hu, W., Peng, C., Lu, M., Li, X., Zhang, Y., Chen, N., Fan, C, Huang, Q. (2011). "Protein corona-mediated mitigation of cytotoxicity of graphene oxide ". ACS Nano **5** (5): 3693-3700.

Huang, Y., Chen, S., Bing, X., Gao, C., Wang, T. and Yuan, B. (2011)." Nanosilver Migrated into Food-Simulating Solutions from Commercially Available Food Fresh Containers". Packaging Technology and Science **24** (5): 291-297.

International Starch Institute (2018). "Technical Memorandum on wheat starch". Retrieved from http://www.starch.dk/isi/starch/tm33wheat.asp

ISO/TS 80004-1 (2015). "Nanotechnologies-Vocabulary-Part 1: Core Term". Geneva: International Organization for Standardization. Retrieved from https://www.iso.org/obp/ui/#iso:std:iso:ts:80004:-1:ed-2:v1:en

ISO/TS 80004-2 (2015). "Nanotechnologies-Vocabulary-Part 2: Nano-Objects." Geneva: International Organization for Standardization. Retrieved from https://www.iso.org/obp/ui/#iso:std:iso:ts:80004:-1:ed-2:v1:en

ISO/TS 80004-4 (2015). "Nanotechnologies-Vocabulary-Part 4: Nanostructured Materials". Geneva: International Organization for Standardization. Retrieved from https://www.iso.org/obp/ui/#iso:std:iso:ts:80004:-1:ed-2:v1:en

Jarak, I., Carrola, J., Barros, A.S., Gil, A.M., Pereira, M.L., Corvo, M.L. and Duarte I.F. (2017). "From the cover: Metabolism modulation in different organs by silver nanoparticles: an NMR metabolomics study of a mouse model." Toxicological Sciences **159** (2): 422-435.

Ji, JH., Jung, JH., Kim, SS., Yoon, JU., Park, JD. And Choi, BS. (2007). "Twenty-eight-day inhalation toxicity study of silver nanoparticles in Sprague-Dawley rats". Inhalation Toxicology **19** (10) : 857-871.

Jia, J., Li, F., Zhou, H., Bai, Y., Liu, S., Jiang, Y. et al. (2017)." Oral exposure to silver nanoparticles or silver ions may aggravate fatty liver disease in overweight mice". Environmental Science & Technology **51**: 9334-9343.

Jiang, X., Foldbjerg, R., Miclaus, T., Wang, L., Singh, R., Hayashi, Y. *et al*. (2013)." Multi-platform genotoxicity analysis of silver nanoparticles in the model cell line CHO-K1", Toxicology Letters **222**: 55–63.

Jiang, X., Miclaus, T., Wang, L., Foldbjerg, R., Sutherland, D. S., Autrup, H. *et al*. (2015)." Fast intracellular dissolution and persistent cellular uptake of silver nanoparticles in CHO-K1 cells: implication for cytotoxicity." Nanotoxicology **9**: 1841-189.

Jung, J. Raghavendra, G.M., Kim, D. and Seo, J. (2018). "One-step synthesis of starch-silver nanoparticle solution and its application to antibacterial paper coating". Int J Biol Macromol **107** (Pt B): 2285-2290.

Kästner, C., Lichtenstein, D., Lampen, A. and Thünemann, A.F. (2017)." Monitoring the fate of small silver nanoparticles during artificial digestion". Colloids and Surfaces A: Physicochemical and Engineering Aspects **526**: 76-81.

Keat, L.C., Aziz, A., Eid, M.A. and Elmarguzi, A.N. (2015)." Biosynthesis of nanoparticles and silver nanoparticles", Bioresources and Bioprocessing a Springer Open Journal **2**:47.

Keller, A. A., McFerran, S., Lazareva, A. and Suh S. (2013). "Global life cycle releases of engineered nanomaterials" Journal of Nanoparticle Research **15** :1692.

Kelly, PM., Åberg, C., Polo, E., O'Connell, A., Cookman, J., Fallon, J., Krpetić, Z. and Dawson, A.K. (2015). "Mapping protein binding sites on the biomolecular corona of nanoparticles". Nature Nanotechnology **10**: 472-479.

Khan, I., Saeed, K. and Khan, I. (2017). "Nanoparticules: properties, applications and toxicities ". Arabian Journal of Chemistry.

Khatab H. (2016). "Colloid". retrieved from https://fr.slideshare.net/hassankhatab/colloid-62075135.

Kholoud, M.M., Abou, E-N., Abdulrhman, A-W., and Reda, A.A.A. (2010)." Synthesis and applications of silver nanoparticles", Arabian Journal of Chemistry **3** (3): 135-140.

Kim,Y.S., Kim, J.S., Cho, H.S., Rha, D.S. and Kim, J.M. (2008). "Twenty-eight-day oral toxicity, genotoxicity, and gender-related tissue distribution of silver nanoparticles in sprague-dawley rats". Inhalation Toxicology **20** (6): 575-583.

Kittler, S., Greulich, C., Gebauer, J.S., Diendorf, J., Treuel, L., Ruiz, L. et al. (2010). "The influence of proteins on the dispersibility and cell-biological activity of silver nanoparticles ". Journal of Materials Chemistry **20** (3): 521-518.

Klein, C.L., Comero, S., Stahlmecke, B., Romazanov, J., Kuhlusch, T.A.J, Van Doren, E. et al. (2011). "NM-Series of Representative Manufactured Nanomaterials NM-300 Silver - Characterization, Stability, Homogeneity". JRC Scientific and Technical Reports.

Kokkinopoulou, M., Simon, J., Landfester, K., Mailänder, V. and Lieberwirth, I. (2017). "Visualization of the Protein Corona: towards a biomolecular understanding of nanoparticle-cell-interactions ". Nanoscale **9** (25):8858-8870.

Kroll, A., Pillukat, M.H., Hahn, D. and Schnekenburger, J. (2009). "Current in vitro methods in nanoparticle risk assessment: Limitations and challenges". European Journal of Pharmaceutics and Biopharmaceutics 72: 370-377.

Kvítek,L., Panáček, A.,Soukupová,J, Kolář,M., Večeřová,R., Prucek,R., Holecová,M and Zboril R. (2008). "Effect of Surfactants and Polymers on Stability and Antibacterial Activity of Silver Nanoparticles (NPs)", J. Phys. Chem. 112 (15): 5824-5834.

Labille, J. and Brant, J.A. (2010). "Stability of nanoparticles in water", Nanomedicine 5 (6): 985-998.

Laloux, L. (2013). " Etude in vitro de l'impact d'une digestion de nanoparticules d'argent sur leurs propriétés physico-chimiques et sur leur toxicité dans un modèle cellulaire de barrière intestinale. "

Lankveld,D.P., Oomen, A.G., Krystek, P., Neigh, A., Troost-de Jong, A., Noorlander, C.W et al. (2010). "The kinetics of the tissue distribution of silver nanoparticles of different sizes." Biomaterials 31 (32) : 8350-8361.

Lau, CP., Abdul-Wahab, M.F., Jaafar, J., Chan, G.K. and Rashid, N.A.A. (2016). "Effect of pH and biological media on polyvinylpyrrolidone-capped silver nanoparticles ". AIP Conference Proceedings 1756 (1).

LCI (2018). "Nanoparticules dissimulées dans l'alimentaire et les cosmétiques : le dioxyde de titane au cœur des soupçons." retrieved from https://www.lci.fr/conso-argent/plaintes-de-l-ufc-que-choisir-contre-les-nanoparticules-dissimulees-dans-l-alimentaire-et-les-cosmetiques-le-dioxyde-de-titane-au-coeur-des-soupcons-2028374.html

Le Ferrec, E., Chesne, C., Artusson, P., Brayden D., Fabre, G., Gires, P., et al. (2001). "In vitro models of the intestinal barrier", Alternatives to Laboratory Animals ATLA 29: 649-668.

Le Ouay, B. and Stellacci, F. (2015). "Antibacterial activity of silver nanoparticles: a surface science insight." Nano Today 10: 339-354.

Lesniak, A., Fenaroli, F., Monopoli, M., Åberg, C., Dawson, K., and Salvati, A. (2012). "Effect of the presence or absence of a protein corona on silica nanoparticle uptake and impact on cells", ACS Nano 6 (7): 5845-5857.

Li, W.R., Xie, X.B., Shi, Q.S., Zeng, H.Y., Ou-Yang, Y.S. and Chen, Y.B. "Antibacterial activity and mechanism of silver nanoparticles on *Escherichia coli* ". Appl. Microbiol. Biotechnol 8 :1115–1122

Lichtenstein, D., Ebmeyer, J., Knappe, P., Juling, S., Böhmert, L., Selve, S. et al. (2015). "Impact of food components during *in vitro* digestion of silver nanoparticles on cellular uptake and cytotoxicity in intestinal cells". Biological Chemistry 396 (11): 1255-1264.

Lim, H.K., Lal Gurung, R. and Prakash Hande, M. (2017). "DNA-dependent protein kinase modulates the anti-cancer properties of silver nanoparticles in human cancer cells". Mutation Research/Genetic Toxicology and Environmental Mutagenesis 824: 32-41.

Liu, W., Wu, Y., Wang, C., Li, H. C., Wang, T., Liao, C. Y. *et al.* (2010). "Impact of silver nanoparticles on human cells: effect of particle size". Nanotoxicology 4: 319–330.

Lövestam, G., Rauscher H., Roebben, G., Klüttgen, B.S., Gibson, N., Putaud, JP. And Stamm, H. (2010). "Considerations on a definition of nanomaterial for regulatory purposes". JRC Reference Reports, European Commission.

Lunqvist, M., Stigler, J., Elia, G., Lynch, I., Cerdevall, T. and Dawson, KA. (2008). "Nanoparticle size and surface properties determine the protein corona with possible implications for biological impacts." Proc Natl Acad Sci U S A 105 (38): 14265-14270.

Maayan, G. and Liu, LK. (2011). "Silver nanoparticles assemblies mediated by functionalized biomimetic oligomers". Biopolymers 96 (5): 679-687.

Mao, B.H., Chen, Z.Y., Wang, Y.J. and Yan, SJ. (2018). "Silver nanoparticles have lethal and sublethal adverse effects on development and longevity by inducing ROS-mediated stress responses". Scientific Reports 8: 2445.

Marambio-Jones, C. and Hoek, E.M.V. J. (2010)." A Review of the antibacterial effects of silver nanomaterials and potential implications for human health and the environment", Journal of Nanoparticle Research 12 (5): 1532-1551.

Markell, L.K., Wezalis, S.M., Roper, J.M., Zimmermann, C. and Delaney, B. (2017). "Incorporation of in vitro digestive enzymes in an intestinal epithelial cell line model for protein hazard identification". Toxicology in Vitro 44: 85-93.

Márquez, M., Fernández Gutiérrez del Álamo, C. and Girón-González, J.A. (2016). "Gut epithelial barrier dysfunction in human immunodeficiency virus-hepatitis C virus coinfected patients: Influence on innate and acquired immunity". World Journal of Gastroenterology 22 (4): 1433-1448.

Martirosyan, A., Bazes, A. and Schneider, Y-J. (2014). "In vitro toxicity assessment of silver nanoparticles in the presence of phenolic compounds – preventive agents against the harmful effect?" Nanotoxicology 8 (5): 573-582.

Martínez-Maqueda, D., Miralles, B. and Recio, I. (2015) "HT29 Cell Line". In: Verhoeckx K. et al. (eds) The Impact of Food Bioactives on Health. Springer, Cham. pp 113-124.

McCracken, C., Zane, A., Knight, D., Hommel, E., Dutta, P.K. and Waldman, W.J. (2015). "Oxidative stress-mediated inhibition of intestinal epithelial cell proliferation by silver nanoparticles." Toxicology In Vitro 29: 1793 – 1808.

McQuillan, J.S., Infante, H.G., Stokes, E. and Shaw, A.M. (2012). "Silver nanoparticle enhanced silver ion stress response in Escherichia coli K12". Nanotoxicology 6: 857–866.

Mendis, P., de Silva, R.M., Nalin de Silva, K.M., Wijenayaka, L.A., Jayawardana, K. and Yan, M. (2013). "Nanosilver Rainbow: A rapid and facile method to tune different colours of nanosilver through the controlled synthesis of stable spherical silver nanoparticles." Journal Name 00: 1-3.

Meng, J., Sindberg, G. and Roy, S. (2015). "Disruption of gut homeostasis by opiods accelerates HIV disease progression ". Frontiers in Microbiology 6: 643.

Mignard, L. (2016). " Influence d'une digestion in vitro sur la toxicité de nanoparticules et des ions argent sur un modèle de coculture de la barrière intestinale. "

Minekus, M., Alminger, M., Alvito, P., Balance, S., Bohn, T., Bourlieu, C., et al. (2014). "A standardized static *in vitro* digestion method suitable for food - an international consensus" Food & Function **5** (6): 1113–1124.

Mirzajani, F., Ghassempour, A., Aliahmadi, A. and Esmaeili, M.A. (2011). "Antibacterial effect of silver nanoparticles on Staphylococcus aureus". Res. Microbiol. **162** (5): 542-549.

Mittal, R.K. (2011)." Motor function of the pharynx, esophagus and its sphincters", Morgan & Claypool Life sciences, San Rafael (CA).

Monopoli, M.P., Pitek, A.S., Lynch, I. and Dawson, KA. (2013). "Formation and characterization of the nanoparticle–protein corona". Methods Mol Biol **1025**: 137-155.

Monopoli, M.P., Walczyk,D. , Campbell,A., Elia, G., Lynch, I., Baldelli Bombelli, F., and Dawson K.A. (2011). "Physical-Chemical aspects of protein corona: relevance to in vitro and in vivo biological impacts of nanoparticles". Journal of the American Chemical Society **133**: 2525-2534.

Monteiro-Riveire, N.A., Inman, AO. And Zhang, LW. (2009). "Limitations and relative utility of screening assays to assess engineered nanoparticle toxicity in a human cell line". Toxicology and Applied Pharmacology **234** (2): 222-235.

Monteiro-Riviere, N.A., Samberg, M.E., Oldenburg, S.J. and Riviere, J.E. (2013). "Protein binding modulates the cellular uptake of silver nanoparticles into human cells: Implications for in vitro to in vivo extrapolations? ". Toxicology Letters **220** (3): 286-293.

Munjar, C.W. and Gilbert, B.D. (2017). "Synthesis and characterization of lipid coated nanoparticles as drug delivery vehicles". Retrieved from http://digitalcommons.linfield.edu/cgi/viewcontent.cgi?article=1239&context=symposium

Munger, MA., Radwanski, P., Hadlock GC., Stoddard, G., Shaaban, A., Falconer, J. et al. (2014). "In vivo human time-exposure study of orally dosed commercial silver nanoparticles." Nanomedicine **10** (1): 1-9.

Mwilu, S.K., El Badawy, A.M., Bradham, K., Nelson, C., Thomas, D., Scheckel, K.G. (2013). "Changes in silver nanoparticles exposed to human synthetic stomach fluid: Effects of particle size and surface chemistry". Science of the Total Environment **447**: 90-98.

Nanocomposix (2018). "Silver Nanoparticles: Optical Properties ". retrieved from https://nanocomposix.eu/pages/silver-nanoparticles-optical-properties

Nash, JA., Ballard, TN., Weaver, TE., and Akinbi, HT. (2006). "The peptidoglycan-degrading property of lysozyme is not required for bactericidal activity in vivo ", Journal of Immunology **177** (1): 519-526.

Nollevaux, G., Devillé, C., El Moualij, B., Schneider, YJ., Zorzi, W., et al. (2006). "Development of a serum-free co-culture oh human intestinal epithelium cell-lines (Caco-2/HT29-5M21) ". BMC Cell Biology **7**: 20.

OSHA Occupational Safety and Health Administration (2018). "Nanotechnology Applications". Retrieved from https://www.osha.gov/dsg/nanotechnology/nanotech_applications.html

Ouellette, AJ. (2006). “Paneth cell alpha-defensin synthesis and function”. Curr Top Microbiol Immunol 306: 1-25.

Pal, S., Tak, Y.K and Song, J.M. (2007).” Does the antibacterial activity of silver nanoparticles depend on the shape of the nanoparticle? A study of the gram-negative bacterium *Escherichia Coli*”, Appl. Environ. Microbiol. 73 (6) :1712.

Pan, F., Han, L., Zhang, Y., Yu., Y. and Liu, J. (2015).” Optimization of Caco-2 and HT29 co-culture in vitro cell models for permeability studies”. International Journal of Food sciences and Nutrition 66 (6): 680-685.

Park, EJ., Yi, J., Kim, Y., Choi, K. and Park, K. (2010). “Silver nanoparticles induce cytotoxicity by a Trojan-horse type mechanism.” Toxicology in Vitro 24: 872-878.

Park, K., Park, EJ., Chun, IK., Choi, K., Lee, SH., Yoon, J. and Lee, BC. (2011). “Bioavailability and toxicokinetics of citrate-coated silver nanoparticles in rats.” Arch Pharm Res 34 (1): 153-158.

PEN, The Project on Emerging Nanotechnologies (2013). “Consumer Products Inventory. An Inventory of nanotechnology-based consumer products introduced on the market”. Retrieved from http://www.nanotechproject.org/cpi/

Piccinno, F., Gottschalk, F., Seeger, S. and Nowack, B. (2012).” Industrial production quantities and uses of ten engineered nanomaterials in Europe and the world”, Journal of Nanoparticle Research, 14: 1109.

Pinďáková, L., Kašpárková, V., Kejlová, K., Dvořáková, M., Krsek, D., Jírová, D. and Kašparová, L. (2017). “Behaviour of silver nanoparticles in simulated saliva and gastrointestinal fluids “. Int J Pharm 527 (1-2): 12-20.

Promega (2018). “CellTiter-Blue® Cell Viability Assay – Technical Bulletin “. Retrieved from https://www.promega.com/-/media/files/resources/protocols/technical-bulletins/101/celltiter-blue-cell-viability-assay-protocol.pdf

Promega (2018). “CellTiter-Glo® Luminescent Cell Viability Assay – Technical Bulletin “. Retrieved from https://www.promega.com/-/media/files/resources/protocols/technical-bulletins/0/celltiter-glo-luminescent-cell-viability-assay-protocol.pdf

Pubchem Open Chemistry Database (2018). “Glyceryl Trioleate”. Retrieved from https://pubchem.ncbi.nlm.nih.gov/compound/Triolein#section=Top

Pulit-Prociak, J. and Banach, M. (2016). “Silver nanoparticles–a material of the future …? “Open Chem 14: 76–91.

Rai, M., Ingle, A.P., Paralikar, P., Gupta, I., Medici, S and Santos, CA. (2017). “Recent advances in use of silver nanoparticles as antimalarial agents “. International Journal of Pharmaceutics 526 (1-2): 254-270.

Rambaud, JC., Buts, JP., Corthier, G., and Flourié B. (2004). " Flore microbienne intestinale : Physiologie et pathologie digestives ", John Libbey Eurotext, Paris, pp. 61-74.

Ramos, K., Ramos, L. and Gómez-Gómez, M.M. (2017). “Simultaneous characterisation of silver nanoparticles and determination of dissolved silver in chicken meat subjected to in vitro human

gastrointestinal digestion using single particle inductively coupled plasma mass spectrometry". Food Chemistry 221: 822-828.

Ravindran, A., Singh, A., Raichur, A.M., Chandrasekaran, N. and Mukherjee, A. (2010). "Studies on interaction of colloidal Ag nanoaprticles with Bovine Serum Albumin (BSA)." Colloids and surfaces B: Biointerfaces 76: 32-37.

Research and Markets (2018). "Global Nanotechnology Market Outlook 2018-2024". Retrieved from https://www.researchandmarkets.com/research/9d2zws/global?w=4 .

Reidy, B., Haase, A., Luch, A., Dawson, K.A. and Lynch I. (2013). "Mechanisms of silver nanoparticle release, transformation and toxicity: a critical review of current knowledge and recommendations for future studies and applications ". Materials (Basel) 6 (6): 2295-2350.

Ribet, A., Mirouze, J., and Renard, E. (2018). "Pancréas". In Encyclopaedia Universalis retrieved from http://www.universalis-edu.com/encyclopedie/pancreas/

Ribeiro, M.J, Maria, V.L., Scott-Fordsmand, J.J. and Amorim, M.J.B. (2015). "Oxidative Stress Mechanisms Caused by Ag Nanoparticles (NM300K) are Different from Those of AgNO3: Effects in the Soil Invertebrate *Enchytraeus crypticus*". Int. J. Environ. Res. Public Health 12: 9589-9602.

Rockland antibodies & assays (2018). "Bovine Serum Albumin Overview". Retrieved from https://rockland-inc.com/bovine-serum-albumin.aspx

Sambuy, Y., De Angelis, I., Ranaldi, G., Scarino, ML., Stammati, A. and Zucco, F. (2005). "The Caco-2 cell line as a model of the intestinal barrier: influence of cell and culture-related factors on Caco-2 cell functional characteristics". Cell Biology and Toxicology 21 (1): 1-26.

Schneider, G. (2017). "Antimicrobial silver nanoparticles- regulatory situation in the European Union". Materials today: Proceedings 4: 200-207.

Sharma, M., Salisbury, RL., Maurer, El., Hussain, SM. And Sulentic, CE. (2014). "Gold nanoparticles induce transcriptional activity of NF-κB in a B-lymphocyte cell line." Nanoscale 5 (9): 3747-3756.

Sherwood, L. (2012). "Fundamentals of Human Physiology", 4th edition, Brooks/Cole, Cengage Learning, pp. 436-477.

Shin, S.W., Song, I.H. and Um, S.H. (2015). "Role of physicochemical properties in nanoparticle toxicity". Nanomaterials 5: 1351-1365.

Shrivastava, S., Bera,T., Roy, A., Singh, G., Ramachandrarao, P. and Das, D. (2007) "Characterization of enhanced antibacterial effects of novel silver nanoparticles" Nanotechnology 18 (22).

Šidàk, Z. (1967)." Rectangular confidence region for the means of multivariate normal distributions ". Journal of the American Statistical Association 62: 626–633.

Sigma-Aldrich (2011). "Silver nanoparticles: properties and applications ". Retrieved from https://www.sigmaaldrich.com/technical-documents/articles/materials-science/nanomaterials/silver-nanoparticles.html

Sigma-Aldrich (2018). “Bovine Serum Albumins”. Retrieved from https://www.sigmaaldrich.com/life-science/biochemicals/biochemical-products.html?TablePage=103994915

Sigma-Aldrich (2018). “Pancreatin from porcine pancreas”. Retrieved from https://www.sigmaaldrich.com/catalog/product/sigma/p3292?lang=fr&region=BE

Sinnecker, H., Ramaker, K. and Frey, A. (2014). “Coating with luminal gut-constituents alters adherence of nanoparticles to intestinal epithelial cells”. Beilstein Journal of Nanotechnology **5**: 2308-2315.

Stensberg, MC., Wei, Q., McLamore, E.S., Porterfield, D.M., Wei, A. and Sepulveda, M.S. (2011). “Toxicological studies on silver nanoparticles: challenges and opportunities in assessment, monitoring and imaging.” Nanomedicine **6** (5): 879-898.

Suresh, A.K., Pelletier, D.A., Wang, W., Morrell-Falvey, J.L., Gu, B. and Doktycz, M.J. (2012). “Cytotoxicity induced by engineered silver nanocrystallites is dependent on surface coatings and cell types”. Langmuir **28** (5): 2727-2735.

Syafiuddin, A., Salim,M.R., Kueh, A.B.H., Hadibarata, T. and Nur, H. (2017). “A review of silver nanoparticles: research trends, global consumption, synthesis, properties, and future challenges.” Journal of the Chinese Chemical Society **64** (7).

Tai, JT., Lai, C-S., Ho, H-S., Yeh, Y-S., Wang, H-F, Ho, R-M. et al. (2017). “Protein- silver nanoparticle interactions to colloidal stability in acidic environments “. Langmuir **30** (43): 12755-12764.

Taniguchi, N. (1974).” On the Basic Concept of Nanotechnology”. Proceedings of the International Conference on Production Engineering, Tokyo, Part II, Japan Society of Precision Engineering, 18-23.

The Nanodatabase (2018). “Analysis/Consumer products”. Retrieved from http://nanodb.dk/en/analysis/consumer-products/#chartHashsection

Thermo Fischer Scientific (2018). “Micro BCA™ Protein Assay Kit “. Retrieved from https://www.thermofisher.com/order/catalog/product/23235

Thursby, E., and Juge, N. (2017). “Introduction to the human gut microbiota”. Biochemical Journal **474** (11): 1823-1836.

Tran, Q. H., Nguyen, V. Q. and Le, A. T. (2013). “Silver nanoparticles: synthesis, properties, toxicology, applications and perspectives “. Adv. Nat. Sci. **4** (3).

Treuel, L., Malissek, M., Grass, S., Diendorf, J., Mahl, D. Meyer-Zaika, W. and Epple, M. (2012). “Quantifying the influence of polymer coatings on the serum albumin corona formation around silver and gold nanoparticles”. Journal of Nanoparticle Research **14**: 1102.

USDA United States Department of Agriculture. (2015). “How many calories are in one gram of fat, carbohydrate, or protein? “. Retrieved from https://www.nal.usda.gov/fnic/how-many-calories-are-one-gram-fat-carbohydrate-or-protein

U.S. FDA Food and Drug Administration (2014). “Considering Whether an FDA-Regulated Product Involves the Application of Nanotechnology” retrieved from https://www.fda.gov/RegulatoryInformation/Guidances/ucm257698.htm

Vance, M. E., Kuiken, T., Vejerano, E. P., McGinnis, S. P., Hochella, M. F. Jr., Rejeski, D. and Hull, M. S. (2015). ". Beilstein Journal of Nanotechnology **6** :1769–1780.

Van den Brule, S., Ambroise, J., Lecloux, H., Levard, C., Soulas, R., De Temmerman, P.J., Palmai-Pallag, M., Marbaix, E. and Lison, D. (2016). "Dietary silver nanoparticles can disturb the gut microbiota in mice." Part Fibre Toxicol, **13**: 38.

Van der Zande, M., Vandebriel, R.J., Van Doren, E., Kramer, E., Herrera Rivera, Z., Serran-Rojera, C.S et al. (2012). "Distribution, elimination, and toxicity of silver nanoparticles and silver ions in rats after 28-day oral exposure". ACS Nano **6** (8): 7427-7442.

VIVO Pathophysiology. (2018). "Absorption in the stomach ". retrieved from http://www.vivo.colostate.edu/hbooks/pathphys/digestion/stomach/absorb.html

Völker, C., Oetken, M. and Oehlmann, J. (2013). "The biological effects and possible modes of action of nanosilver". Rev Environ Contam Toxicol **223**: 81 -106.

Von Goetz, N., Fabricius, L., Glaus, R., Weitbrecht, V., Günther, D. and Hungerbühler, K. (2013). "Migration of silver from commercial plastic food containers and implications for consumer exposure assessment." Food Additives & Contaminants: Part A **30**: 612-620.

Waalewijn-Kool, P.L., Klein, K., Forniès, P.M. and van Gestel, C. (2014). "Bioaccumulation and toxicity of silver nanoparticles and silver nitrate to the soil arthropod *Folsomia candida*". Ecotoxicology **23**: 1629-1637.

Walczak, AP., Fokkink, R., Peters, R., Tromp, P., Herrera Rivera, Z., Rietjens, IM. et al. (2013). "Behaviour of silver nanoparticles and silver ions in an in vitro human gastrointestinal digestion model". Nanotoxicology **7** (7): 1-13.

Wang, G., Lu, Y., Hou, H. and Liu, Y. (2017). "Probing the binding behavior and kinetics of silver nanoparticles with bovine serum albumin". RSC Advances **7**: 9898-9401.

Wasmuth, C., Rüdel H., Düring, R.A. and Klawonn, T. (2016). "Assessing the suitability of the OECD 29 guidance document to investigate the transformation and dissolution of silver nanoparticles in aqueous media". Chemosphere **144**: 2018-2023.

Wen, R., Hu, L., Qu, G., Zhou, Q. and Jiang, G. (2016). "Exposure, tissue distribution, and biotransformation of nanosilver". NanoImpact **2**: 18-28.

Wheeler, MW., Park, RM. And Bailer, AJ. (2006). "Comparing median lethal concentration values using confidence interval overlap or ratio tests". Environmental Toxicology and Chemistry **25** (5): 1441-1444.

Wijhoven, S., Peijnenburg, W., Herberts, C., Hagens, W., Oomen, A., Heugens, E. et al. (2009). "Nano-silver – a review of available data and knowledge gaps in human and environmental risk assessment". Nanotoxicology **3** (2): 109-138.

Williams, K.M., Gokulan, K., Cerniglia, C.E. and Khare, S. (2016). "Size and dose dependent effects of silver nanoparticle exposure on intestinal permeability in an in vitro model of the human gut epithelium". J. Nanobiotechnol. **14** (62).

Wilson, V.T. (2007). “How sword swallowing works”. In Howstuffworks.com, retrieved from https://entertainment.howstuffworks.com/arts/circus-arts/sword-swallowing2.htm

Winuprasith, T., Chantarak, S., Suphantharika, M., He, L. and McClements, DJ. (2014). “Alterations in nanoparticle protein corona by biological surfactants: impact of bile salts on β-lactoglobulin-coated gold nanoparticles.” J Colloid Interface Sci **426**: 333-340.

Xue, Y., Zhang, S., Huang, Y., Zhang, T., Liu, X., Hu, Y. (2012). “Acute toxic effects and gender-related biokinetics of silver nanoparticles following an intravenous injection in mice “. Journal of Applied Toxicology **32** (11): 890-899.

Yeshchenko, O.A., Dmitruk, I.M., Alexeenko, A.A., Kotko, A.V., Verdal, J. and Pinchuk, O. (2012). “Size and temperature effects on the surface plasmon resonance in silver nanoaprticles”. Plasmonics **7** (4): 685-694.

Yi, F., Chen, G., Zeng, G., Guo, Z., Liu, W., Huang, Z., He, K. and Hu, L. (2016). “Influence of cysteine and bovine serum albumin on silver nanoparticle stability, dissolution, and toxicity to *Phanerochaeta chrysosporium*”. RSC Advances 108.

Yoder, S.M., Kindel T.L., and Tso P. (2010). “Using the lymph fistula rat model to study incretin secretion”. Vitamins & Hormones **84**: 221-249.

Zhang, X-F., Liu, Z-G., Shen, W. and Gurunathan, S. (2016). “Silver nanoparticles: synthesis, characterization, properties, applications, and therapeutic approaches.” International Journal of Molecular Sciences **17** (9).

Zhang, Z., Shen, W., Xue, J., Liu, Y., Liu, Y., Yan, J., Liu, J. and Tang, J. (2018). “Recent advances in synthetic methods and applications of silver nanostructures”. Nanoscale Research Letters **13** (54).

Zhu, Y., Li, W., Li, Q., Li, Y., Li, Y., Zhang, X. and Huang, Q. (2009). “Effects of serum proteins on intracellular uptake and cytotoxicity of carbon nanoparticles “. Carbon **47** (5): 1351-1358.

Université catholique de Louvain

Impact of food components and digestive enzymes on silver nanoparticles cytotoxicity in a coculture model of the intestinal barrier

Présenté par Donika Kastrati

Abstract

Known as "the material of the 21st century", nanomaterials have revolutionized many industrial sectors during the last decades. Concerning the food industry, engineered nanomaterials (ENMs) have been added intentionally in commercial food products to enhance their quality, safety or shelf-life but also to provide specific flavors or colors. Silver nanoparticles (AgNPs) are currently the nanomaterial found in the highest number of consumer products thanks to their antibacterial properties: dietary supplements, plastic food containers, fridges, …

The inevitable use of these products leads to the unintentional exposure of consumer's digestive system to AgNPs. Indeed, the risk of AgNPs ingestion due to their migration from the products is recognized and reported in many studies, such as their deleterious effects *in vitro* and *in vivo*. Such considerations raise the need of toxicological studies about AgNPs, especially that account for the physico-chemical transformations of AgNPs occurring when they are incorporated into food and digested as they transit the gastro-intestinal tract (GIT). Although the GIT and food have been demonstrated to alter AgNPs cell's interactions, only few studies take in account these effects.

In this master thesis however, we investigated the impact of food components and digestion on the toxicity of AgNPs. Thanks to a modelized food matrix and an *in vitro* digestion process, these two effects could be reproduced and their impact on the cytotoxic effect of AgNPs assessed in a coculture model of the human intestinal epithelium consisting of Caco-2 and HT29-MTX cells.

The food matrix seemed to reduce AgNPs inherent toxicity while digestive enzymes worsened it. Together, digestive enzymes and food component induced such changes that the toxicity of AgNPs was also increased. Further characterization and protein quantification experiments gave us lines of explanations. Indeed, the presence of a protein corona is strongly indicated and can explain the protective effect of food components. Digested enzymes were suggested to alter AgNPs characteristics or have a potential higher activity consequently to their interaction with AgNPs. Our results indicate that toxicity of AgNPs can be strongly influenced by the presence of food components and digestive enzymes and reproducing both parameters is important to draw realistic and truthful interpretations.

Further experiments should focus on the characterization of the composition of the protein corona upon incubation of AgNPs with the food matrix but also throughout the whole digestion process to have an insight of the new biological identity acquired by AgNPs.

Keywords: silver nanoparticles, toxicity, digestion, food matrix, GI tract

AGRO LOUVAIN